Advanced Photon Source Upgrade Project

Preliminary Design Report

September 2017

Chapter 5: Front Ends and Insertion Devices

Document Number : APSU-2.01-RPT-002
ICMS Content ID : APSU_1705610

Table of Contents

List of Figures

List of Tables

Acronyms and Abbreviations

3D	three dimensional
3PW	3 pole wiggler
APPLE	Advanced Planar Polarized Light Emitter
APS	Advanced Photon Source
APS-U	Advanced Photon Source Upgrade
BINP	Budker Institute of Nuclear Physics
BIV	beamline isolation valve
BM	bending magnet
BMFE	bending magnet front end
BMR	bending magnet front end retrofit
BPLD	beam position limits detector
BPM	beam position monitor
CDR	Conceptual Design Report
CFR	canted front end retrofit
CM	clearing magnet
CUFE	canted undulator front end
DCS	Dynamic Compression Sector
DOF	degree of freedom
DS	downstream
EM	exit mask
FEV	front end exit valve
FEv1.2	front end version 1.2
FEv1.5	front end version 1.5
FM	fixed mask
FReD	Functional Requirements Document
GRID	grazing-incidence for insertion device
HGVPU	horizontal-gap vertically-polarizing undulator
HHLFE	high heat load front end

HHLR	high heat load front end retrofit
HPM	hybrid permanent magnet
HPMU	hybrid permanent magnet undulator
ID	insertion device
IDVC	insertion device vacuum chamber
IEX	Intermediate Energy X-ray
IM	intensity monitor
LHe	liquid helium
LPPS	low power photon shutter
MBA	multi-bend achromat
MPS	machine protection system
NEG	non-evaporative getter
PIN	P-type, intrinsic, and N-type material
PM	permanent magnet
PRD	Physics Requirements Document
PS	photon shutter
rf	radio frequency
RFBPM	radio frequency beam position monitor
SCAPE	superconducting arbitrary polarization emitter
SCU	superconducting undulator
SRV	storage ring exit valve
SS	safety shutter
SV	slow valve
UHV	ultra high vacuum
US	upstream
XBPM	x-ray beam position monitor
XRF	x-ray fluorescence

5 Front Ends and Insertion Devices

5-1 Introduction

The Advanced Photon Source (APS) Upgrade Project is a major redesign of the accelerator in the current operating machine. The upgraded APS will be operating at 6 GeV and 200 mA of stored beam with a new low emittance lattice. To fully support the APS Upgrade (APS-U), the front ends and insertion devices (IDs) located inside the storage ring tunnel need to be upgraded. This chapter describes the front ends, IDs, and bending magnet (BM) sources where capabilities must be improved to maximize the potential of the APS Upgrade Project.

Most of the front ends at the APS were designed more than 20 years ago and have been in operation since then. The BM front ends were designed to handle power from the APS operating at 300 mA current at 7 GeV. The ID front ends were originally designed to handle 100 mA of beam from a 2.4-m-long undulator A of period 3.3 cm. Recently, the APS has designed ID front ends capable of handling higher heat loads from two 2.4 m undulator A's in a straight section. The APS Upgrade will require all the original ID front ends to be replaced in order to handle the increased power. In addition, all ID front ends will have next-generation x-ray beam position monitors (XBPM) to provide long-term stability for the beamlines. The current BM front ends will undergo minor modifications and will be reused. Section 5-2 discusses the front end plans for the APS-U.

At the current time, the APS has 54 IDs in operation over 33 beamlines. Most of the devices were optimized more than 20 years ago for 7-GeV operation, providing full energy tunability in the hard x-ray range. There are some devices with smaller periods and two electromagnetic devices for soft x-ray beamlines. The upgraded APS machine will operate at 6 GeV and will require replacement of most of the IDs. Over the years, user requirements have been refined, and requests for special devices like superconducting undulators and variable polarizing undulators have increased. To maximize the brightness and flux for all the beamlines (also part of the APS-U), most of the IDs will be replaced with smaller period devices. In addition, because of user requirements, more special devices will be installed in the new upgraded machine. Section 5-3 discusses the ID plans for the APS-U.

Currently, there are 23 BM front ends installed, of which only 20 beamlines are in operation. The BM beamlines can use up to 6 mrad in a horizontal fan of radiation. With the multi-bend achromat (MBA) lattice for the APS-U, the BM source is changing. The MBA reverse bend lattice makes the BM source a complex combination of radiation from multiple sources. Section 5-4 will discuss the various options for the existing bending magnet sources.

5-2 Front Ends

5-2.1 Introduction and Scope

Front ends are the sections tangential to the storage ring. Most of the front end components, except for the exit table, are housed inside the storage ring tunnel enclosure. The synchrotron beam extracted from the storage ring must pass through the front ends first. At the APS, there are a total of 40 sectors, 35 of which have beam ports and are capable of extracting a synchrotron beam. Each sector consists of an ID and a BM beam port. An overview of both ID and BM front ends of the APS-U for one sector is shown in Figure 5.1.

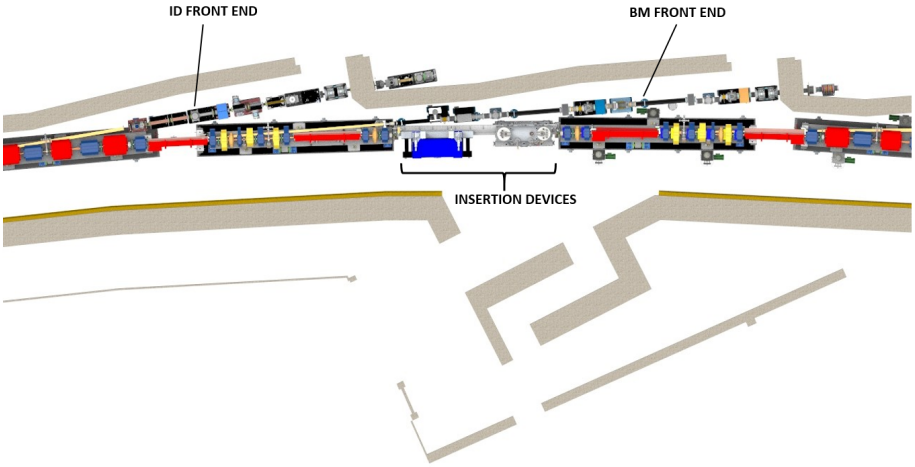

Figure 5.1. Overview of ID and BM front ends in relation to the storage ring components.

The APS Upgrade will build out front ends for the entire 35 ID ports and 23 BM front ends. All existing original ID front ends that were built in the 1990s cannot handle the heat load and will be replaced by new front ends. The ID front ends built in the 2000s can handle the heat load and will be retrofitted to have clearing magnets and next generation XBPMs. All BM front ends will be retrofitted to have clearing magnets. The total scope and top level WBS is shown in Table 5.1.

Table 5.1. Type of front ends and their WBS

WBS	Type of front end	Qty
U2.05.02.01	High Heat Load Front Ends (HHLFE)	17
U2.05.02.02	Canted Undulator Front Ends (CUFE)	6
U2.05.02.03	High Heat Load Front Ends Retrofit (HHLR)	5
U2.05.02.04	Canted Front End Retrofit (CFR)	7
U2.05.02.05	Bending Magnet Front End Retrofit (BMR)	23
U2.05.02.06	Front End Test and Assembly	

5-2.2 Requirements

The APS Upgrade requires three types of front ends:

1. High Heat Load Front End (HHLFE) for two inline undulators
2. Canted Undulators Front End (CUFE) for two undulators at 1.0 mrad canting angle between them
3. Bending Magnet Front End (BMFE) for bending magnet sources

All front ends must have the following features:

1. Must have a clearing magnet to deflect and dump the electron beam in case the electrons escape the storage ring during the swap out injection while the safety shutter is open. This is a new requirement on the front end exclusively from the APS-U. In current APS operation, electron trace studies have been performed for each type of front end to ensure that no electrons can escape from the storage ring and pass through the front end during top-up injection. These studies depend on the front-end shielding aperture arrangement and must be re-done if the shielding aperture changes. For the APS-U lattice, due to the large number of magnets, it is difficult to perform simulations for all cases, so a clearing magnet will be used in the front end to meet the required safety for swap out injection. The clearing magnet must be a permanent magnet.
2. Must have next generation XBPMs system. This is a new requirement for the APS-U. Due to the stringent beam stability requirements for the APS-U beam, the XBPM plays an important role.
3. Must handle heat load from anticipated sources.
   (a) HHLFE must be able to handle the heat load from 6 GeV, 200 mA operation with two inline 2.4 m long undulators. The HHLFE must be able to handle a total power of 21 kW and a peak power density of 590 kW/mrad^2.
   (b) CUFE must be able to handle heat load from 6 GeV 200 mA operation with two 2.1 m long canted undulator at 1.0 mrad canting angle. The CUFE must be able to handle a total power of 20 kW and a peak power density of 280 kW/mrad^2.
   (c) BM front ends must be able to handle the heat load from APS-U magnets at 6 GeV, 200 mA operation.
4. Must provide radiation safety. The front end must confine the synchrotron radiation and bremsstrahlung radiation within a defined opening angle, and provide a means of stopping and absorbing the radiation upstream of the ratchet wall in order to allow personnel access to stations outside the ratchet wall. The major components that will fulfill these functions are photon masks, photon shutters, bremsstrahlung collimators, and safety shutters.
5. Must provide vacuum protection to the storage ring. The front end must function as a vacuum buffer zone between the beamline vacuum and storage ring vacuum. It must be able to maintain the ultra-high vacuum (UHV) requirements of the storage ring. It must monitor vacuum quality and isolate the storage ring vacuum from the beamline vacuum when necessary. Components for vacuum protection are vacuum pumps, gauges, valves, and x-ray exit windows.

5-2.3 Front End Design

5-2.3.1 Overview of Existing Front Ends and Design History

Over the past 20 years, front end design has been constantly improving to enhance the capability to handle higher heat loads, deliver canted beams, and provide mechanisms for improving beam stability. Over the past few years, the design has also been improved in its manufacturability, ease of alignment, ease of maintenance, and engineering value. As of today, there are five types of ID front ends in the APS storage ring. This document describes the existing front ends and what needs to be done to upgrade them so they are compatible with the APS Upgrade.

The majority of the existing front ends are version 1.2 front ends (FEv1.2), which are the original front ends installed in the current APS storage ring. This type of front end is compatible with both the undulator and wiggler operation and has very large apertures to pass the wiggler beam. The heat-load limit for FEv1.2 is about 7 kW of total power and 200 kW/mrad^2 peak power density, which is equivalent to a single undulator A (period 33mm) of 11-mm gap at 130 mA. In the mid-to-late 1990s, an improved version of the front end, referred to as the version 1.5 front end (FEv1.5), was designed and installed in four locations: 16-ID, 22-ID, 31-ID, and 32-ID. FEv1.5 exercised value engineering, improving the components' manufacturability and raising the heat load limit equivalent to one undulator A at 150 mA. The detailed thermal analysis of these two types of front ends can be found in APS technical bulletin TB-50 [1]. In 2003, driven by having two beams in a single beam port, a canted undulator front end was designed and installed in three locations: 21-ID, 23-ID, and 24-ID. All masks and photon shutters for the canted undulator front end were redesigned, and the heat load limit was raised to 20 kW of total power and 281 kW/mrad^2 peak power density [2]. In 2004, driven by the requirement to handle the higher heat load from dual inline undulators, a high-heat-load front end (HHLFE) was designed and installed in 26-ID and 30-ID, which further raised the heat-load-handling limit to 21 kW total power and 590 kW/mrad^2 peak power density [3]. In 2009, a modified version of the HHLFE, capable of handling a beam from vertical and circular polarized undulators, was designed and installed at 29-ID. Between 2010 and 2012, three FEv1.2 and one FEv1.5 front ends were replaced by canted undulator front ends at 12-ID, 13-ID, 16-ID, and 34-ID. In 2013, driven by the need to improve beam stability and incorporate next-generation XBPM systems into the front ends, the HHLFE was redesigned. The new HHLFEs were installed at 27-ID and 35-ID in May 2014. In 2016 the 6-ID front end was changed from FEv1.2 to FEv1.5 to handle higher heat loads. The type of ID front ends that currently exist in the APS storage ring, along with their heat load capability, are listed in Table 5.2. Except for 25-ID and 28-ID, which are vacant, all ID ports have front ends.

Table 5.2. Type of existing ID front ends and their heat-load limits

Type of front end	FEv1.2	FEv1.5	CUFE	HHLFE	HHLFE with GRID
Sector location	1,2,3,4,5, 7,8,9,10,11, 14,15,17,18, 19,20,33	22, 31, 32, 6	12, 13, 16, 21, 23, 24, 34	26, 29, 30	27, 35
Total power (kW)	6.9	8.9	20	21	21
Peak power density (kW/mrad^2)	198	245	281	590	590

Table 5.3. Comparison of heat load of the APS HHLFE with current ring versus APS-U

	HHLFE design parameter with current APS	**APS-U with U27.5**	**APS-U with U30**	**APS-U with SCU18**
Storage ring energy (GeV)	7	6	6	6
Radiation angle $1/\gamma$ (μrad)	73	85	85	85
Design beam current (mA)	180	200	200	200
Undulator minimum magnetic gap (mm)	10.5	8.5	8.5	9.0
Undulator period length (cm)	3.3	2.75	3.0	1.8
Total periods for two 2.4-m undulators (N)	144	172	158	167
K_{peak} at minimum gap	2.76	2.44	2.92	1.56
Total power (kW)	21.28	19.46	23.43	11.79
Peak power density at second photon shutter at 22.4 m (W/mm^2)	1193	903	912	843
Total power at second photon shutter (kW, beam aperture at PS2 is 5.60 × 6.72 mm)	14.8	13.1	13.6	10.3
Maximum peak temperature (°C)	218	190	193	176
Maximum von Mises stress (MPa)	369	315	321	286
Cooling wall temperature (°C)	87	79	80	74

For the APS-U, all ID front ends must be able to handle the heat loads from two IDs in either an inline or a canted configuration. The FEv1.2 and FEv1.5 will not meet the heat load requirement. In addition, the apertures in these front ends are too large, so these two types of front ends must be replaced. The low emittance lattice of the APS-U has a higher level of requirement for beam stability, resulting in the need for better beam diagnostics in front ends. All front ends are required to be equipped with next-generation XBPMs. The existing design of the masks and photon shutters in the CUFE and HHLFE will meet the heat load requirement of the APS-U with 200 mA operation. A preliminary selection of sources have been determined for each beamline. Based on the selection, the likely choice is to replace the widely used 3.3 cm period undulator (undulator A) with a device of period between 2.8 cm (U28) and 2.75 cm (U27.5) with a minimum gap of about 8.5 mm. The power profile of the U27.5 is being used as a benchmark for preliminary thermal design of the front end components. In addition, two more devices with period of 3.0 cm (U30) and a superconducting undulator of period 1.8cm (SCU18) are used for the benchmark.The comparison of the power load and thermal analysis for the photon shutter is shown in Table 5.3.

5-2.3.2 Thermal Design and Failure Criteria

The thermal design criteria have been in existence since the APS was built. The three design criteria used are listed below in order of importance:

1. The maximum temperature of the cooling wall should not locally exceed the boiling point of water at the cooling channel water pressure, and thus only single-phase water is allowed. An APS front end has a typical cooling water header pressure of 130 to 150 psig. The typical pressure for evaluating water boiling is set at 60 psig, corresponding to a water boiling point of 153 °C. This is the most important criterion, to ensure that catastrophic failure, such as thermal burn out, does not occur.
2. The maximum surface temperature, generally occurring at the center of the beam footprint,

should not exceed 300 ℃.

3. The maximum von Mises stress for photon shutters should not exceed 400 MPa, which is the room temperature yield stress of plate stock GlidCop Al-15. The maximum stress allowed on fixed masks in the corners at extreme missteering conditions is relatively relaxed because such missteering cases are very rare. Following this criterion essentially ensures an infinite life for the device.

Over the past 10 years, efforts have been under way to try to establish fatigue-based criteria. In the past four years, many GlidCop samples were tested under very high heat loads at an APS beamline (29-ID). New, more relaxed criteria have been proposed [4], which suggest raising the maximum temperature limit to 375 ℃ and eliminate the need for stress evaluation for flat surfaces as long as the peak temperature is below 375 ℃. These new criteria are under an internal review and approval process. The APS-U front end easily meets the original design criteria, however the new criteria maybe helpful for the front end to be used for very high power SCUs in the future.

5-2.3.3 High Heat Load Front End (HHLFE)

The new HHLFE for APS-U must have a clearing magnet as far upstream as possible to deflect the electrons away from the safety shutter's aperture in the event that the electrons enter the front end during the swap out injection. In addition, it must have the next generation XBPM system. For the high heat load front end the next generation XBPM is the Grazing Incidence for Insertion Devices (GRID) XBPM. The requirements and the design of the clearing magnet and the NG XBPM system are discussed later in Sections 5-2.4 and 5-2.5. The aperture size and location of the masks are determined by the need to protect the clearing magnet from synchrotron beam strikes and by the requirement to provide the full view of the beam profile for the GRID-XBPM. Based on the proposed undulator sources for the APS-U, the existing HHLFE masks and photon shutters meet the thermal design criteria. The plan is to use most of the existing component designs; however, if a mask needs to be redesigned it will have the same thermal handling capacity as the existing components. The most recent design of the HHLFE with the GRID-XBPM installed in 27-ID and 35-ID will be used as the design base. For value engineering, we plan to harvest and reuse the safety shutters from the FEv1.2 front ends. The design of the HHLFE is at the final design phase. We plan to build out one HHLFE early and install it in a vacant port of 28-ID for an R&D beamline. Procurement of masks has started for the HHLFE for installation in 28-ID.

The HHLFE design layout is shown in Figure 5.2. For a detailed layout and ray tracing drawing, refer to drawing U2520101-210000. The aperture designs of the masks are determined by the following factors: In order to protect the clearing magnet from synchrotron radiation strikes, the first fixed mask and second fixed mask must restrict the beam in both the horizontal and vertical planes. The inlet aperture of FM1 remains the same as the current APS ring which is 38(H) x 26(V) mm in anticipation that the APS-U beam missteering will be the same as or less than the existing APS ring. Details for the beam mistering and the FE requirements are discussed in the front end FReD document. For the HHLFE a missteering beam envelope of no more than ±1.0 mrad(H) x ±0.67mrad (V) was used to determine the FM1 inlet aperture at 17 m to be at least 34(H) x 23(V)mm.

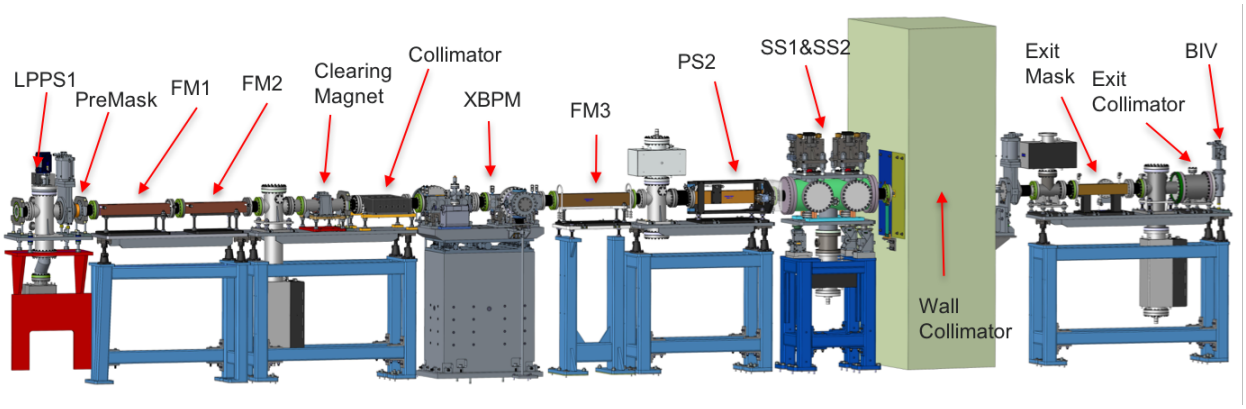

Figure 5.2. The HHLFE for APS-U with clearing magnet and the next-generation XBPMs.

The benchmark heat load for the APS-U front end is equivalent to the heat load from two 2.4 m long, 2.75 cm period undulators at 8.5-mm gap, operating at 6 GeV and 200 mA. This heat load is less than the heat load of two 3.3 cm period undulator A at 10.5-mm gap at 180 mA in the 7 GeV ring. Therefore, all of the high heat load components designed for the existing HHLFE will work

for the future APS-U storage ring. The new masks are also designed to the same standards.

The description of the HHLFE for APS-U from upstream to downstream is as follows:

1. Low Power Photon Shutter (LPPS). The function of the LPPS is to protect the slow valve immediately downstream from the dipole. The LPPS cannot withstand the heat load from the ID source and when LPPS is closed, the ID gap must be open. The LPPS is an existing APS design and is currently installed and operating in 27-ID and 35-ID.
2. Slow Valve (SV). The function of the SV is to isolate the front end vacuum from the storage ring vacuum in case there are front end faults during operation. When the SV is commanded to close, it will dump the stored beam followed by the closure of the LPPS. The storage ring can resume operation only when the ID gap is verified to be at open position and the LPPS is closed. The slow valve and LPPS can be used to isolate the front end from the storage ring and will allow for operation of the storage ring with the ID gap open.
3. Premask. The function of the premask is to protect the stainless steel flange of FM1 from the dipole radiation. the premask has an aperture of 36(H) x 26(V) mm to allow the ID beam to pass. The premask is an existing APS design.
4. First Fixed Mask (FM1). The FM1 is a missteering protection mask. Under normal operating conditions, the beam will pass right through without touching the mask. FM1 and FM2 together define the required aperture for the GRID XBPM. The inlet aperture of the FM1 is 38(H) x 26(V) mm, which is sufficient to accept a beam missteering cone of $\pm$1.0(H) x 0.67(V) mrad. This is the same aperture used in the current APS ring. The exit aperture of FM1 is 20(H) x 16(V) mm and is determined by the allowed beam incidence angle from thermal analysis. The FM1 is a new design. The design and thermal analysis will be discussed next.
5. Second Fixed Mask (FM2). The FM2 inlet aperture is 24(H) x 20(V) mm, which has a 2 mm all around overlap with the FM1 exit aperture. The FM2 exit horizontal aperture is defined by the GRID-XBPM. For proper functionality of the GRID-XBPM, the full beam footprint is passed through the FM2 exit aperture. Based on the various possible undulator sources, a 9.0-mm exit horizontal aperture is required for the FM2. The GRID-XBPM is not sensitive to the vertical aperture. So the FM2 vertical aperture is defined by the allowed beam incidence angle from thermal analysis. The exit aperture of FM2 is 9(H) x 12(V) mm. The FM2 design is similar to FM1 and the design and thermal analysis will be discussed next.
6. Pump support chamber. The only purpose of this chamber is to support a vacuum pump and allow mounting of vacuum gauges to the chamber. This configuration uses the least amount of space along the beam to mount the larger size pump. This pump is needed to pump out FM1, FM2 and clearing magnet.
7. Clearing Magnet (CM). The clearing magnet is a device with a rectangular vacuum chamber of 13(H) x 20(V) mm optical aperture. The magnets are on the inboard and outboard side of the chamber. It has an 18-mm magnetic gap in the horizontal direction. The magnetic field can bend the electron beam 6.52 mrad towards the floor. There is a magnetic shield around the clearing magnet to prevent it from interfering with the nearby storage ring magnets. The CM will be discussed later in detail in Section 5-2.5.
8. Lead Collimator. This is a shielding component. Its construction consists of a square vacuum tube surrounded by lead. The optical aperture is the tube's ID and the aperture is designed so that it can pass the maximum missteered synchrotron beam with at least a 3.0-mm clearance. The lead aperture is the shielding aperture. It has a 19.5(H) x 19.5(V) mm optical aperture and 26(H) x 26(V) mm shielding aperture. The collimator design is modified from the existing

HHLFE collimator design with the aperture changes.

9. GRID-XBPM. This is the primary component of the NG XBPM system. It consists of two horizontal half masks. The upstream mask collimates the inboard half of the beam and the downstream mask collimates the outboard half of the beam. The relative position between the two half masks is fixed at installation so the exit aperture is set at 1.6 mm total in the horizontal dimension. The GRID masks do not have a vertical aperture. For the upstream mask, the detector is mounted at the outboard side of the mask to sense the X-ray florescence created by the inboard mask. For the downstream mask, the detector is mounted at the inboard side to sense the florescence created by the outboard mask. The horizontal beam position is detected by comparing the inboard and outboard detector signal. The vertical position is detected using the pin hole camera principle in the detector. The GRID mask assembly is mounted to precision slides to allow horizontal movement. The GRID-XBPM will be discussed in detail later in Section 5-2.4.
10. Third Fixed Mask (FM3). The function of this mask is to further collimate the synchrotron beam to protect the photon shutter, safety shutter, wall collimator and exit mask. FM3 has an inlet aperture of 16(H) x 47(V) mm and an exit aperture of 3.6(H) X 6(V) mm.
11. Pump Chamber. The function of this chamber is to mount a vacuum pump and valves to pump out. The vacuum pump is required to pump the section between the FM3 and the PS2. This is an existing design.
12. Photon Shutter 2 and Intensity Monitor 1 (PS2/IM1) Assembly. This is the high heat load photon shutter. It was designed in 2004 and is installed and operational in five sectors. It pivots horizontally towards the inboard to close the beam. Two intensity monitors are mounted directly at the upstream and downstream of the shutter to measure the X-ray florescence when the shutter is closed. The IM1 is a diagnostic tool for alignment of the GRID-XBPM when the PS2 is closed.
13. Safety Shutter. This is the existing safety shutter from FEv1.2. As part of value engineering the Fev1.2 shutters will be reused in the HHLFE. This shutter was originally designed for undulator/wiggler and is not ideal for HHLFE. Its aperture of 72(H) x 20(V) mm is large and it will not function as a collimator when it is at open position. This shutter is also longer along the beam direction so it occupies more floor space. This shutter is expected to be retrofitted with a new air cylinder as part of APS operations. In addition, due to changes in the ACIS/PSS, two additional close switches for a total of 4 switches at the closed position will be installed. A HHLFE safety shutter design is available with 16(H) X 16(V) mm aperture and installed in five sectors. The decision for reuse of the FEv1.2 safety shutter may be re-evaluated at a later date.
14. Wall collimator. This collimator is based on the design of the existing HHLFE wall collimator. There are five such wall collimators installed at the APS. The wall collimator consists of a rectangular vacuum tube surrounded by lead. The optical aperture is the vacuum chamber's internal aperture and the shield aperture is the nominal lead aperture.
15. Front End Valve (FEV). This valve isolates the front end components inside the ratchet wall from the components outside the ratchet wall. Any vacuum fault downstream of this valve will trigger the FEV to close.
16. Pump Chamber. this pump chamber was designed to house XBPM2 detectors for the 27-ID and 35-ID front end. In the new design for the APS-U, the detectors for the XBPM2 are directly mounted on the exit mask side port so this chamber acts as a vacuum pump support.
17. Exit Mask/XBPM2. This is an integrated unit of an exit mask and XBPM2. As an exit mask, it is an RSS component with an inlet aperture of 10(H) x 38(V) mm and exit aperture

of 2(H) x 2(V) mm. The mask consists of two inclined planes forming a "y" shape in the bottom view. The outboard has the short edge of the "y" and stops 1 mm away from the beam center plane. The inboard side is the long edge of the "y" and extends far beyond the beam center plane. There is a slot cut into the long edge of the "y" to allow the beam to pass. The overlap from the long edge to the short edge is 2 mm. The detectors are mounted on the side port in the outboard side to detect the florescence generated by the inboard plane. The angle of the tapered plane is 1.1°, which is the same as the exit mask of the 27-ID so the thermal handling ability remains the same. The exit aperture of the mask is 2x2 mm. This mask is a new design.

18. Pump chamber. This is an existing design and supports the vacuum pump.
19. Tungsten collimator. This is a shielding component. This is the existing design as in 27-ID. It is an in-vacuum tungsten design. Both the optical and shielding aperture are 10(H) x 7(V) mm.
20. Beamline isolation valve (BIV). BIV is used to isolate front end vacuum from the beamline vacuum for windowless beamlines. For a beamline with a window, the beamline will terminate with the Be window or diamond window.

The HHLFE aperture table is shown in Table 5.4.

Table 5.4. HHLFE Components Aperture Table

APS-U HHLFE Components	Distance to center of straight section (m)	Aperture Optical H (mm) x V (mm)	Shielding Aperture H (mm) x V (mm)	Comments
Premask	16.5	36 x 26		Same as 27-ID
First Fixed Mask (FM1)	17.3	38 x 26 (inlet) 20 x 16 (outlet)		New design
Second Fixed Mask (FM2)	18.0	24 x 20 (inlet) 9 x 12 (outlet)		New design
Clearing Magnet (CM)	18.7	12 x 40	18 x ∞ (magnet gap)	New design
Lead Collimator	19.2	19.5 x 19.5	26 x 26 (Pb)	New design
GRID-XBPM	20.0	15.3 x 50 (inlet) 1.6 x 50 (outlet)		New design
Third Fixed Mask (FM3)	21.3	16 x 47.8 (inlet) 3.6 x 6 (outlet)		Same as 27-ID
Photon Shutter (PS)	22.4	10 x 47.8 (inlet) 5 x 47.8 (outlet)		Same as 27-ID
Safety Shutter (SS)	22.9	72 x 20	72 x 20 (W)	Reuse FEv1.2
Wall Collimator	23.6 (upstream concrete)	27 x 17	37 x 26 (Pb)	Same as 27-ID
Exit Mask (EM)/XBPM2	25.6	10 x 38 (inlet) 2 x 2 (outlet)		New design
Exit Collimator	26.2	10 x 7	10 x 7 (W)	Same as 27-ID

A retrofit must be performed on the older versions of the HHLFE at locations 26-ID, 27-ID, 29-ID, 30-ID, and 35-ID to place a clearing magnet and have next-generation XBPMs. In these front ends, the photon shutter, safety shutter, some masks, and most shielding components and vacuum pumps can be harvested and reused.

Thermal Analysis There are five high heat load components in the HHLFE subject to the ID beam. They are FM1, FM2, FM3, PS2, and Exit Mask. For the current APS 7 GeV ring, the bench mark heat load is two 3.3 cm period undulators at 10.5-mm gap at 180 mA. For the APS-U ring, the bench mark heat load is two 2.75 cm period undulators at 8.5-mm gap at 200 mA. Two ID sources will be used for the analysis:

1. For initial installation at 7 GeV ring, two 2.4 m long U33 at 180 mA at 10.5-mm gap (k=2.76, N=144, γ=13700)
2. For APS-U ring at 6 GeV, two U27.5 at 200 mA at 8.5 mm gap (k=2.44, N=172, γ=11743)

For each component, the heat load will be calculated as power density distribution and fit into a Gaussian formula and applied to the component. For the FM1 and FM2, the material is GlidCop, the beam center location will simulate the vertical, horizontal, and corner beam missteering, and at these missteering locations, the maximum power is absorbed into the mask's top surface, side surface, and corner, respectively. All calculations used the convective cooling coefficient of 0.015 W/mm^2 ℃ for all the cooling channels. This cooling coefficient is easily achievable with wire coil inserts which induce turbulence in the cooling channel. All APS HHLFE and CUFE components have wire coil inserts to enhance the heat transfer coefficient. The cooling water temperature is 25.6 ℃. The summary of the FM1 thermal analysis data is shown in Table 5.5 and the maximum temperature of beam vertical missteering for APS-U is shown in Figure 5.3.

Table 5.5. Thermal analysis summary of FM1

ID Source	7 GeV U33, k=2.76, N=144, 180 mA			6 GeV U27.5, k=2.44,N=172, 200 mA		
Distance to source	17.0 m			17.0 m		
Total power seen by FM1	21135 Watts			18781 Watts		
Peak normal incidence power density	2071 W/mm^2			1581 W/mm^2		
Beam missteering	*Case 1 vertical*	*Case 2 horizontal*	*Case 3 corner*	*Case 1 vertical*	*Case2 horizontal*	*Case3 corner*
Beam center coordinates [x,y] mm	[0,10.5]	[14.5,0]	[13.9, 9.9]	[0,10.5]	[14.5,0]	[13.9, 9.9]
Beam incidence angle	0.48°	0.86°	Vary	0.48°	0.86°	Vary
Peak incidence power density (W/mm^2)	17.35	31.08	35.41	13.24	23.73	27.03
T_{max} (℃)	300.0	243.1	265.0	240.6	209.4	222.0
T_{wall} (℃)	133.0	85.0	106.8	110.6	77.3	93.8
Max. σ_{vm} (Mpa)	528.5	425.2	571.4	414.5	358.1	471.1

The thermal analysis of FM2 is very similar to the FM1 and the result summary is shown in Table 5.6. The stress plot of the beam corner missteering with APS-U source is shown in Figure 5.4.

As seen from the results table, for the APS-U source at 200 mA, the peak temperature is well below 300℃ under all cases for both FM1 and FM2. For the missteering masks, the stress slightly above the yield stress is not a concern because these missteering cases are very rare and being slightly above yield stress will not affect the component service life.

The FM3 was first designed and installed at 27-ID and 35-ID front end. Thermal analysis was completed at the time of the component design for the APS 7 GeV ring with two U33 at 10.5-

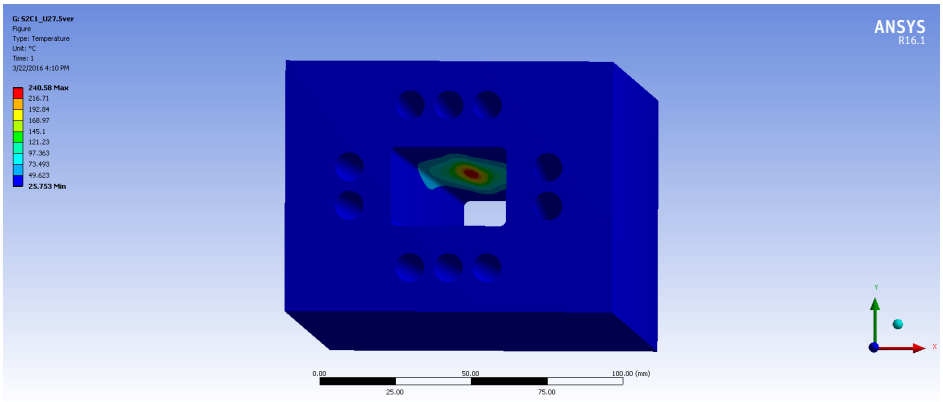

Figure 5.3. FM1 temperature distribution with APS-U source of two U27.5 at 200 mA at vertical beam missteering.

Table 5.6. Thermal analysis summary of FM2

ID Source	7 GeV U33, k=2.76, N=144, 180 mA			6 GeV U27.5, k=2.44,N=172, 200 mA		
Distance to source	17.7 m			17.7 m		
Total power seen by FM2	21280 Watts			18530 Watts		
Peak normal incidence power density	1910 W/mm^2			1469 W/mm^2		
Beam missteering	*Case 1 vertical*	*Case 2 horizontal*	*Case 3 corner*	*Case 1 vertical*	*Case2 horizontal*	*Case3 corner*
Beam center coordinates [x,y] mm	[0,8]	[8.35,0]	[7.7,7.4]	[0,8]	[8.35,0]	[7.7,7.4]
Beam incidence angle	0.48°	0.86°	Vary	0.48°	0.86°	Vary
Peak incidence power density (W/mm^2)	15.33	28.67	29.97	11.79	22.05	23.03
T_{max} (°C)	255.1	222.8	242.6	205.9	188.7	201.6
T_{wall} (°C)	100.1	75.6	96.2	84.5	68.2	83.9
Max. σ_{vm} (Mpa)	448.2	390.8	551.6	353.4	324.9	452.1

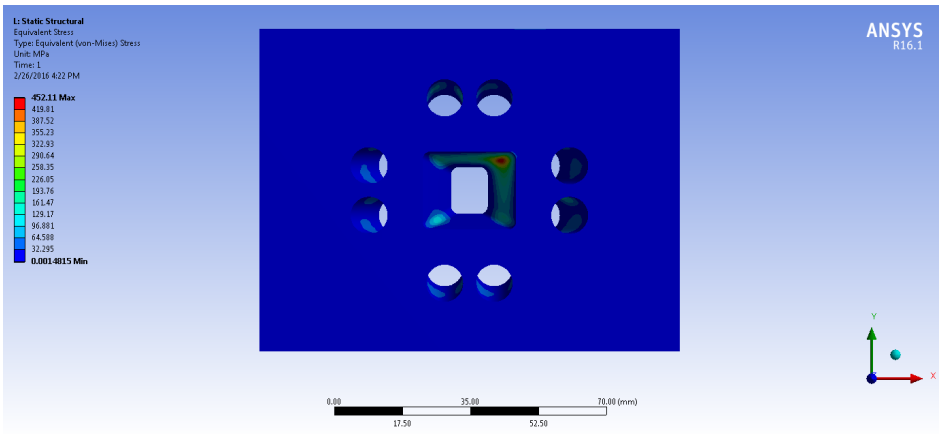

Figure 5.4. FM2 von Mises stress with APS-U source of two U27.5 at 200 mA at beam corner missteering.

mm gap at 180 mA. The thermal analysis report was generated and is in ICMS as APS_1431811. Compared to 27-ID and 35-ID, the FM3 installation location for the new APS-U HHLFE is moved downstream by 1.0 m. It will be at 20.8 m instead of at 19.8 m. There is no need to redo the analysis since the heat load is decreased.

The photon shutter (PS2) was designed in 2004 when the first HHLFE was designed. Thermal analysis was completed at that time for APS 7 GeV ring with two U33 at 10.5-mm gap at 180 mA. This photon shutter is currently installed in five sectors, and the thermal analysis is referenced in the design report in ICMS as APS_1001198. The heat load for APS-U with U27.5 at 200 mA is less than that of APS 7 GeV two U33 at 180 mA. The installation location is the same so there is no need to redo the analysis.

The exit mask is a new component and is now integrated with detectors to function as a XBPM2. The exit mask is made by brazing two GlidCop halves. The taper angle is 1.1° which is the same as all other exit masks. The inlet aperture is 10(H) x 38(V) mm and the exit aperture is 2(H) x 2(V) mm. The detectors are mounted at the side port of the exit mask. Beam intercepted by the inboard side will generate signals to be read by the detector on the outboard side. The top sectional view of the exit mask is shown in Figure 5.5.

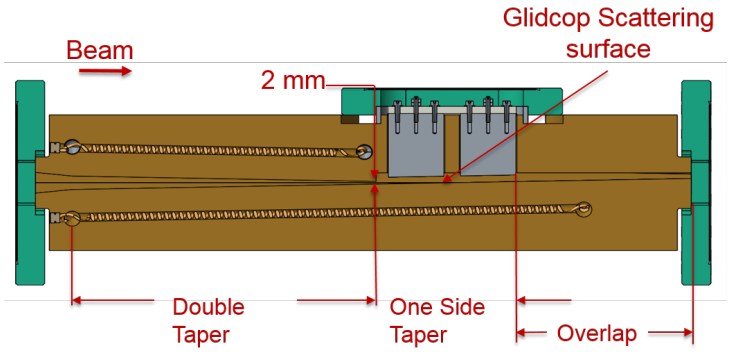

Figure 5.5. Top sectional view of the exit mask at the mid plane.

Two cases are analyzed: one with the beam center at the center of the aperture, allowing the center of the beam to pass through the aperture. This represents the normal operating conditions. The second case is when beam is missteered by [1,1], which places the center of the beam at the corner of the aperture. The results are tabulated in Table 5.7. And the temperature plot is shown in Figure 5.6.

Front End Interfaces The interface to the storage ring and to the beamline will be described in this section. The front end aperture opening must be able to accept a beam missteering envelope of ±1.0 mrad horizontal and ±0.67 mrad vertical as specified in the FReD. The front end FM1 inlet aperture size of 38(H) x 26(V) mm satisfies that requirement.

The front end exit aperture will be 2(H) x 2(V) mm as default. This aperture is sufficient to pass the central cone of the beam. The front end will end with a BIV for windowless beamlines and end with a diamond window for beamlines that require a window.

Table 5.7. Thermal analysis results for exit mask.

ID Source	7 GeV U33, k=2.76, N=144, 180 mA		6 GeV U27.5, k=2.44,N=172, 200 mA	
Distance to source	25.3 m		25.3 m	
Upstream aperture and location	3.6 x 6.0 @ 21.3 m		3.6 x 6.0 @ 21.3 m	
Total power seen by exit mask	10772 Watts		9430 Watts	
Peak normal incidence power density	935 W/mm^2		714 W/mm^2	
Beam missteering	*Case 1 no missteering*	*Case 2 missteering*	*Case 1 no missteering*	*Case2 missteering*
Beam center coordinates [x,y] mm	[0,0]	[1,1]	[0,0]	[1,1]
Beam incidence angle	1.1°(H)	1.1°(H)	1.1°(H)	1.1°(H)
Total power absorbed by the exit mask (W)	8791	11186	8088	9894
Peak incidence power density (W/mm^2)	17.95	17.95	13.70	13.70
T_{max} (°C)	204.0	228.4	177.4	201.1
T_{wall} (°C)	70.0	77.2	63.9	71.4
Max. σ_{vm} (Mpa)	289.7	330.7	247.2	278.7

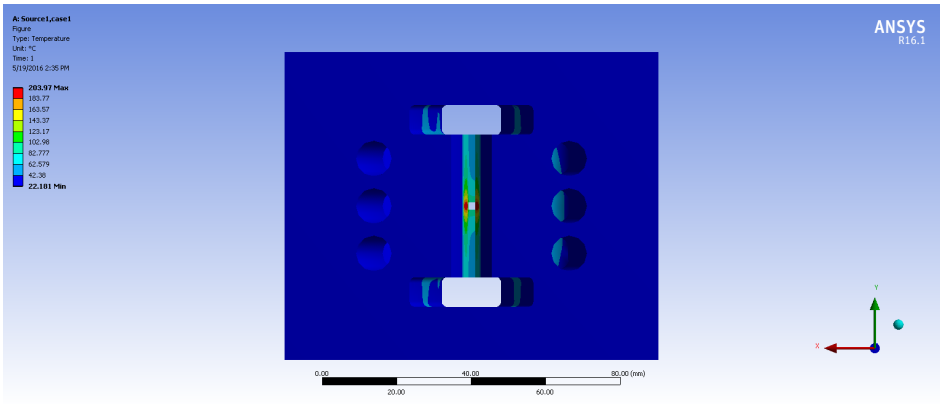

Figure 5.6. Temperature plot of exit mask with APS 7 GeV source when beam is missteered.

The front end vacuum interface to the storage ring will be the slow valve (SV).

The interfaces between the front end and the storage ring are addressed in the front end interface documents. The interfaces to each of the ID beamlines are addressed in the beamline to ID and Front End interface documents.

5-2.3.4 Canted Undulators Front End(CUFE)

The CUFE is designed to deliver two undulator beams with 1.0 mrad angle between them in the horizontal plane. Similar to the HHLFE, the new CUFE for APS-U must have a clearing magnet as far upstream as possible to deflect the electrons away from the safety shutter's aperture in the event the electrons enter the front end during the swap out injection. In addition, it must have the next generation XBPM system. The requirements and the design of the NG XBPM system and the clearing magnet are discussed later in Sections 5-2.4 and 5-2.5. The aperture size and location of the masks are determined by the need to protect the clearing magnet from synchrotron beam strikes and to provide adequate aperturing for the NG-XBPM. For the thermal design, the existing CUFE masks and photon shutters meets the thermal design criteria of the APS-U for nearly all anticipated undulators. There are currently seven existing canted undulator front ends installed at the APS. They are at locations 12-ID, 13-ID, 16-ID, 21-ID, 23-ID, 24-ID, and 34-ID. The plan is to use most of the existing component designs; however, if a mask needs to be redesigned it will have the same thermal handling capacity as the existing components. The CUFE design layout is shown in Figure 5.7.

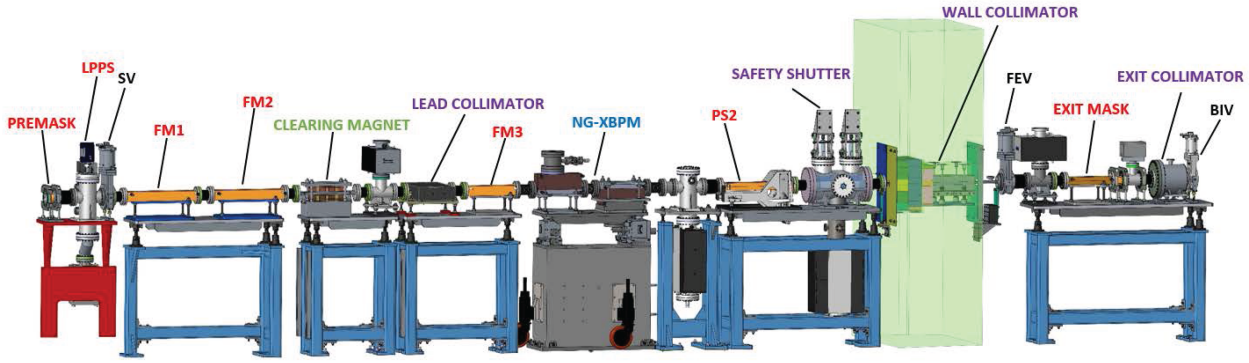

Figure 5.7. Canted undulator front end with next-generation XBPMs and clearing magnet.

The FM1 and FM2 use existing design, and the aperture contains both the beams from the two canted undulator sources. The FM2 has an exit aperture of 26(H) x 5(V) mm and will be used to protect the clearing magnet. Due to the large horizontal aperture and small vertical aperture of FM2, the clearing magnet is orientated to use the vertical plane for the magnet gap and bend the beam inboard. The schematic of the clearing magnet is shown in Figure 5.26 for the required deflection angle. The FM3 is a splitter mask, and it has dual apertures separated by 1.0 mrad to ensure that the XBPM design has the maximum flexibility to prevent beam cross talking. The photon shutter and safety shutter are existing designs. For the next generation XBPM two possible options are in the process of being explored. Figure 5.7 shows a GRID-XBPM similar to the HHLFE but rotated 90° with detectors on top and bottom. The other option currently under R&D is based on Compton scattering and is discussed in Section 5-2.4.5. Compton XBPM is more compact in space than the GRID-XBPM. The space reserved in the layout is sufficient for both the GRID-XBPM and the Compton XBPM.

The benchmark heat load for the canted APS-U front end is equivalent to the heat load from two 2.1 m long, 2.75 cm period undulators with 8.5-mm gaps, operating at 6 GeV and 200 mA at 1.0 mrad canting angle. This heat load is less than the heat load of two 2.1 m long 3.3 cm period undulator A's at 10.5-mm gap at 200 mA in the 7 GeV ring, which the original CUFE was designed

for. Therefore, all of the photon components designed for the existing CUFE will work for the future APS-U storage ring. The new masks are also designed to the same standards.

Similar to the HHLFE, the existing CUFEs at locations 12-ID, 13-ID, 16-ID, 21-ID, 23-ID, 24-ID, and 34-ID must be retrofitted to replace the photo emission style XBPMs with next-generation XBPMs and the clearing magnet. Components such as photon shutters, safety shutters, some masks, and all shielding components, some vacuum pumps, and valves can be harvested and reused.

The CUFE components description from upstream to downstream as follows:

1. Low Power Photon Shutter (LPPS). The function of the LPPS is to protect the slow valve immediately downstream from the dipole. The LPPS cannot withstand the heat load from the ID source and when LPPS is closed, the ID gap must be open. The LPPS is an existing APS design and is the same as used in HHLFE and is currently installed and operating in 27-ID and 35-ID.
2. Slow Valve (SV). The function of the SV is to isolate the front end vacuum from the storage ring vacuum in case there are front end faults during operation. When the SV is commanded to close, it will dump the stored beam followed by the closure of the LPPS. The storage ring can resume operation only when the ID gap is verified to be at open position and the LPPS is closed. The slow valve and LPPS can be used to isolate the front end from the storage ring and will allow for operation of the storage ring with the ID gap open.
3. Premask. The function of the premask is to protect the stainless steel flange of FM1 from the dipole radiation. The premask has an aperture of 62(H) x 26(V) mm to allow the ID beam to pass. The horizontal aperture of the premask is smaller than the FM1 horizontal aperture. This premask is a new design due to the existing premask has an asymmetric aperture.
4. First Fixed Mask (FM1). This is an existing design. The FM1 is a missteering mask. Under normal operating condition, the beam will pass right through without touching the mask. FM1 aperture allows both beams to pass through. The inlet aperture of the FM1 is 64(H) x 26(V) mm which is sufficient to accept a beam missteering cone of $\pm$1.67(H) x 0.67(V) mrad. The exit aperture is 40(H) x 14(V) mm.
5. Second Fixed Mask (FM2). This is an existing design. FM2 aperture allows both beams to pass through. The FM2 exit aperture is 26(H) x 5(V) mm. The vertical aperture of 5 mm will be used to protect the clearing magnet.
6. Clearing Magnet (CM). The clearing magnet is a device with a rectangular vacuum chamber of 40(H) x 9(V) mm optical aperture. The magnets are on the top and bottom side of the chamber. It has an 16-mm vertical magnetic gap. The magnetic field can bend the electron beam 13.5 mrad towards the inboard. There is a magnetic shield around the clearing magnet to prevent it from interfering with the nearby storage ring magnets. The CM will be discussed later in detail in Section 5-2.5.
7. Pump support chamber. The only purpose of this chamber is to support a vacuum pump and allow mounting of vacuum gauges to the chamber. This configuration use the least amount of space along the beam to mount the large size pump. This pump is needed to pump out FM1, FM2 and clearing magnet.
8. Lead Collimator. This is a shielding component and is an existing design. Its construction consists of a rectangular vacuum tube surrounded by lead. The optical aperture is the tube's ID and the aperture is designed so that it can pass the maximum missteered synchrotron beam with at least a 3.0-mm clearance. The lead aperture is the shielding aperture. It has a

40(H) x 16(V) mm optical aperture and 46(H) x 22(V) mm shielding aperture.

9. Third Fixed Mask (FM3). This mask is a new design. It is a splitter mask,and has dual aperture that is one mrad apart. The mask must be installed at the exact location in order to function properly. If for some reason the canting magnet does not separate the beams by 1.0 mrad, the beam will be absorbed by the FM3. The FM3 provides thermal protection to the PS2 and exit mask. It also offers flexibility to the XBPM design. The FM3 beam splitter will allow a divider to be installed in the XBPM to prevent cross talk without the divider being exposed to the synchrotron beam. The vertical aperture of the FM3 must be 4 mm or less in order to reuse the existing PS2 and exit mask. The horizontal aperture is flexible and the current choice is dual 8x4 mm to allow the maximum beam pass.
10. NG-XBPM. This is a space holder at this time. The downselection of the XBPM for the canted undulator front end will be made after the completion of the R& D. The XBPM will be discussed later in Section 5-2.4.
11. Pump Chamber. The function of this chamber is to mount a vacuum pump and may be used to house intensity monitor detectors. The vacuum pump is required to pump the section between the XBPM and the PS2.
12. Photon Shutter2 (PS2). This is an existing design. The photon shutter pivots down to close.
13. Safety Shutter. This is an existing design. However, a small modification is needed to have four closed switch mounted on the shutters.
14. Wall Collimator. This is an existing design. There are seven such wall collimators installed at the APS. The wall collimator consists of a rectangular vacuum tube surrounded by lead. The optical aperture is the vacuum chamber's internal aperture and the shield aperture is the nominal lead aperture.
15. Front End Valve (FEV). This valve isolates the front end components inside the ratchet wall from the components outside the ratchet wall. Any vacuum fault downstream of this valve will trigger the FEV to close.
16. Pump Chamber. This pump chamber was designed to house XBPM2 detectors. The decision whether to integrate the exit mask with the XBPM2 detector has not been made. The assumption is the fluorescence generated by the exit mask will be used by detectors inside this pump chamber.
17. Exit mask. This is an existing design. This mask is a splitter mask, and it has dual exit aperture of 3x2 mm and is 1.0 mrad apart.
18. Pump chamber. This is an existing design and supports the vacuum pump.
19. Tungsten Collimator. This is a shielding component. This is a new design because the existing design uses tungsten and lead combination and is difficult to fabricate and takes much space along the beam. This is an in-vacuum tungsten design. It has a dual exit aperture of 7x6 mm.
20. Beamline isolation valve (BIV). BIV is used to isolate front end vacuum from the beamline vacuum for windowless beamlines. For a beamline with a window, the beamline will terminate with the Be window or diamond window.

The APS-U CUFE aperture table is shown in Table 5.8.

Table 5.8. APS-U CUFE Components Aperture Table

APS-U CUFE Components	Distance to center of straight section (m)	Aperture Optical H (mm) x V (mm)	Shielding Aperture H (mm) x V (mm)	Comments
Premask	16.5	62 x 26		New design
First Fixed Mask (FM1)	17.3	64 x 26 (inlet) 40 x 14 (outlet)		Existing design
Second Fixed Mask (FM2)	18.0	46 x 17 (inlet) 26 x 5 (outlet)		Existing design
Clearing Magnet (CM)	18.6	40 x 9 (magnet gap)	∞ x 16	New design
Lead Collimator	19.3	40 x 16	46 x 22 (Pb)	Existing design
Third Fixed Mask (FM3)	20.2	50 x 10 (inlet) Dual 8 x 4 (outlet)		New design
NG-XBPM	20.9	TBD		New design
Photon Shutter (PS)	22.7	50 x 10 (inlet) 50 x 5 (outlet)		Existing design
Safety Shutter (SS)	23.1	50 x 16	50 x 16 (W)	Existing design
Wall Collimator	23.5 (upstream concrete)	47.6 x 16.8	56 x 26 (Pb)	Existing design
Exit Mask (EM)	25.6	50 x 9 (inlet) Dual 3 x 2 (outlet)		Existing design
Exit Collimator	26.1	Dual 7 x 6	Dual 7 x 6 (W)	Existing design

5-2.3.5 BM Front End

There are a total of 23 BM front ends at the APS. All of them, except for the three front ends at 11-BM, 23-BM, and 24-BM, are the original BM front ends, as shown in Figure 5.8. The BM front ends at 11-BM, 23-BM, and 24-BM are a newer style and were designed in 2003. Many components in the newer BM front ends have been redesigned to make them more compact, and the locations and apertures of masks are different compared to those of the original front ends. Currently three locations at 15-BM, 18-BM, and 34-BM have front ends but no beamlines. The initial plan is to upgrade the original 20 front ends for the 20 beamlines and use the newer BM front ends for future BM beamlines.

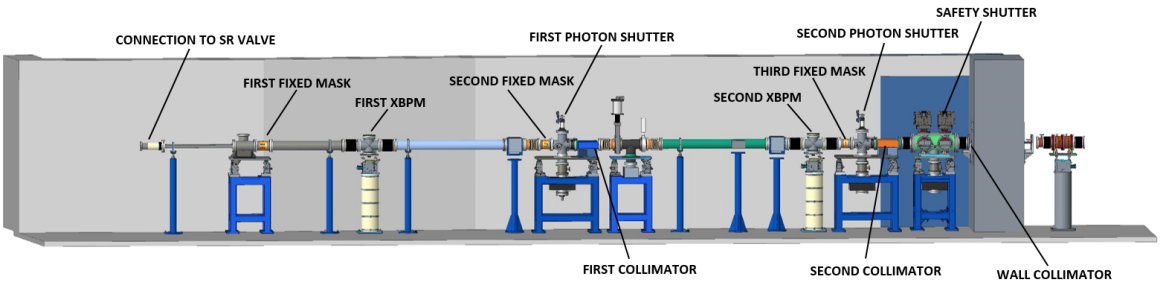

Figure 5.8. APS original BM front end layout.

The original BM front ends were designed for the 7 GeV machine operating at 300 mA. Most BM front ends terminate in double beryllium windows and allow a 6-mrad horizontal fan of BM radiation to pass through the front end. For the APS-U, at the time of CDR, a 3 pole wiggler (3PW) was considered to be the BM source. Based on the space and the usability of the 3PW radiation, the planned use of the 3PW has been dropped. So the bending magnet beamline source for the APS-U will be a combination of M3, Q8, and M4, as shown in Figure 5.9.

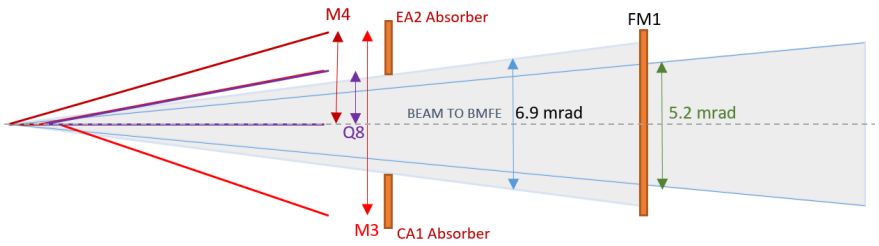

Figure 5.9. APS-U bending magnet sources.

Compared to the APS 7 GeV BM sources, the APS-U BM source point has shifted upstream by 2.929 m and the centerline of the BM front end will be shifted inboard by 43.6 mm. The heat load comparison of the new source versus the original 7 GeV source is tabulated in Table 5.9.

As shown in Table 5.9, both the total power and peak power density for the APS-U are less than those of the current 7 GeV dipoles. The existing BM front end can handle the combined heat load from M4+M3+Q8. No thermal analysis is necessary for the existing masks and shutters.

The plan to upgrade the APS BM front end is to fit a clearing magnet in as far upstream a position

Table 5.9. Comparison of heat load of APS 7 GeV dipole BM with APS-U BM sources

Parameters	**APS Now**	**APS-U**	**APS-U**	**APS-U**	**APS-U**
Magnets	*BM Dipole*	*M4 upstream*	*M3 downstream*	*Q8*	*M4+M3+Q8 (outboard) M3 (inboard)*
Machine energy (GeV)	7	6	6	6	6
Ring current (mA)	300	200	200	200	200
Critical energy (keV)	19.6	15.872	16.232	4.357	N/A
Peak field (T)	0.6	0.663	0.678	0.182	N/A
Total power per mrad horizontal fan (W)	260.5				239
Total power entering front end (W)	1860 (7.1 mrad)	315	322	86	1045 (723 outboard) (322 inboard)
Peak power density (kW/mrad^2)	2.342	0.937	0.958	0.256	2.151

as possible while preserving the current layout. The two photo emission XBPMs are planned to be used as is, mechanically, and only upgrade the XBPM electronics. The clearing magnet location is planned to be just downstream of the FM1. The existing FM1, which has a very large vertical aperture of 18 mm, will be replaced by a new design with a 4-mm vertical aperture with the same length as the original FM1. The inlet aperture of the new FM1 will remain the same as the existing FM1 and the exit aperture will change from 60(H) x 18(V) mm to 60(H) x 4(V) mm. The new FM1 design and thermal analysis will be discussed next. The wall collimator will be replaced due to the horizontal shift and there is a plan to replace the original lead shots with lead bricks. The rest of the BM components will remain the same and will be harvested and reinstalled at the installation shut down. The BM front end will retain the storage ring exit valve (SRV) and operate with the current EPS and PSS logic with two photon shutters and two safety shutters. The shift of the BM source point upstream by 2.929 m and the the fixed mask apertures remaining the same, the fan that passes through the BM front end will be 5.2 mrad instead of 6.0 mrad in the original design. The new BMFE layout with the clearing magnet is shown in Figure 5.10. The clearing magnet specification will be discussed later in Section 5-2.5 The BMFE aperture table is shown in Table 5.10.

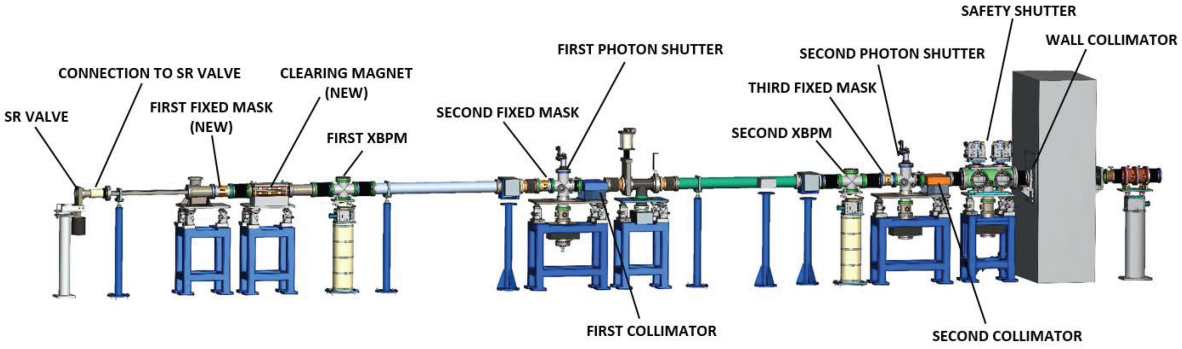

Figure 5.10. The APS-U BM front end layout. The clearing magnet is added and the FM1 is replaced with a new design.

For the description of the existing BM components, refer TB-5 Functional Description of APS

Table 5.10. APS-U BM front end aperture table

Component	Distance from Source [m]	Optical Aperture [mm x mm]	Shielding Aperture [mm x mm]	Comments
First Fixed Mask (FM1)	12.2	129 x 30 (inlet) 60 x 4 (outlet)		New design
Clearing Magnet(CM)	12.8	73 x 10		New design
XBPM1	13.9	90 x 24		Reuse
Second Fixed Mask (FM2)	16.7	110 x 36 (inlet) 84 x 12 (outlet)		Reuse
Photon Shutter (PS1)	17.0	124 x 22		Reuse
First Collimator	17.3	92 x 20	98 x 27 (Pb)	Reuse
XBPM2	20.9	125 x 18		Reuse
Third Fixed Mask (FM3)	21.5	125 x 20 (inlet) 111 x 5 (outlet)		Reuse
Photon Shutter (PS2)	21.8	124 x 22		Reuse
Second Collimator	22.1	122 x 20	129 x 27 (Pb)	Reuse
Safety Shutter (SS)	22.9	132 x 20	132 x 20 (W)	Reuse
Wall Collimator	23.5 (upstream wall)	138 x 20	145 x 26 (Pb)	Existing design
Be window	24.9	145 x 12		Reuse

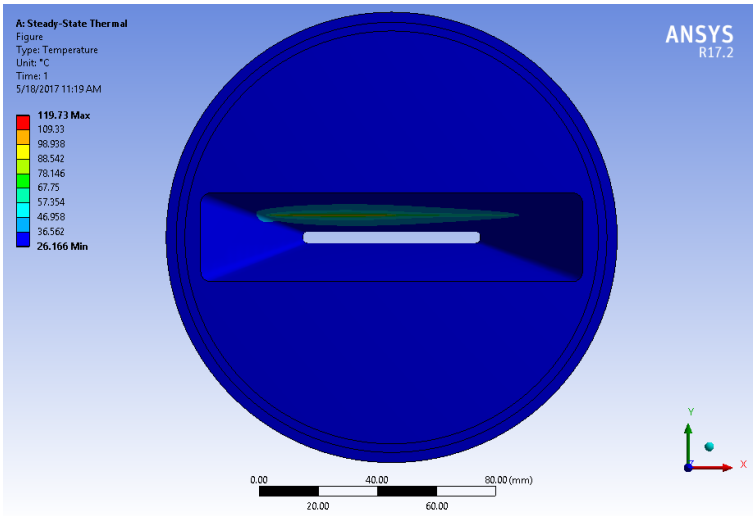

Figure 5.11. New APS-U FM1 temperature plot (distance from source 12.08 m, total power 1324 Watts).

Beamline Front Ends.

The new FM1 is made from OFHC copper with an inlet aperture of 129(H) x 30(V) mm and 60(H) x 4(V) mm exit. It intercepts a total of 6.9 mrad horizontal fan with M4+M3+Q8 in the outboard and M3 in the inboard. The maximum temperature is shown in Figure 5.11.

5-2.4 X-ray Beam Position Monitors

The x-ray beam position monitor (XBPM) plays an important role in maintaining the angular stability of the x-ray beams entering the user beamline. The XBPM fills a significant blind spot left by the RFBPM: the field error steers the electron trajectory inside the undulators, making the x-ray beam axis different from the straight line defined by the RFBPMs outside of the undulator. Furthermore, the temperature change and ground motion of the ring will move the storage ring chamber and the RFBPMs around, dragging the x-ray beam along with them. The XBPM monitors beam motion at locations near the user beamline and enables the long-term x-ray beam stability to be maintained.

5-2.4.1 Technical Specifications

Table 5.11 lists the e-beam stability requirements for the APS-U (see Chapter 4, Section 4.3.8.5, Beam-Size Monitors). In the most favorable case, beam motion in position and angle is uncorrelated, and the x-ray beam motion is derived at the first XBPM, 20 m from the source (Table 5.12). If the requirements are partitioned equally between the feedback system and the position detectors, the derived resolution requirements for the XBPM are listed in the last two columns of Table 5.12.

*Table 5.11. Beam stability requirements for APS-U lattice (RMS)**

	AC motion (0.01–1000 Hz)		**Long-term drift (7 days)**	
	Position (μm)	**Angle (μrad)**	**Position (μm)**	**Angle (μrad)**
Horizontal	1.7	0.25	1	0.6
Vertical	0.4	0.17	1	0.5

* Beam stability requirements are based on 10% of beam sizes.

Table 5.12. Beam stability requirements at the XBPM (Z = 20.0 m)

	Total beam motion (μm)		**XBPM resolution specifications* (μm)**	
	AC	**Long-term**	**AC**	**Long-term**
Horizontal	4.9	11.1	3.5	7.9
Vertical	3.2	9.3	2.2	6.6

* XBPM resolution is 70% of the beam stability requirement.

5-2.4.2 Rationale for Next-Generation X-ray Beam Position Monitors

At first glance, sub-micron resolution RFBPMs should be able to stabilize the e-beam source in both the position and angle, as specified in Table 5.11. However, because of imperfections in the undulator field, especially in the end sections, the e-beam position at the two end points of the ID chamber is not a very reliable measurement of x-ray beam position and angle. Figure 5.12 shows the calculated electron trajectory through a typical APS undulator, based on magnetic measurement data. The x-ray beam source location and angle differ from those predicted by the electron beam measurements (at the location of the RFBPM) by about 10 μm in position and 5 μrad in angle for the horizontal plane. To make the situation worse, as a function of the undulator gap, the vertical plane behaves similar to the horizontal plane. The bottom panel of Figure 5.13 shows measurements

performed with two undulators in 29-ID, closing their gaps one at a time. When the RFBPMs are used to control e-beam positions, steering by the two undulators causes the monochromatic beam positions to differ by 100+ μm at the beamline slits, 25 m from the source. The top panel of Figure 5.13 shows the same measurements, however using the GRID XBPM to to position the electron beam.

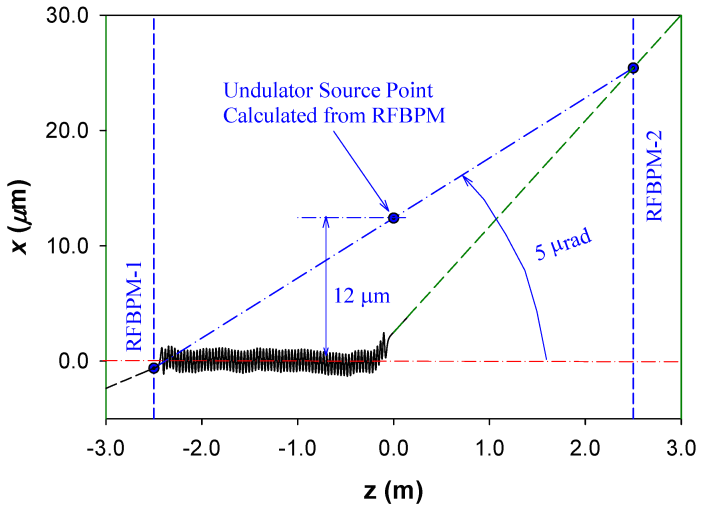

Figure 5.12. Electron trajectory in an APS undulator based on magnetic measurement data.

While periodic measurements of undulator steering could be used to partially compensate for steering effects, an XBPM capable of monitoring the hard x-ray beam position in real time provides the most direct solution to the problem, since it not only provides a uniform solution to reduce gap-dependent beam motion for all beamlines, it also monitors x-ray beam motion in real time, regardless of the source of the disturbance.

The most challenging issue facing the XBPM design is the conflict between the high undulator power (10's kW) and the micrometer precision requirements. In the APS-U front ends, different power levels require us to use different XBPM designs. While the bend magnet (BM) front ends will use an existing XBPM without modification, all ID front ends will require a next generation XBPM: the canted undulator front ends (CUFE) XBPM will use a compact design based on x-ray scattering from diamond blades; and the high heat load front ends (HHLFE) will use x-ray fluorescence (XRF) from the GlidCop absorbers to withstand the highest power density in the ring.

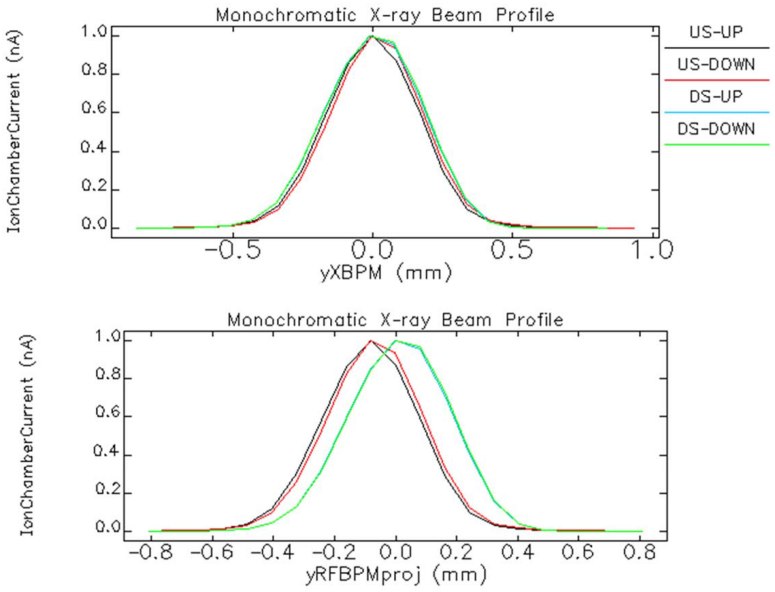

Figure 5.13. (Bottom) Monochromatic beam intensity through the beamline entrance slits of the upstream and downstream undulators, respectively, when the e-beam scans across the entrance slits, controlled by the RFBPM. (Top) Same as bottom but the e-beam scans were controlled by the GRID-XBPM.

5-2.4.3 Bending Magnet XBPM

The first-generation XBPMs in the APS were based on photoemission from blades insulated from the ground. Figure 5.14 shows the copper holder of the blades, which is mounted on a water-cooled platform. Since the BM radiation has a stable spatial spectral distribution and is the only beam in the front end, the photoemission XBPM works well for the vertical beam angle measurements. We plan to reuse these XBPMs in the APS-U BM front ends. No major redesign has been planned.

A relatively minor change will be made to the BM XBPM for the APS Upgrade due to the presence of multiple synchrotron radiation sources in the BM port: M4, Q8, and M3. While all these sources can be seen on the outboard side of the BM axis, only M3 is visible on the inboard side. It is thus desirable to position the XBPM blade on the inboard side of the BM port axis, either through modification of the blade mount or a simple displacement of the XBPM chamber.

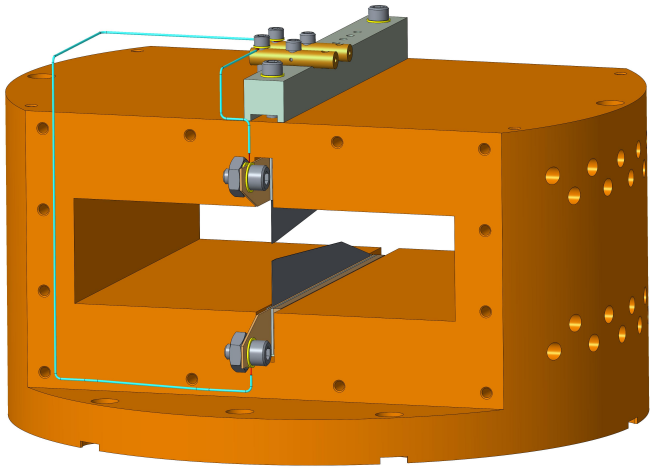

Figure 5.14. Photoemission blade holder of the BM front end XBPM.

5-2.4.4 High Heat Load Front End XBPM

The first generation ID XBPM in the APS was based on photoemission from gold-coated diamond blades, which are more sensitive to low-energy x-rays generated copiously by the main dipoles, as well as steering magnets and focusing quadrupoles [5]. This resulted in a very strong undulator-gap-dependent XBPM offset. Implementation of Decker distortion of the lattice in 2000 reduced these background signals by an order of magnitude, and reduced gap-dependent XBPM offsets from hundreds of microns to about 100 microns. Implementation of software compensation further reduced the offset to tens of microns, but the offsets are still short of the APS-U requirements shown in Table 5.12.

Next generation XBPMs should satisfy the following requirements:

- They should use hard x-ray signals to improve signal-to-background ratio;
- They should be able to handle the onslaught of full undulator beams; and
- They should meet the resolution requirements in Table 5.12.

A new, hard x-ray BPM has been developed for the HHLFE. It is based on x-ray fluorescence (XRF) signals from a copper absorber receiving the undulator beam in grazing-incidence (GRID-XBPM) [6, 7]. The top panel of Figure 5.13 shows test data of a prototype at 29-ID, demonstrating that the position measurements of the XBPM agree with that of the monochromatic x-ray beam by the beamline. The first HHLFE with integrated GRID-XBPM was installed in May 2014 in 27-ID and 35-ID front ends. The unit in 27-ID was integrated into the orbit control system in July 2015, and has operated continuously since. No weekly calibration is needed like other, first-generation XBPMs. No significant changes in calibration were noticed in the periodic checks approximately three times a year.

In Figure 5.15, the three-dimensional (3D) model of the new GRID-XBPM is shown on the left and a photo of the installed assembly is shown on the right. It uses two vertical GlidCop absorbers to intercept the unused wing of the white undulator beam and two pinhole-camera arrangements to read out the position of the Cu-K edge XRF footprint left by the intercepted beam. The readout detectors use silicon PIN diodes in combination with stainless steel screens to down-convert the x-ray intensity. Figure 5.16 shows the undulator signal-to-BM background ratio of 27-ID GRID-XBPM as a function of undulator gap, along with those of the legacy APS photoemission XBPMs. For the same undulator source, the bend magnet background is suppressed 30-fold with hard x-ray XBPM.

In Figure 5.17, we show the GRID-XBPM data from eight weeks of user operations. In the first week, the GRID-XBPM is not in the feedback loop. The beam positions in both planes move outside the APS-U specification denoted by the horizontal red lines. After the XBPM is included in the feedback loop, the beam position stayed well within the APS-U specification. The slight dependence on stored current, within 2 μm in the horizontal plane and 1 μm in the vertical plane, can be seen in the 324 bunch non top-up operations (black traces), when the beam is filled twice daily from ~90 mA to 102 mA. The recovery of beam positions within 5μm after each machine study period can be seen by the segments of straight lines occurring about once a week.

These performance data show that we have a sound GRID-XBPM baseline design for the HHLFE.

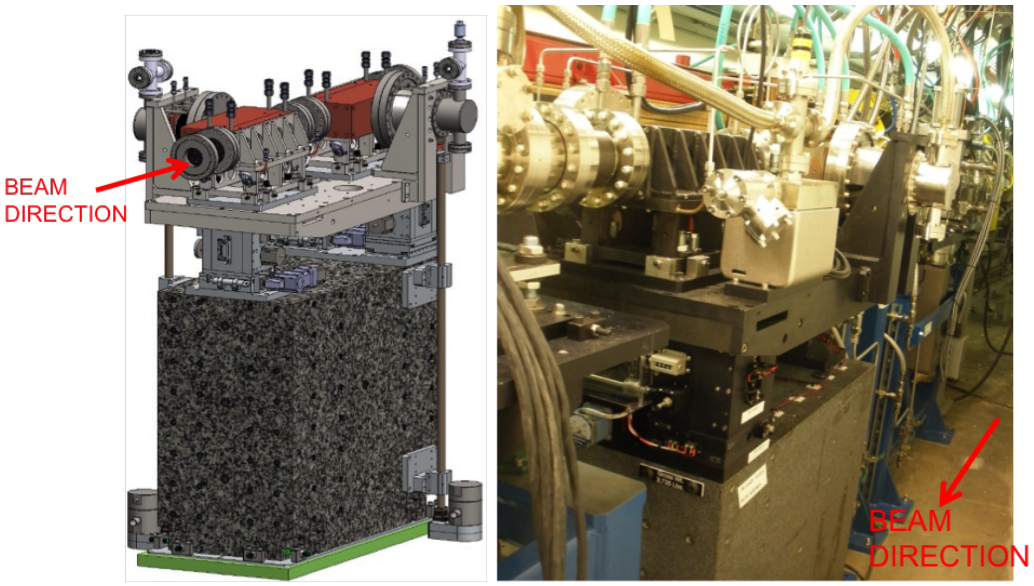

Figure 5.15. (Left) Three-dimensional model of the GRID-XBPM for the HHLFE. (Right) GRID-XBPM installed in the HHLFE.

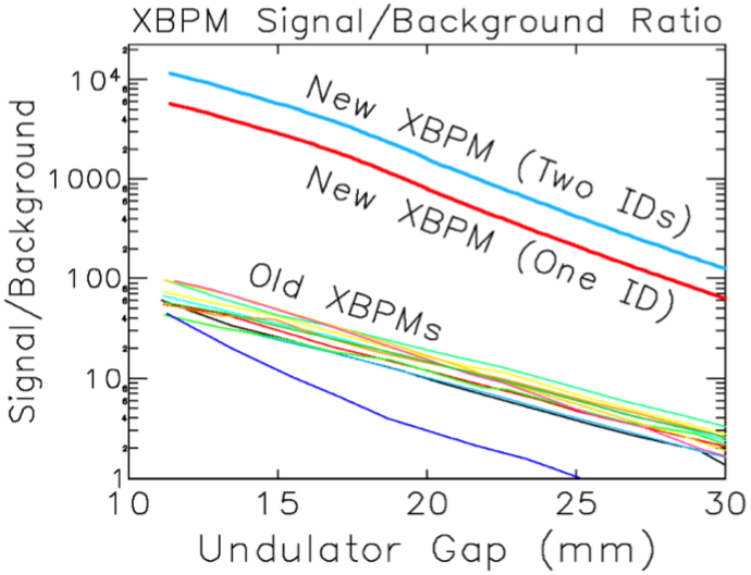

Figure 5.16. Measured undulator beam signal-to-bend magnet background ratio of the 27-ID GRID-XBPM as a function of undulator gap. Compared to the legacy APS photoemission XBPM, the new XBPM demonstrates significant improvement.

However, further improvements are still required to deal with the increased bending magnet background radiation in the APS-U 41-pm lattice.

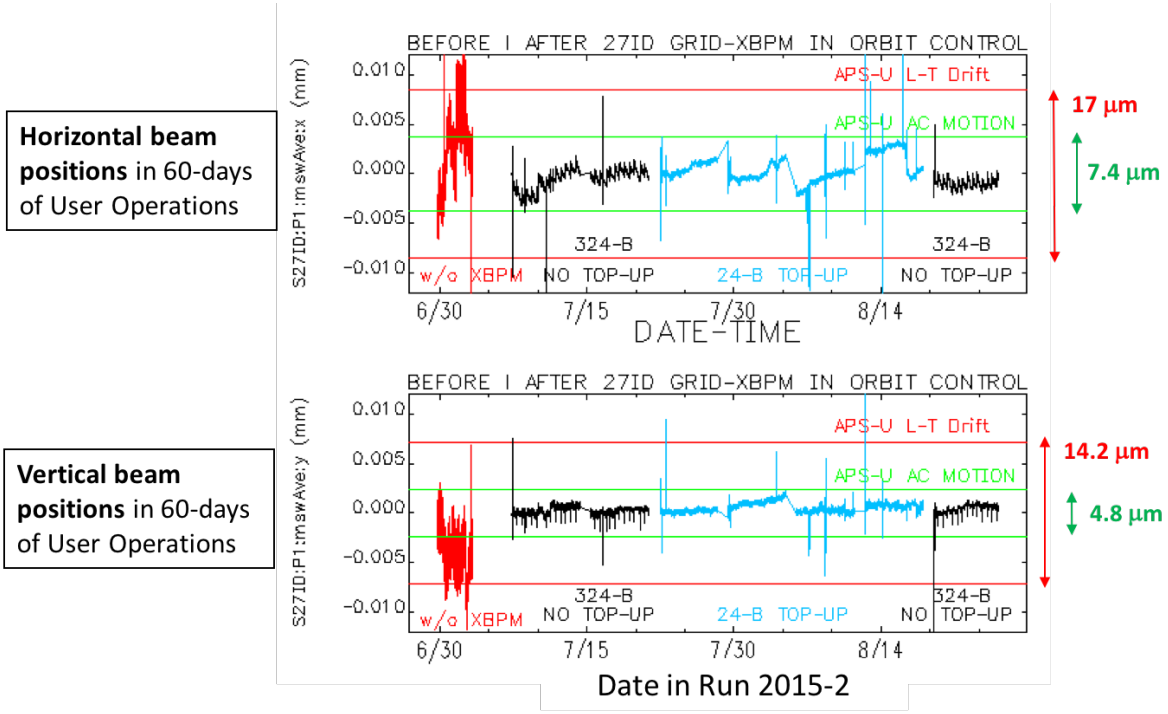

Figure 5.17. GRID-XBPM position data in seven weeks user operation show that the 27-ID beam met the APS-U angular stability requirements.

5-2.4.5 Canted Undulator Front End XBPM

For the CUFE, each device delivers only half of the power in the HHLFE. We have developed a new XBPM based on x-ray scattering from diamond blades in normal incidence. Figure 5.18 shows a prototype design compatible with the existing XBPM platform. The XBPM uses two diamond blades with ∼3 mm vertical spacing to scrape the undulator beam from above and below. Two pairs of collimators distribute the scattered x-ray photons proportionally to the horizontal beam position on the opposing blades; and four YAG/Si-PIN photodiodes read out the flux of the scattered x-ray signal at the end of the collimators. During spring 2017, the prototype has been tested during the weekly machine study period. The highlights from these tests include:

- The principles of operation have been successfully demonstrated in both planes within the limited aperture of the front end Exit Mask.
- The vertical calibration factor is in the range of 0.15 - 0.30 mm, and the horizontal calibration factor is in the range of 3 - 5 mm, both depending on the undulator gaps. These ranges are narrower than that of the horizontal calibration factor for the GRID-XBPM.

A full test is scheduled to commence in June 2017 for the full-width, full-power undulator beam. Assuming a successful outcome of this final test, we will install two Compton XBPMs in each CU front ends.

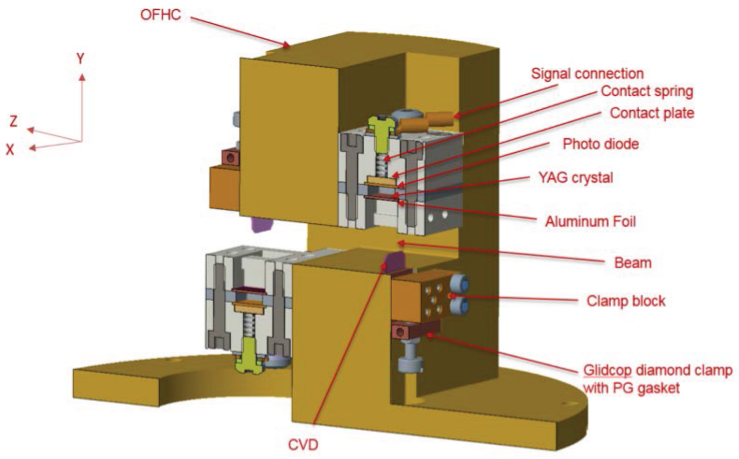

Figure 5.18. Component view of the Compton XBPM.

5-2.5 Clearing Magnets

The APS-U will be operating the storage ring with regular swap-out injection as frequently as every 5 seconds. During these injections, the beamlines will be operating with the shutters open, and, as part of radiation safety, no electrons are allowed to exit the storage ring enclosure. Therefore, as part of the beamline, a passive device located inside the storage ring tunnel will be employed to ensure that the electrons cannot exit the storage ring enclosure.

A permanent magnet dipole (Clearing Magnet) will be located in the front end (part of the beamline between the storage ring exit and the concrete shield wall towards the beamline) to deflect any electrons escaping the storage ring and to prevent them from exiting through the front end apertures and on to the experiment floor.

5-2.5.1 Clearing Magnets for HHLFE

Figure 5.19 is a schematic representation of a possible electron particle trajectory through a clearing magnet in the high heat load front end. The safety shutter is the last shielding component in the front end inside the shield wall of the storage ring. When the safety shutter is open, electron particles are not allowed to exit through the opening in the shutter. A clearing magnet is located 4 m upstream of the safety shutter and is immediately after a fixed mask FM2. Based on the geometry of the front end and the location of the clearing magnet, the requirements for the clearing magnet are shown in Table 5.13.

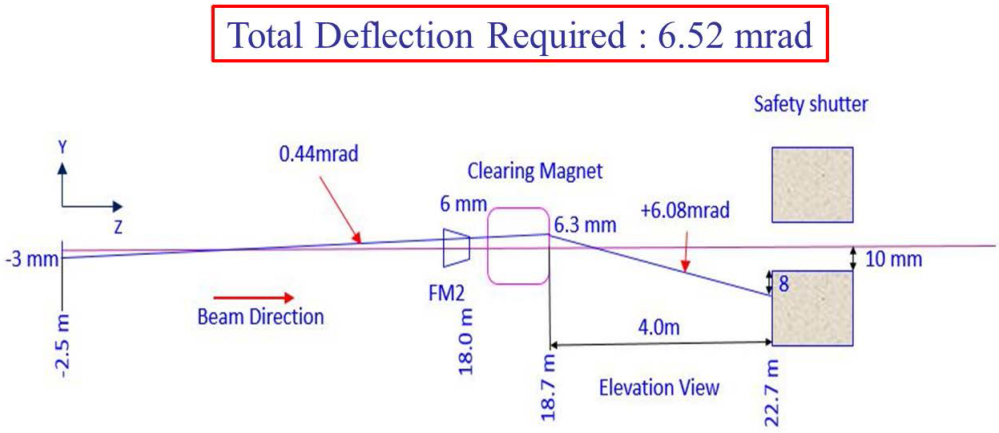

Figure 5.19. Schematic diagram of a electron particle trajectory through a clearing magnet in the high heat load front end.

A permanent magnet (PM) dipole was designed to produce a field of about 1T for a magnetic gap of 1.8 cm. An H-shaped hybrid PM dipole, that creates a B_x field, was designed with Opera 3D as shown in Figure 5.20. The beam direction is along the Z-axis and the magnetic gap of 1.8 cm is along the X-axis. For this reference design, the magnetic material of choice is NdFeB in grade N42SH, from Shin-Etsu Rare Earth Magnet, and the pole material is 1010 steel (soft iron). The N42SH has the following properties: B_r=1.26T (25°C) and intrinsic demagnetization field, H_{cj} = 20.5 kOe.

To minimize shunting of the magnetic field, the shields were placed as far from the magnetic structure

Table 5.13. Requirements for HHL front end clearing magnet

Parameter	Value	Unit
Ring Energy	6.6	GeV
Deflecting Angle	6.52	mrad
Gap	1.8	cm
Insertion Length	30	cm
Deflecting direction (electron beam)	Toward floor	–
Deflecting height at the safety shutter	≥ 2.0	cm
Distance of the safety shutter from the clearing magnet	400	cm
Deflecting range in vertical (Y)	± 0.6	cm
Field at 20 cm from the magnet center	≤ 1	G

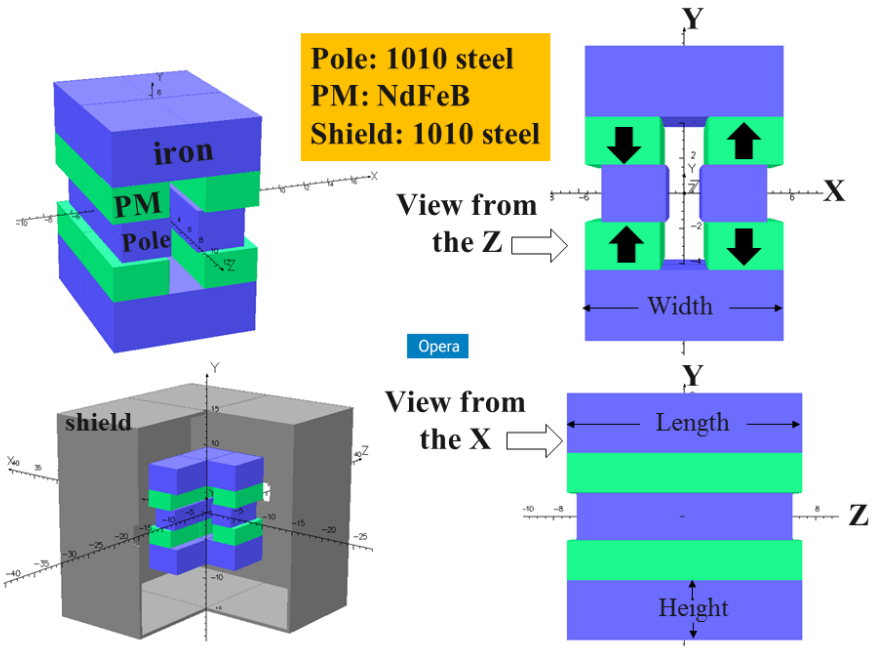

Figure 5.20. Different views of the clearing magnet. The blue colored parts are 1010 steel, the green colored parts are PMs, and the grey is 1010 steel for the shield. The arrows depict the magnetic moment orientation.

as reasonably possible, based on the space constraints within the front end. The shield keeps the stray fields fully contained, as there are other storage ring magnets in close proximity, and also provides personnel safety. The magnets are recessed 0.3 cm back from the pole tips as shown in the right top image in Figure 5.20. The magnets are 1.25 cm thick. The thickness of the iron parts on the top and bottom is 3.75 cm. A 0.5 cm thick shield was placed 7.75 cm away from the magnet to contain all stray fields for safety. The design parameters of the magnets are shown in Table 5.14. Figure 5.21 shows the trajectories of the 6.6 GeV electron beam at 3 different Y locations as it passes through the clearing magnet. The outgoing angle, α, was defined as the trajectory at the zero field region (Z=20 cm) at the downstream end of the clearing magnet. The outgoing angle of the electron beam is -6.77 mrad at the beam mid-plane (Y = X= 0). As seen in Figure 5.21, the worst case for Y at 0.6 cm is -6.68 mrad, which is more than the required 6.52 mrad, as shown in Table 5.13.

Table 5.14. Design parameters of the magnets for the HHLFE clearing magnet

Parameter	Value	Unit
Peak Field, Bx	10082	G
Magnetic force in YZ-plane at X=0	3859	N
Absolute maximum demagnetization fields on PMs at 25℃	9.95	kOe
Maximum field, B, at ±20 cm in Y from the center of the gap	0.8	G
Maximum field, B, at ±20 cm in X from the center of the gap	1.2	G
Maximum field, B, at ±20 cm in Z from the center of the gap	1.0	G

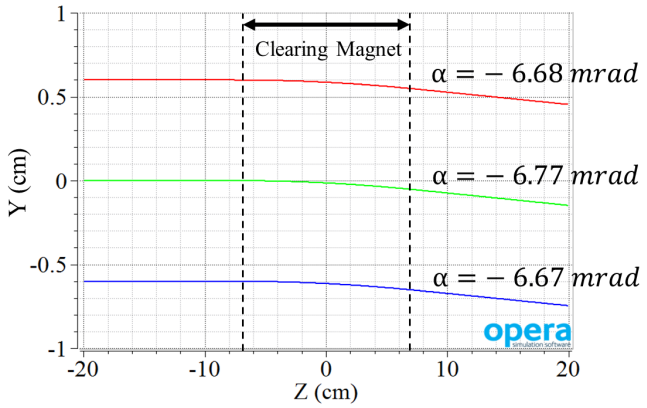

Figure 5.21. Electron beam trajectory though the clearing magnet with a ring energy of 6.6 GeV. The outgoing angle, α, was determined at the zero field region at the downstream end of the magnet.

Figure 5.22 shows the B_x field along the electron beam trajectories as in Figure 5.21. The differences in the outgoing angles of the beam, as shown in Figure 5.21, are due to the small field differences, as shown in the inset of Figure 5.22.

In this design, the permanent magnets are recessed 0.3 cm back from the poles, thereby decreasing the Bx field at the center of the gap. However, this helps to decrease the maximum demagnetization field on the PM edges. The absolute maximum H_y field on the PM was 9.9 kOe for this design, which allows for the temperature to rise up to 121 ℃ before demagnetization effects start affecting the magnet.

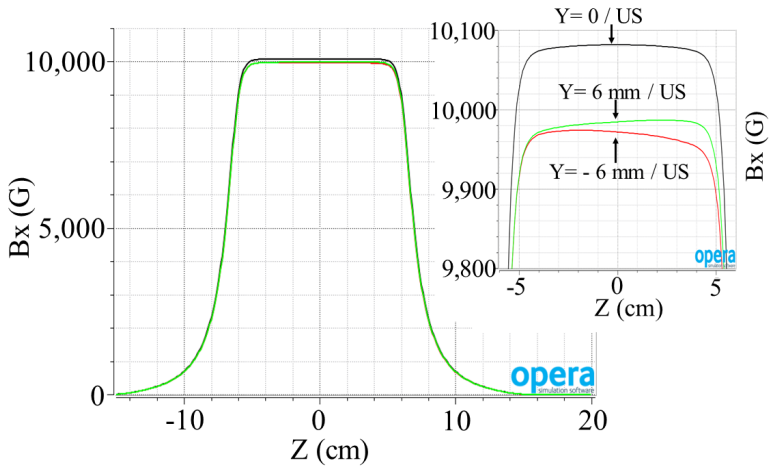

Figure 5.22. B_x field along the beam direction at 3 different Y positions. Z of 0 is the middle of the clearing magnet. The top inset plot is an enlargement over a smaller range of Z.

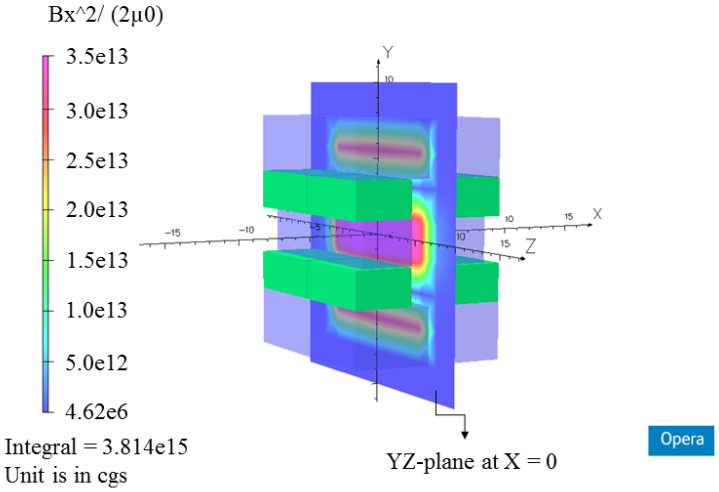

Figure 5.23. Magnetic force on YZ-lane at X=0 as generated with Opera 3D.

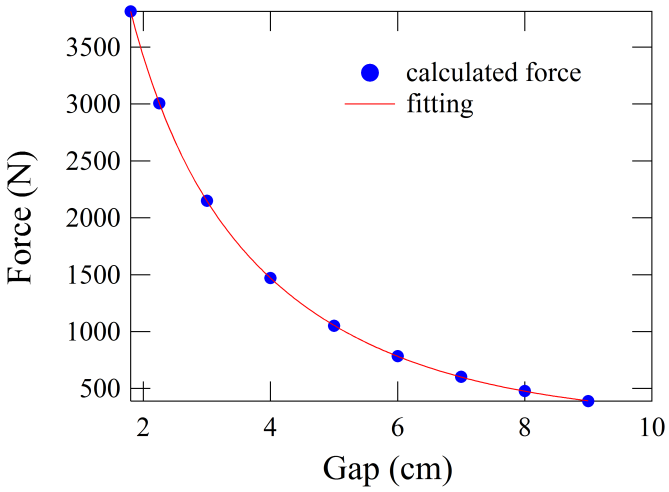

Figure 5.24. Magnetic force on the YZ-plane at X=0 at different gaps. The filled circles are the calculated forces from the model of the clearing magnet, and the red curve is the fit.

The magnetic force on the YZ-plane at X=0 as simulated is shown in Figure 5.23. The integrated force on the plane was 3859 N at an 1.8 cm gap (typical operational gap). Due to the large forces involved, the mechanical design has to take into consideration the assembly and maintenance processes. Towards this end, the magnet was split into two halves along the YZ plane. The splitting of the magnet has a two-fold advantage: for ease of assembly, and also for operational purposes, when the vacuum chamber between the magnets has to be baked for vacuum conditioning. Hence, the magnetic forces were calculated as a function of the gap between the two halves. Figure 5.24 is a plot of the force as a function of the magnetic gap. As expected, the force decreases exponentially with increasing gap.

Figure 5.25 is a conceptual model of the clearing magnet with the integrated vacuum chamber and all associated support systems. The top left model is in its operating condition. The top right is the end view of the clearing magnet when the two halves are separated for vacuum baking of the vacuum chamber in the middle. The bottom model is a rendering of the complete assembly with the two magnets shown separated. The mechanical design takes into consideration the forces and has a force compensation spring to assist in assembly and disassembly.

Table 5.15 shows the net resulting location of the possible electron beam at the safety shutter due to the clearing magnet in the HHLFE. It has achieved the required deflecting height of 20 mm at the safety shutter with a safety margin of 10% in the electron beam energy of 6.6 GeV.

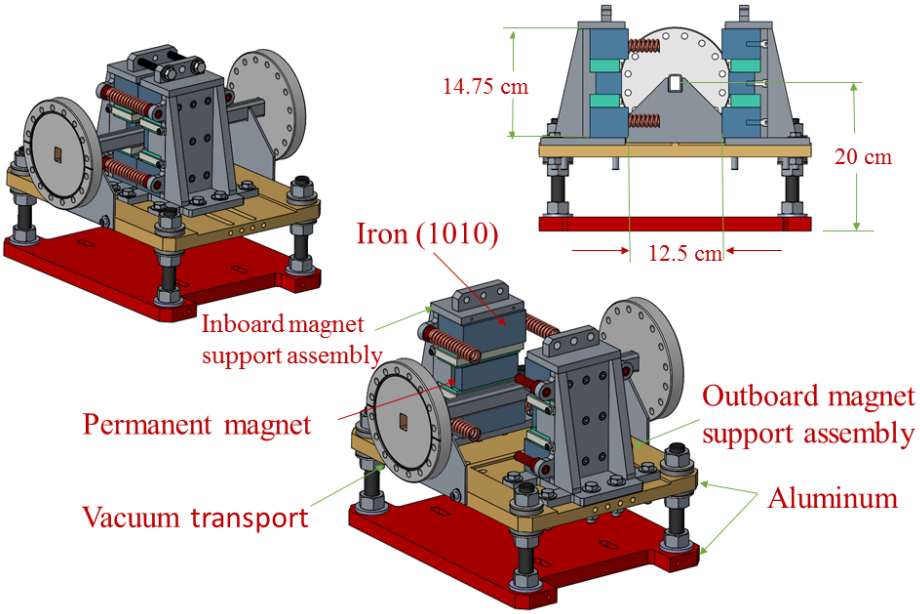

Figure 5.25. Three different views of the mechanical model of clearing magnet and its associated support systems.

Table 5.15. Location of the possible electron beam at the safety shutter due to the clearing magnet in the HHLFE.

Parameter	Operations at 6.0 GeV Value	Margin	Operation at 6.6 GeV Value	Margin	Unit
Beam outgoing angle, α Y= 0.6 cm	-7.36	0.92	-6.68	0.24	mrad
Beam outgoing angle, α Y= 0	-7.52	1.08	-6.77	0.23	mrad
Beam outgoing angle, α Y= -0.6 cm	-7.34	0.90	-6.67	0.23	mrad
Deflecting height at the safety shutter (Z= 400 cm) Y = 0.6 cm at US	-23.44	3.44	-20.72	0.72	mm
Deflecting height at the safety shutter (Z= 400 cm) Y = 0 at US	-30.08	10.08	-27.08	7.08	mm
Deflecting height at the safety shutter (Z= 400 cm) Y = - 0.6 cm at US	-35.36	15.36	-32.68	12.68	mm

5-2.5.2 Clearing Magnets for CUFE

Figure 5.26 is a schematic representation of a possible electron particle trajectory through a clearing magnet in the canted undulator front end. Similar to the high heat load front end, the safety shutter is the last shielding component in the front end inside the shield wall of the storage ring. When the safety shutter is open, electron particles are not allowed to exit through the opening in the shutter. A clearing magnet is located 4 m upstream of the safety shutter and is immediately after a fixed mask (FM2). Based on the geometry of the front end and the location of the clearing magnet, the requirements for the clearing magnet are shown in Table 5.16. Unlike the HHLFE clearing magnet, the CUFE clearing magnet will deflect the beam sideways as it has a large horizontal aperture to allow the photon beam to pass through.

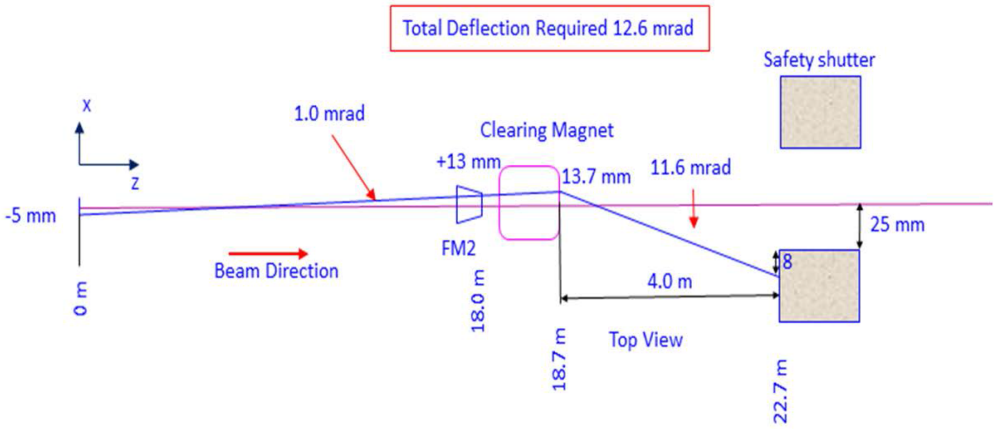

Figure 5.26. Schematic diagram of a electron particle trajectory through a clearing magnet in the canted undulator front end.

Table 5.16. Requirements for CU front end clearing magnet

Parameter	Value	Unit
Ring Energy	6.6	GeV
Deflecting Angle	-12.6	mrad
Gap	1.6	cm
Insertion Length	50	cm
Deflecting direction (electron beam)	Inboard	–
Distance of the safety shutter from the clearing magnet	400	cm
Deflecting distance inboard	3.3	cm
Deflecting range in horizontal (X)	2.64	cm

A permanent magnet (PM) dipole will be designed to produce a By field in the gap of this clearing magnet. The clearing magnet for this front end will be similar to the bending magnet front end clearing magnet discussed in Section 5-2.5.3. An H-shaped hybrid PM dipole similar to the BMFE clearing magnet is under consideration to efficiently produce the required B_y field integral with a gap of 1.6 cm. The pole width at the US end will be narrower than the clearing magnet for the BMFE since the required stay clear range in X is only 2.64 cm for this clearing magnet. The estimated length of this clearing magnet is shorter than 30 cm. The magnet material, NdFeB in grade N42SH, from Shin-Etsu Rare Earth Magnet, will be used for the magnetic design for the PMs and the pole material will be 1010 steel.

5-2.5.3 Clearing Magnets for BMFE

Figure 5.27 is a schematic representation of a possible electron particle trajectory through a clearing magnet in the bending magnet front end. Similar to the high heat load front end, the safety shutter is the last shielding component in the front end inside the shield wall of the storage ring. When the safety shutter is open, electron particles are not allowed to exit through the opening in the shutter. A clearing magnet is located 9.44 m upstream of the safety shutter and is immediately after a fixed mask (FM1). Based on the geometry of the front end and the location of the clearing magnet, the requirements for the clearing magnet are shown in Table 5.17. Unlike the HHLFE clearing magnet, the BMFE clearing magnet will deflect the beam sideways as it has a large horizontal aperture to allow the photon beam to pass through.

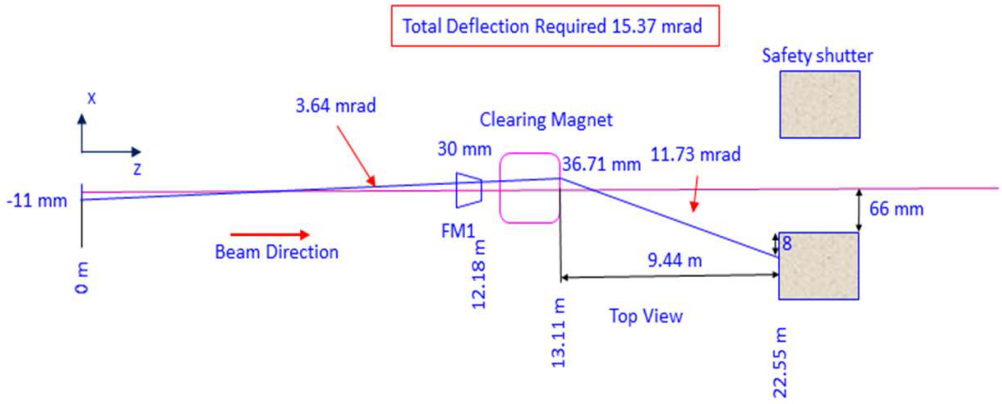

Figure 5.27. Schematic diagram of a electron particle trajectory through a clearing magnet in the bending magnet front end.

Table 5.17. Requirements for BM front end clearing magnet

Parameter	Value	Unit
Ring Energy	6.6	GeV
Deflecting Angle	-15.37	mrad
Gap	1.6	cm
Insertion Length	80	cm
Deflecting direction (electron beam)	Inboard	–
Distance of the safety shutter from the clearing magnet	944	cm
Deflecting distance inboard	7.4	cm
Deflecting range in horizontal (X)	6.84	cm

To deflect the outboard beam at X= 3.671 cm at an angle of -15.37 mrad, as shown in Figure 5.27, the B_y field integral along the beam path should be:

$$\int_{-\infty}^{\infty} B_y \, dz = -338,364 \;\; G \; cm$$

A permanent magnet (PM) dipole was designed to produce a By field in the gap of this clearing magnet as shown in Figure 5.28. The green parts are permanent magnet (PM), N49SH-GF, from Shin-Etsu Rare Earth Magnet, and the pole material is 1010 steel (soft iron). The N49SH-GF has

the following properties: B_r=1.36T (20°C) and intrinsic demagnetization field, H_{cj} = 21 kOe. The gap between top and bottom poles is 1.6 cm.

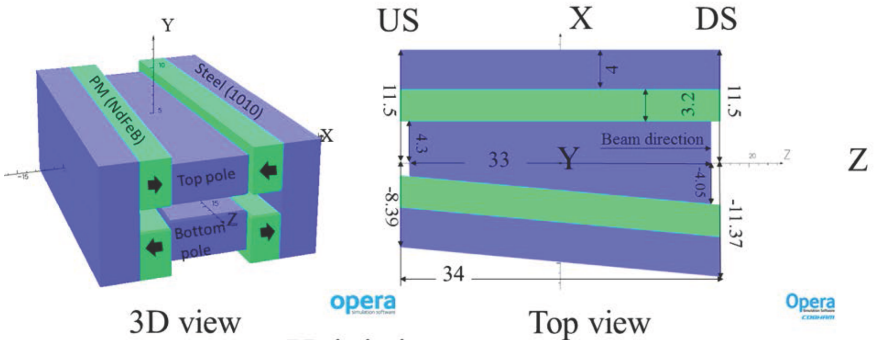

Figure 5.28. 3D and top views of the clearing magnet for the bending magnet front end.

In order to achieve the field efficiently there were two techniques applied to the design: 1) The pole width on the inboard side was tapered from upstream (US) to downstream (DS); 2) the center of the pole was moved outboard by 1.25 cm. The pole length was designed shorter than the PM length by 1 cm in order to increase the field at both ends. The magnets are recessed further than the pole tips by 0.3 cm to reduce damage to the magnets. As the result, the maximum demagnetization field was only 8.9 kOe, which allows the PM to reach a temperature 125°C before damage. All the dimensions in Figure 5.28 were optimized to have the total deflecting angle of the outboard beam with PMs of width 3.2 cm.

Figure 5.29 shows the extreme outboard beam trajectory in the clearing magnet. For the worst case scenario, the beam enters the clearing magnet at an angle of 3.64 mrad, and leaves at a negative angle of -11.847 mrad as shown in Figure 5.29.

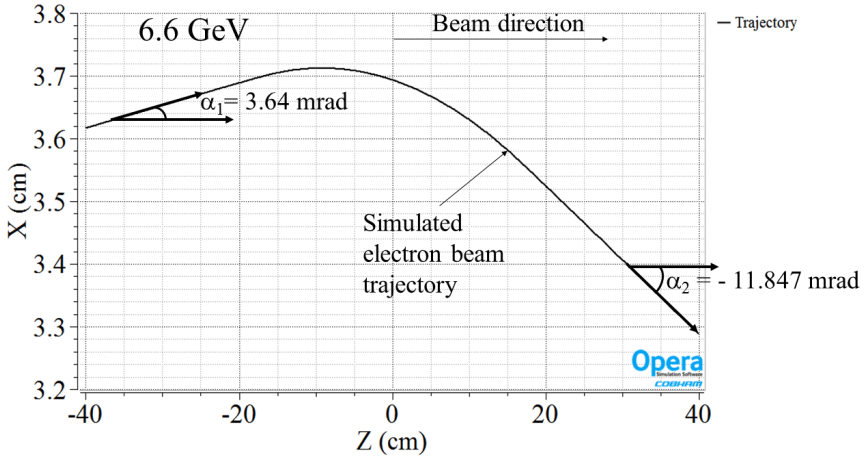

Figure 5.29. Outboard beam trajectory in the clearing magnet.

Figure 5.30 shows the extreme inboard beam trajectory in the clearing magnet. The outgoing angle of the inboard beam is much smaller than the outboard beam to clear the safety shutter aperture.

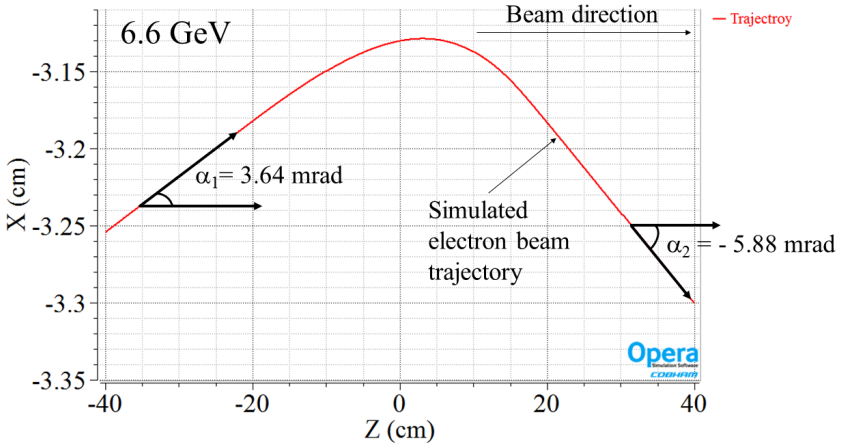

Figure 5.30. Inboard beam trajectory in the clearing magnet.

Figure 5.31 shows the By fields along the trajectory of inboard and outboard beams in the clearing magnet from the US to the DS. The maximum field reached is about 1.0176 T where the outboard beam exits the clearing magnet. If the pole on the inboard side is straight and 8.25 cm wide, then the peak field will be only 0.8 T (at the gap center) with the same PMs width and length. This will result in the clearing magnet length being greater than the current design of 33 cm to achieve the required deflecting angle. Alternatively, if the length is 33 cm, then the PMs need to be much wider (about 6 cm) than the current width of 3.2 cm to get the same required deflecting angle with a uniform pole width of 8.25 cm. The proposed design is efficient and takes advantage of the deflection geometry.

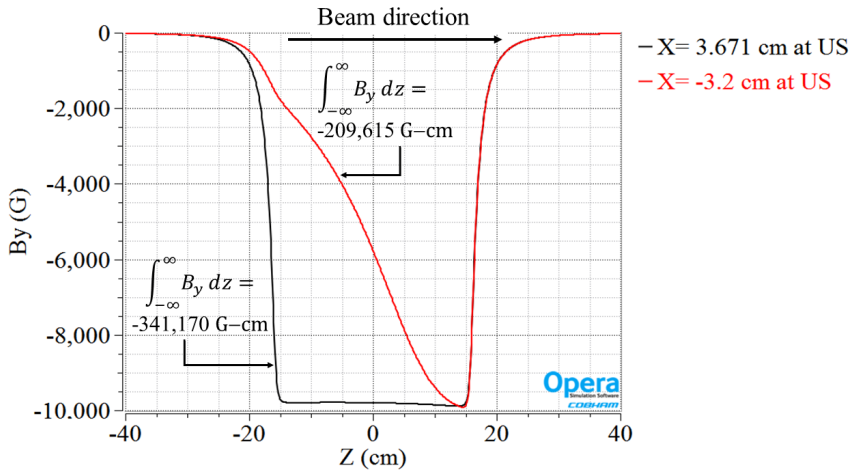

Figure 5.31. By fields along the outboard and inboard beam trajectories in the clearing magnet.

Table 5.18 shows the net resulting location of the possible electron beam at the safety shutter due to the clearing magnet in the BMFE. The magnetic force at the gap center will be calculated from open gap to the closed gap of 1.6 cm for the assembly and supports point of views. The mechanical design will use the data from the magnetic design and will be split as two halves in the vertical

plane. An iron shield is also planned around the clearing magnet to keep the fields contained, due to its close proximity to the insertion devices in the storage ring.

Table 5.18. Location of the possible electron beam at the safety shutter due to the clearing magnet in the BMFE.

Parameter	Operations at 6.6 GeV Value	Margin	Unit
Beam outgoing angle, α X= 3.67 cm	-11.857	0.127	mrad
Beam outgoing angle, α X= 0	-12.39	0.66	mrad
Beam outgoing angle, α X= -3.20 cm	-5.88	-5.85	mrad
Deflecting height at the safety shutter (Z= 944 cm) X = 3.67 cm at US	-75.22	1.22	mm
Deflecting height at the safety shutter (Z= 944 cm) X = 0 at US	-116.96	42.96	mm
Deflecting height at the safety shutter (Z= 944 cm) X = - 3.20 cm at US	-87.51	13.51	mm

5-3 Insertion Devices

5-3.1 Introduction and Scope

Insertion devices (IDs) optimized for small-gap operation as small as 8.5 mm, and potentially smaller for the superconducting undulators (SCUs), which may use thin-wall vacuum chambers, are required to fully utilize the potential of the new APS-U MBA lattice. This includes both out-of-vacuum regular planar hybrid permanent magnet undulators (HPMUs) and planar SCUs, and special-purpose devices for polarization control. With a smaller gap and potential for round beam pipes available for some beamlines, new undulator designs are being developed to enhance the magnetic fields to provide unprecedented brightness over a wide photon energy range from about 2 keV to well above 100 keV.

At the present time, the APS has 54 IDs in operation in over 33 beamlines. Most of the devices were optimized more than 20 years ago for 7-GeV operation, providing full energy tunability in the hard x-ray range. There are some devices with smaller periods and two electromagnetic devices for soft x-ray beamlines. The minimum gap of most devices is 11.0 mm with two devices operating near 9.5 mm. There are also two SCUs installed in the APS storage ring for hard x-ray energies operating at fixed gaps of 9.5 mm.

The upgraded APS machine will operate at 6 GeV and will require replacement of most of the IDs. Over the years, user requirements have been refined, and requests for special devices like superconducting undulators have increased quite dramatically. To maximize the brightness and flux for all the beamlines, most of the IDs will be replaced with shorter-period devices. In addition, because of user requirements, a few special devices will be installed in the upgraded machine. The global APS-U ID design approach to maximize spectral brightness and flux is as follows:

- Continue to use out-of-vacuum hybrid permanent magnet undulators, while at the same time take advantage of new advances in vacuum chamber engineering and fabrication techniques to optimize the design.
- The minimum magnetic gap will become smaller. It is expected to decease from 11.0 mm to 8.5 mm for the HPMUs and about 8.0 mm for the planar SCUs.
- Incorporate a magnetic phase shifter between segmented undulators (max 2 segments per ID straight section) for undulators that operate in tandem to maximize spectral output. Segments will be limited in length to 2.4 m (HPMUs) and 1.8 m (planar SCUs).
- Provide many more 2-headed revolver undulators and make provisions for 3-headed revolvers in the design.
- Tighten tolerances of machined components, which determine pole and magnet heights of planar HPMUs, so that small RMS phase errors of about 3° can be achieved. (A small RMS phase error correlates with high brightness of undulator radiated higher harmonics.)
- Continue to use short-period planar SCUs for hard x-rays (which are superior to in-vacuum cryogenically cooled permanent magnet undulators for period lengths considered for the APS-U).

A preliminary selection of insertion devices and their configurations were determined based on discussion with each beamline and are summarized in Table 5.19. In the table the number next to either SCU or U stands for a undulator period in cm. HGVPU is the Horizontal Gap Vertical

Polarizing Undulator, SCAPE is the Superconducting Arbitrary Polarization Emitter, and, IEX is the variable polarizing electromagnet device for the soft x-ray beamline.

Table 5.19. Preliminary selection of insertion devices for beamlines

Sector	Upstream ID	Downstream ID	Mode	Comments
1	SCU1.65	SCU1.65	Inline	Two SCU of 1.75m each in a cryostat
2	U2.8	U2.8	Canted	Each device of 2.1m long canted at 1mrad
3	U2.3	U2.3	Inline	Two devices of 2.3m each with phase shifter
4	SCAPE	SCAPE	Inline	Two devices of 1.75m each in 1 cryostat
5		U2.8		
6	U2.8	SCU1.8	Inline	One planar 2.3m and one existing SCU of length 1.1m
7		U2.8		
8	U2.5/U2.1	U2.5/U2.1	Inline	Two twin headed revolvers of 2.3m each with phase shifter
9	U2.8	U2.5/U2.1	Inline	A planar and a revolver of 2.3m each with phase shifter
10		U2.8		
11	SCU1.65	SCU1.65	Inline	Two SCU of 1.5m each canted 1mrad in a cryostat
12	U2.8	U2.8	Canted	Each device of 2.1m long canted at 1mrad
13	U3.0	U2.7	Canted	Each device of 2.1m long canted at 1mrad
14	U2.5	U2.1	Inline	Two devices of 2.3m each with phase shifter
15		U2.8		
16	U2.7	U2.5	Canted	Each device of 2.1m long canted at 1mrad
17		U2.8		
18		U2.1		
19	U2.5/U2.1	U2.5/U2.1	Inline	Two twin headed Revolvers of 2.3m each with phase shifter
20	SCU1.65	SCU1.65	Inline	Two SCU of 1.75m each in a cryostat
21	U2.1	U2.8	Canted	Each device of 2.1m long canted at 1mrad
22		U2.8		
23	U2.8	U2.8	Canted	Each device of 2.1m long canted at 1mrad
24	U2.1	U2.8	Canted	Each device of 2.1m long canted at 1mrad
25		U2.7	Canted	Each device of 2.1m long canted at 1mrad
26	U2.5	U2.5	Inline	Two devices of 2.3m each with phase shifter
27	U2.7	U2.7	Inline	Two devices of 2.3m each with phase shifter
28	SCU1.85	SCU1.85	Canted	Two SCU of 1.2m each canted 1mrad in a cryostat
29	IEX		Inline	A 4.8m Variable polarizing electromagnetic device
30	U1.35	U1.35	Inline	Two devices of 2.3m each with phase shifter
31	U2.5	U2.8	Canted	Each device of 2.1m long canted at 1mrad
32	U1.35	U2.8	Canted	Each device of 2.1m long canted at 1mrad
33	HGVPU2.9		Inline	A 4.6m Horizontal Gap hybrid device
34	U2.8/U2.1	U2.8	Canted	A revolver and a planar of each 2.1m long canted at 1mrad
35		U2.3/U1.35		A revolver of 2.3m length

Table 5.20 is the summarization of the ID counts categorized by period and length along with the status of the design.

We note that 53 conventional planar hybrid permanent magnetic (HPMU) structures (44 new and 9 reused) have been requested:

- 39 HPMUs (31 new and 8 reused)
- 7 revolver IDs (14 magnetic structures; 13 new and one reused)

Additionally, a full length HGVPU device, a total of 11 SCUs, which includes the new SCAPE device, has been requested (10 new magnetic structures in 5 new long cryostats and reuse one existing SCU and cryostat).

Table 5.20. Status of Preliminary ID selection

ID Type	Period (cm)	Length (m)	Quantity	Status
HPM	3.00	2.1	1	Existing
HPM	2.80	2.4	8	New design
HPM	2.80	2.1	12	New design
HPM	2.70	2.4	2	Existing
HPM	2.70	2.1	3	Existing
HPM	2.50	2.4	8	New design
HPM	2.50	2.1	2	New design
HPM	2.30	2.4	3	Existing
HPM	2.10	2.4	8	New design
HPM	2.10	2.1	2	New design
HPM	1.35	2.4	3	New design
HPM	1.35	2.1	1	New design
HGVPU	2.90	4.6	1	New design
SCU	1.85	1.2	2	New design
SCU	1.80	1.1	1	Existing
SCU	1.65	1.75	4	New design
SCU	1.65	1.5	2	New design
SCAPE	3.00	1.75	2	New design
IEX	12.50	4.8	1	Existing

5-3.2 Requirements

The ID requirements are divided into two parts, each described separately below.

5-3.2.1 User ID Requirements

The generic user requirements can be summarized by the following key points:

- High brightness of high ID harmonics for high energy x-rays $\Longrightarrow$ small RMS phase errors ($\sim$ 3° desirable)
- Continuous photon energy coverage $\Longrightarrow$ revolver undulators consisting of a combination of short period magnetic arrays
- Operational reliability (keep demagnetization field of permanent magnets for HPMUs within safe margin and keep quenching of SCUs at minimum)
- High photon beam positional/angular stability
- Optimized brightness and flux for given photon energy range of interest

In addition, there are special-purpose requirements such as those for the SCAPE device.

One generally wants to make the period length as short as possible for best performance subject to heat load constraints and engineering/physics constraints such as the minimum allowable magnetic gap. Shorter period lengths than used in current APS will be required because the storage ring energy is reduced from 7.0 GeV to 6.0 GeV. This is clearly demonstrated in Figure 5.32. For the HPMUs, the most commonly requested period lengths are 2.1 – 2.8 cm, and for the SCUs, 1.6 – 1.9 cm.

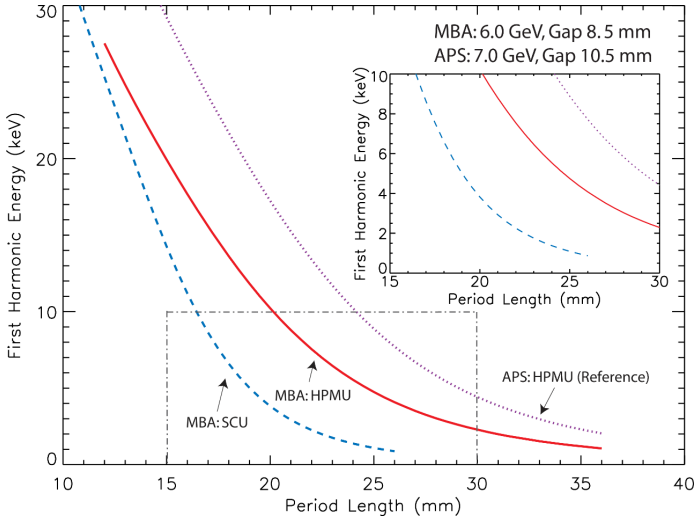

Figure 5.32. First harmonic energy vs period length for HPMUs and SCUs for 6.0 GeV for 8.5-mm magnetic gap.

Small RMS phase errors are directly correlated with high brightness for high undulator harmonics. However, some challenges are anticipated going to a smaller magnetic gap (8.5 mm) to keep the phase errors small. For the APS-U with MBA lattice, with smaller emittance, the effect of magnetic field errors on the spectrum becomes more noticeable, thus there is higher demand for undulators

with smaller phase errors for users that use higher harmonics. Figure 5.33 shows a compilation of the rms phase error of undulators of different period lengths currently installed in the APS storage ring. The typical rms phase error is about 4° near 11 mm gap.

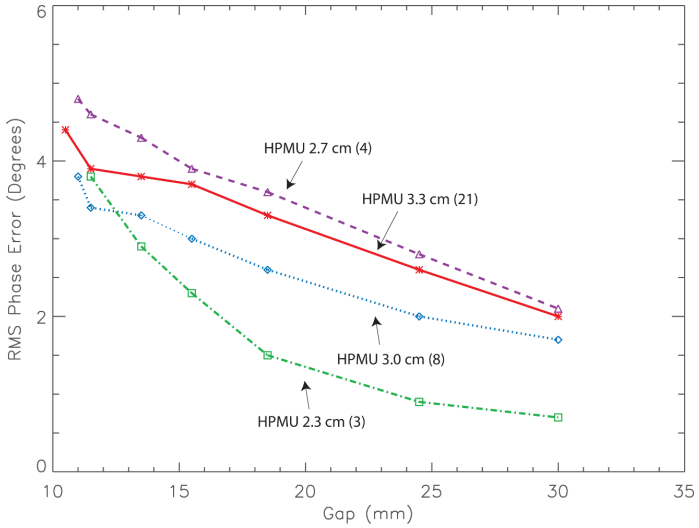

Figure 5.33. Measured RMS phase errors averaged over current APS planar devices. The number of devices used in the analyses is shown in parentheses. The 20-year old original APS specification is 8.0°at 11.5 mm magnetic gap.

Some users demand fast energy scans, however, it is expected that the scanning speed of the current gap separation mechanism will be sufficient. An undulator gap speed of ∼1 mm/s is readily achievable, which translates into an energy scan rate of typically higher than 0.5 keV/s, see Figure 5.34.

The gap setting reproducibility is being revisited to check that it will be sufficient for the new beam energy. It depends on the gap separation mechanism whether it is a 2- or 4-motor drive system – it is typically better than 5 μm for the 4-motor drive systems and in the range of 5 – 10 μm for 2-motor drive systems. Since the change of the first harmonic energy vs gap is $\sim$ 1 eV/μm then (due to the uncertainty in the gap setting) this translates into $\sim$ 5 – 10 eV energy reproducibility at best for either drive system, which may need to be improved for some beamlines.

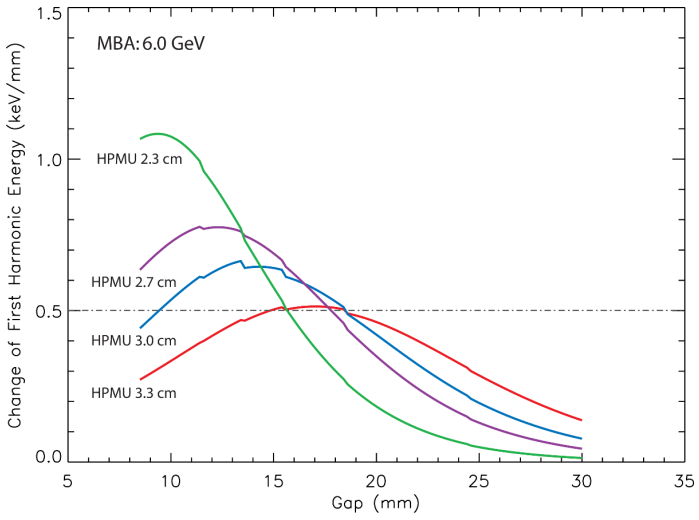

Figure 5.34. Change of first harmonic energy vs gap of different period length undulators currently available at the APS.

5-3.2.2 Storage Ring ID Requirements

Insertion devices may have undesired effects on the electron beam. The effects are normally quantified by two components: one is static field errors, which are measured along a straight-line path, as is done for normal quadrupole and sextupole magnets in the storage ring, and which are also dependent on the gap or current settings of the IDs; and the other one is dynamic field integrals, which introduce additional nonlinearities that the stored beam experiences because of the amplitude of the oscillation.

The latter occurs because in undulators, and to a greater degree in wigglers, the stored beam executes relatively large oscillatory trajectories (in one or both planes), which makes the beam experience slightly different peak fields along one full period due to the finite-width poles. This results in a small net kick in either or both planes that is nonlinearly dependent on the trajectory of the beam, making a wiggler a nonlinear device.

The actual nonlinearity is complex and cannot be described as a simple multipole or sum of multipole components. Planar undulators have relatively wide poles, although the width has been subject to optimization during the magnetic design phase. The divergence is small in the region of interest (injection aperture) near the beam axis, therefore the multipole components model can be used as a rough approximation. On the other hand, the polarizing SCAPE undulator may generate rapid field variation near the beam axis. This also occurs for the electromagnetic devices, such as the CPU and Intermediate Energy X-ray (IEX) undulator in sector 29, with narrower poles because of interleaving vertical and horizontal poles for alternating By and Bx fields. For both cases, the multipole components model is no longer valid in the region of interest (injection aperture). A detailed simulation with a realistic field distribution model is therefore required. Additional details can be found in the Functional Requirements Document (FReD) and the Physics Requirements Document (PRD).

In the past we have used the spectral width of the third harmonic of the undulator brightness radiation to set a guideline for the so-called magnetic field roll-off in the horizontal plane (x) inside the undulator. It was set somewhat arbitrarily, such that when the electron beam transverses the undulator off-axis within a pre-determined good field region, the change in the third harmonic energy shall be less than 10% of its intrinsic width. It has guided us well in the magnet design of planar HPMUs in the past. For the APS-U, we have identified the magnetic good field region to be ± 2.5 mm (which is reduced by a factor of two from ± 5.0 mm used for the present-day APS storage ring). All magnet designs are ultimately verified through detailed beam dynamics simulations and initial results indicate that the chosen (narrower) good field region is large enough.

The HPMUs are planned to be operated near a gap of 8.5 mm, which is much smaller than the current minimum gap of about 10.5 mm. Because strong attractive magnetic forces exist between top and bottom jaws at small gaps, it is highly desirable to reduce the magnetic forces of any new designs. With the smaller good field region we have had an excellent opportunity to reduce the dimensions of both poles and magnets. We have performed detailed undulator magnet design simulations (using codes OPERA and RADIA) of a new design with 2.7 cm period length at 8.5-mm gap. (The period length 2.7 cm was chosen because of an earlier expectation of most commonly requested undulator period length for the APS-U.)

A narrower pole width decreases the magnetic forces, but it tends to increase the magnetic field roll-off. However, optimization of the xx and xy pole chamfers lowered the effect on the roll-off. The following key features of the new design compared to the existing design are noted:

- Volume of magnets and poles reduced by ~30% -> cost savings
- Slightly increased magnetic field on-axis (~1%)
- Reduced magnetic forces by ~20%
- Maintained roll-off with narrower magnets and poles

The optimized magnet length in the beam direction was found to be 9.2 mm and pole length 4.2 mm. The magnet width was reduced from 67 mm to 50 mm from the existing design and the pole width from 44 mm to 40 mm. Figure 5.35 shows the OPERA model and geometry of the design. A tolerance between magnet and pole of 50 μm was used. Also, the magnets are recessed from the pole tips by 500 μm to leave space for shims that are put on the surfaces of the magnets during magnetic tuning of the IDs. The magnetic field roll-offs are compared in Figure 5.36 and the force analysis is shown in Figure 5.37.

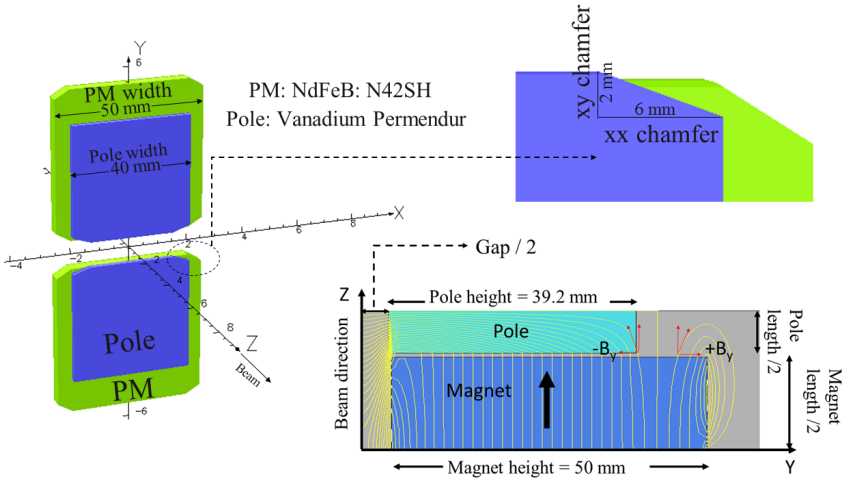

Figure 5.35. OPERA models of magnet and pole geometry for a planar hybrid permanent magnet undulator with 2.7 cm period length used to optimize dimensions and chamfers. Left: A 3D model of a quarter period. Right: A 2D model in the yz plane (x=0) with magnetic flux lines shown. Some of the optimized dimensions are shown.

The storage ring electron beam requirements are derived from the required beam motion listed in Table 5.21.

Table 5.21. Beam motion requirements (RMS)

	AC motion (0.01–1000 Hz)		Long-term drift (7 days)	
	Position (μm)	**Angle (μrad)**	**Position (μm)**	**Angle (μrad)**
Horizontal	1.7	0.25	1	0.6
Vertical	0.4	0.17	1	0.5

Beam stability requirements are based on 10% of beam sizes.

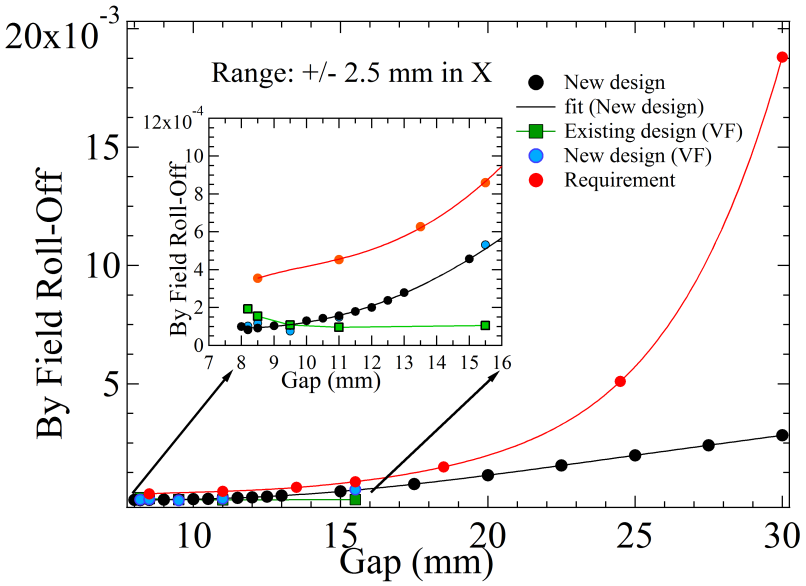

Figure 5.36. The magnetic roll-offs of the new and existing design vs gap. The insert shows an enlarged view at small gaps. The roll-off is defined as ($B_y(x=0)$-$B_y(x=2.5mm)$)/$B_y(x=0)$. The red curve is from the guidance criterion derived from the intrinsic width of the third harmonic undulator brightness.

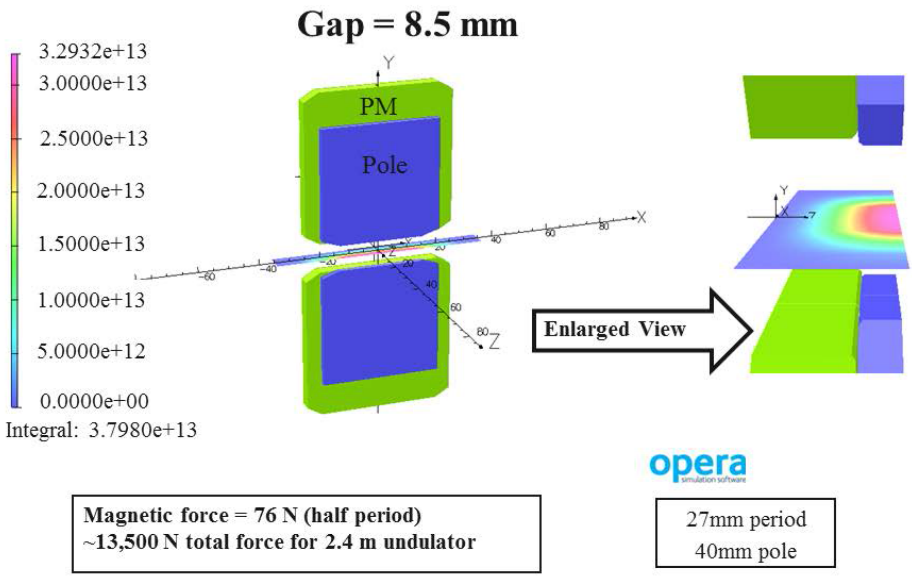

Figure 5.37. Left: Magnetic force analysis of the new design at a gap of 8.5 mm. Right: Enlarged view near the gap center.

It is important to be able to tune the first and second field integrals (which affects the orbit), and multipole errors (which affects the beam lifetime, injection efficiency, etc.) in the magnetic measurement laboratory to predetermined requirements. Those are still evolving at the present time. A set of requirements are listed in tables in the FReD but those are subject to revision. Figure 5.38 illustrates more recent work on local orbit correction with results for the first (I1) and a modified second field integrals (I2-(L/2)I1, symmetric around midpoint of ID) shown in Figure 5.39, assuming a corrector magnet located in the center of the straight section. For a 2.5 m ID on either side of a straight section, the limits on I1 and I2 in the vertical plane, for example, are 100 T-m and 220 T-m^2. This is still a tight requirement for I2 that needs to reevaluated.

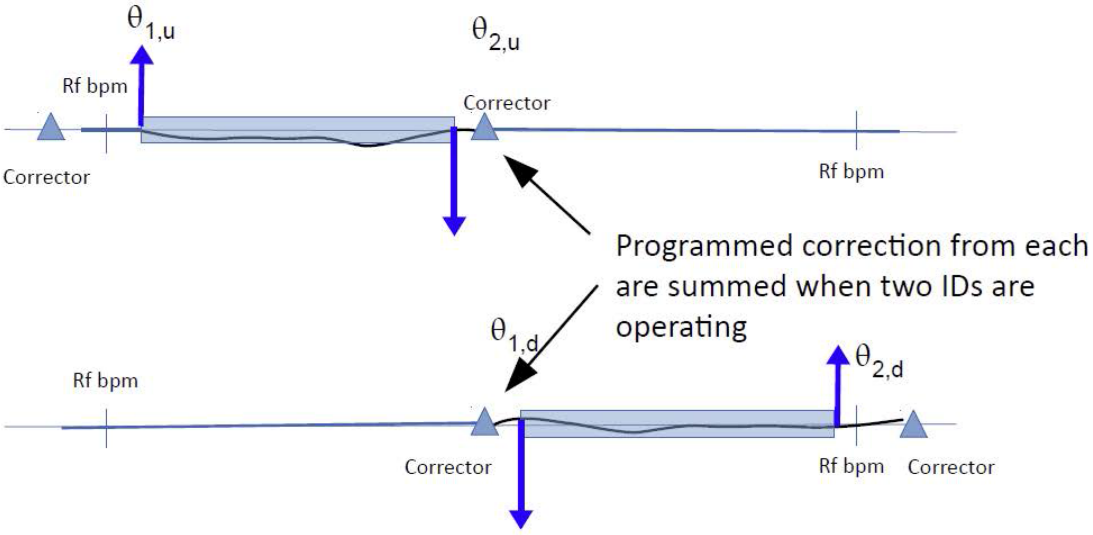

Figure 5.38. Orbit correction with x,y dipole corrector assumed placed in the center of the straight section.

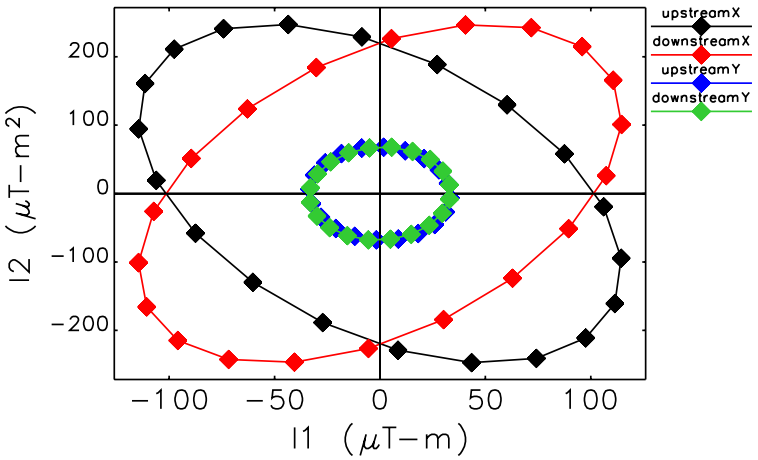

Figure 5.39. Requirements of first (I1) and second integral (I2) generated for electron beam motion of 0.9 μm and 0.13 μrad in x and of 0.2 μm and 0.09 μrad in y over the bandwidth 0.01 – 1 Hz.

5-3.3 Power and Power Density Limitations

The ID front ends were originally designed to withstand a 7.0 GeV beam with 100 mA current from a 2.4-m-long undulator with period of 3.3 cm (undulator A). Subsequently, new ID front ends were capable of handling the higher heat loads from two 2.4 m undulator A's in a straight section. For the APS-U, all 35 ID front ends will be either High Heat Load Front Ends (HHLFE) or Canted Undulator Front Ends (CUFE).

The new limits are 21 kW (HHLFE) and 10 kW (CUFE) for the power, and 590 kW/mrad^2 (HHLFE) and 281 kW/mrad^2 (CUFE) for power density. Figure 5.40 and 5.41 show the total emitted undulator power and on-axis power density, respectively, versus undulator period length for both HPMUs and the SCUs, assuming an 8.5 mm magnetic gap for both. Long period length SCUs will clearly exceed one or both power limits and hence the magnetic lengths need to be shortened for such cases.

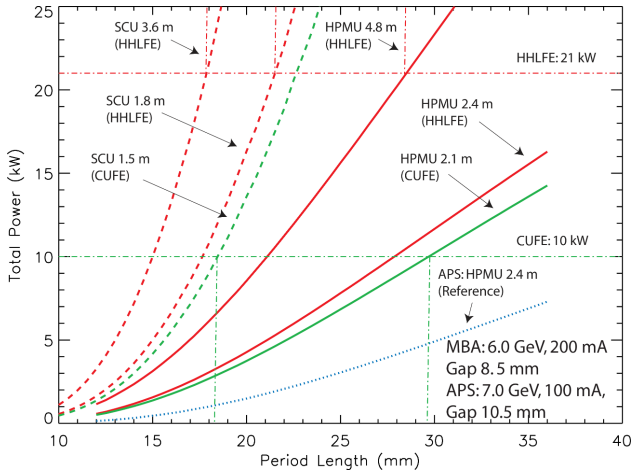

Figure 5.40. Total power vs period length for HPMUs and SCUs for 6 GeV and 8.5-mm magnetic gap (limits indicated by horizontal dashed lines).

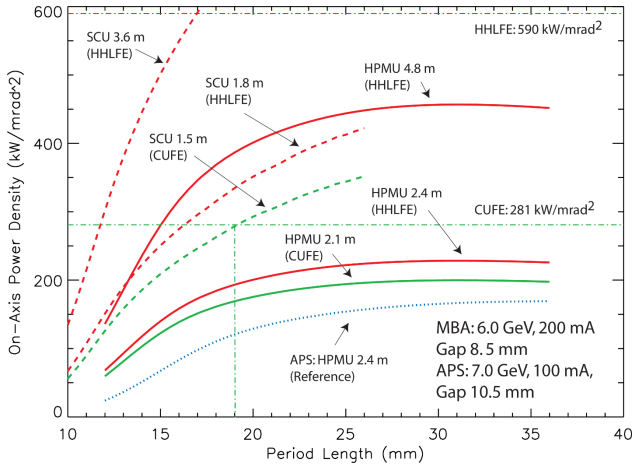

Figure 5.41. On-axis power density vs period length for HPMUs and SCUs for 6 GeV and 8.5-mm magnetic gap (limits indicated by horizontal dashed lines).

5-3.4 Brightness and Flux for the APS-U

The brightness of typical user-requested IDs installed in the APS-U storage ring is compared to the performance of IDs installed in the present-day APS storage ring in Figure 5.42. It was calculated such that for a given photon energy, the optimum period length was that which maximized the brightness. For example, the SCU with 1.8 cm period length (1.1-m long) currently installed in sectors 1 and 6 dominates above 60 keV. The power and on-axis power density constraints imposed by front end high-heat-load limits of the new HHLFE designs were applied. The gap in energy coverage between the first and third harmonics for the APS-U for shorter period devices can be closed by choosing an undulator with a slightly larger period length. The notation U2.5 cm/U2.7 cm indicates a permanent magnet undulator with period lengths of 2.5 cm and 2.7 cm, respectively, (both 4.8 m long with a magnetic gap 8.5 mm) and similarly for the superconducting undulators SCU1.7 cm/SCU1.9 cm (both 3.6 m long with a magnetic gap 7.5 mm). All calculations were performed for the 324-bunch mode with 99% coupling.

With the development of new revolver undulators for the hybrid permanent magnet undulators, enhanced performance may be achieved, by proper choice of periods between the two devices to cover the energy gaps between harmonics. The advantage of the APS-U with the new MBA lattice is significant, with more than two orders of magnitude in brightness enhancement. The increase of the coherent flux is similarly impressive, as it scales with the brightness increase.

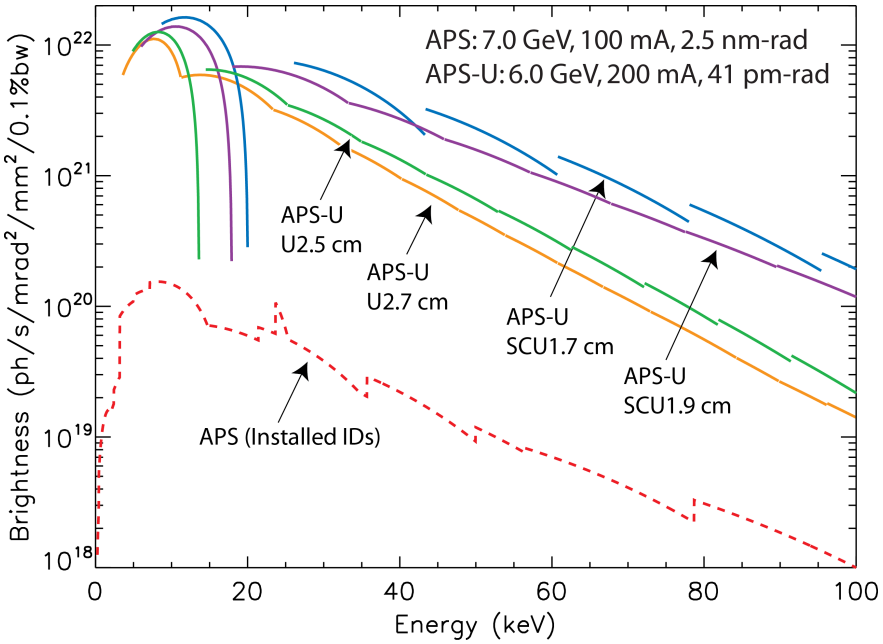

Figure 5.42. Brightness tuning curve comparisons of present-day APS and future APS-U after upgrade with the new MBA lattice. The brightness envelope of all currently installed IDs of the present-day APS are shown. A special 1.72-cm-period undulator (4.8-m long) gives rise to the sharp increase seen at 23.7 keV. The SCU (1.8-cm period, 1.1-m long) dominates above 60 keV.

The flux in the central cone is shown in Figure 5.43. The improvement over the present APS levels is typically in the range of 2 to 3 times for the HPMUs and 3 to 4 times for the SCUs. It is modest in comparison with the brightness increase, but it provides a substantial improvement and will lead

to shortened experiments.

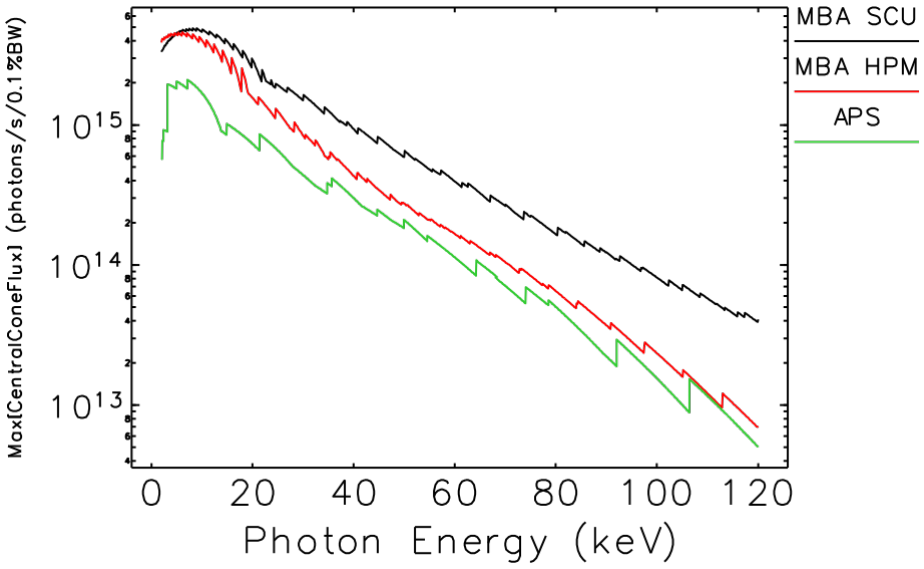

Figure 5.43. Calculated maximum central cone flux of planar IDs on the MBA lattice (6.0 GeV, 200 mA; red curve, HPM undulators; black curve, SCU undulators) compared to the existing HPM undulators in the APS storage ring (7.0 GeV, 100 mA; green curve). For the present-day APS, the existing undulator periods and lengths were used with a 10.75-mm magnetic gap. For the MBA SCUs, periods of 1.2–3.3-cm and 3.7-m magnetic length were used, and for the HPMs, periods of 1.6–3.3-mm and 4.8-m magnetic length were used. Both assumed a magnetic gap of 9.0 mm and a 324-bunch mode with 10% coupling.

5-3.5 Insertion Device Straight Section Configurations

The straight sections for undulator sources for the APS-U with the MBA lattice are literally in the same space as the current APS storage ring. The APS-U lattice shifts the BM beamline inboard by 43.6 mm relative to the current APS lattice. The offset in the bending magnet source point affects available space for IDs and ID vacuum chambers (IDVC), with primary impact on installation and maintenance access rather than limitations on equipment location. Similarly, the support plinths do not directly impact ID and IDVC space, but they do affect planning and execution of installation, calibration, alignment, testing, and maintenance. Figure 5.44 shows plan and elevation views of the straight section with a conventional HPMU at the upstream location in the current APS storage ring. Figure 5.45 shows plan and elevation view of the new straight section for the APS-U storage ring with the HPMU located in the upstream end.

The gross z-axis length available for ID use is positively impacted, relative to the current APS storage ring, by:

- Incorporation of the P0 BPMs in bellows assemblies upstream and downstream of the IDVC.
- A shorter transition length required at the upstream and downstream ends of the IDVC, due to the smaller change in aperture from the SR chamber to the IDVC, relative to the current APS.

The net z-axis length available for multiple ID sources in an inline configuration is negatively impacted, however, by:

- The anticipated need for a corrector magnet between IDs.
- The need for an RF-BPM in the middle, or at least a provision for one.
- The need for a phase shifter between IDs to allow phase matching over a range of X-ray energies.

The positioning of the RF-BPM in the middle, if universal for canted and uncanted use, may be located slightly upstream of the center of the straight section. Similarly, the corrector magnet will be located downstream of the center of the straight section. For canted undulator geometry, a central canting magnet to provide a 1 mrad cant will be located at the center of the straight section. In addition two 0.5 mrad canting magnets will be located in the upstream and downstream ends of the straight section. In the case of two undulators in the uncanted geometry, a phase shifter will be located in the middle of the straight section. Due to the addition of the canting magnets the maximum length of the IDs will be ∼2.1 m each. For the uncanted geometry with two undulators the length of the IDs are expected to be ∼2.3 m each.

The beamline selection and source selection processes have converged to these configurations:

- A single HPM undulator or revolver undulator, as is in common use at the APS today as shown in Figure 5.45.
- Two HPM undulators inline (either can be a revolver); ∼2.3 m each. A phase shifter will be needed between them, together with horizontal/vertical corrector magnet as shown in Figure 5.46. An RF-BPM between the two undulators may also be needed. To date, the APS has not used a phase shifter or an intermediate corrector magnet for dual, inline undulators,

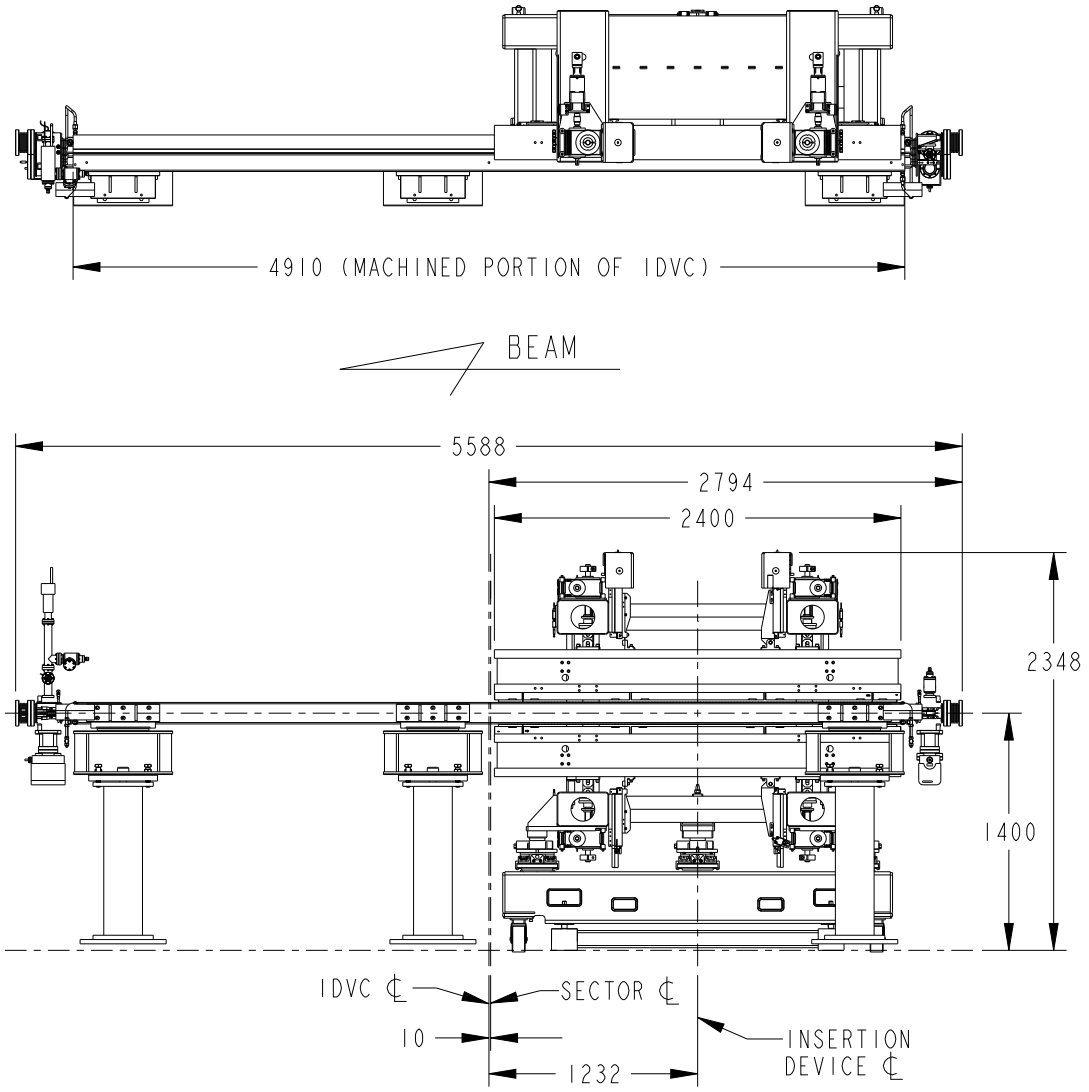

Figure 5.44. Plan and elevation views of the straight section with one undulator in the upstream half of the straight section in the current APS storage ring

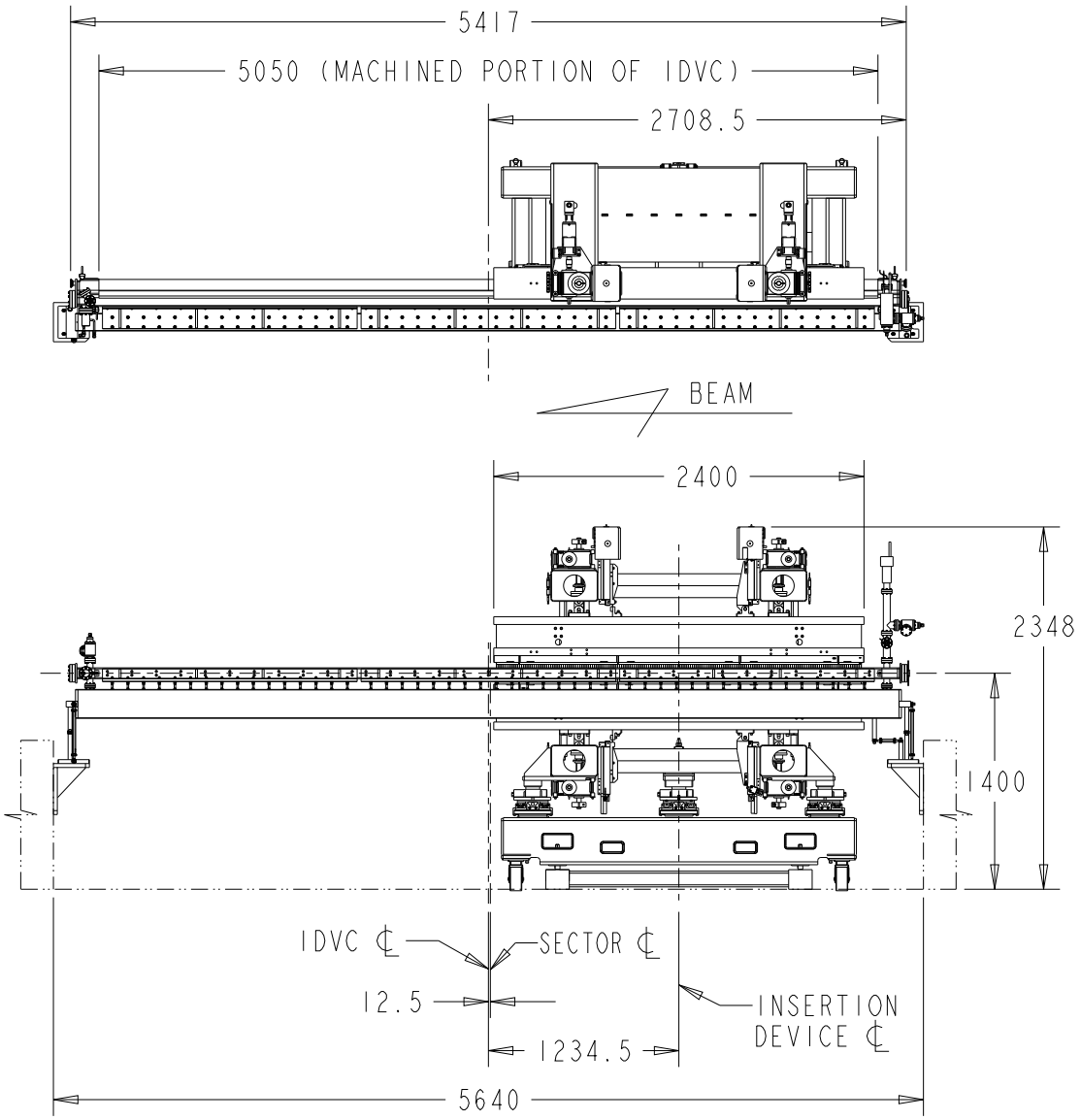

Figure 5.45. Plan and elevation views of the new straight section with one undulator in the upstream half of the straight section in the APS-U storage ring

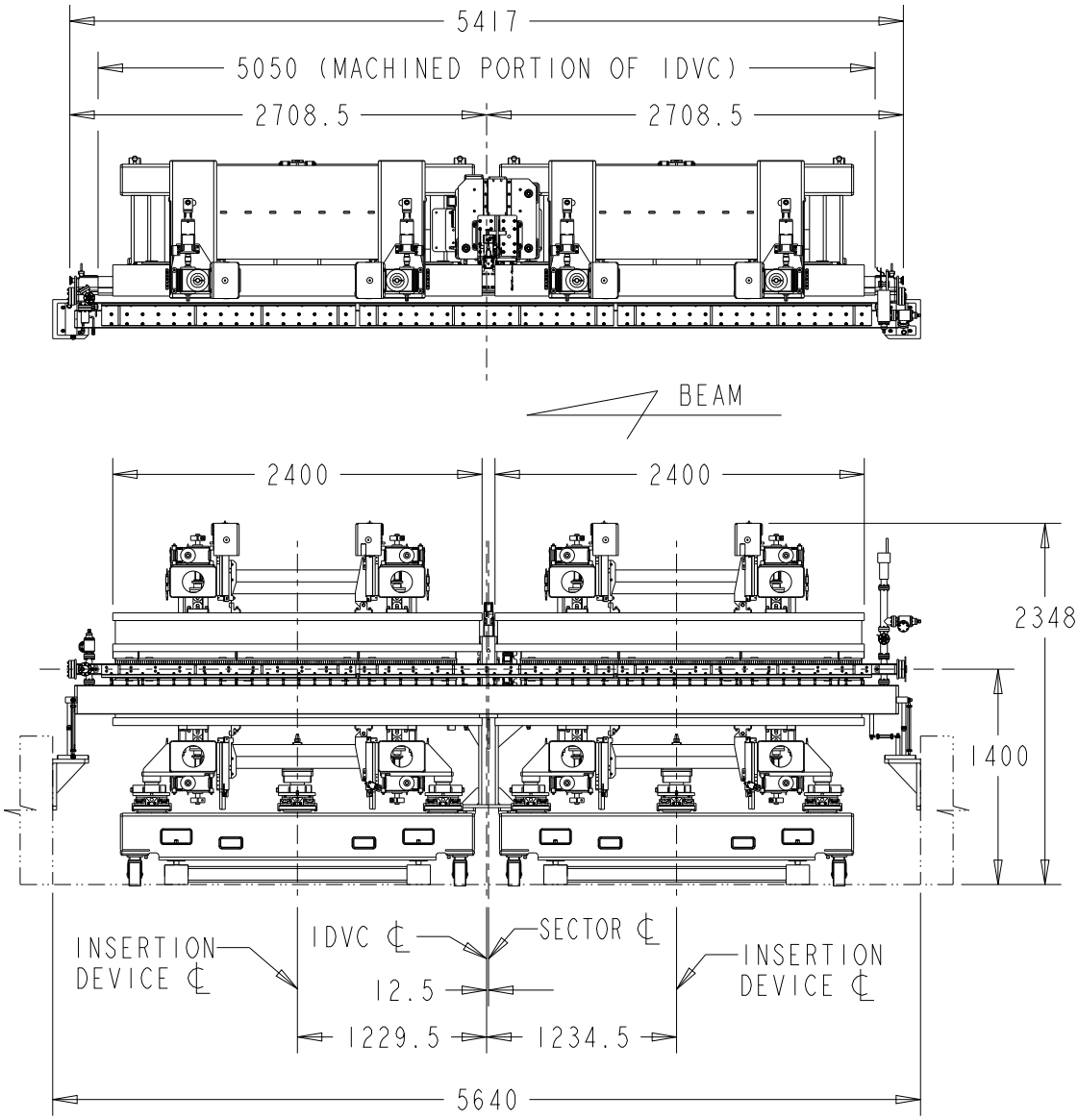

Figure 5.46. Plan and elevation views of the new straight section for uncanted geometry. The straight section consists of two HPMUs, a phase shifter in the middle, and a corrector magnet immediately upstream of the phase shifter.

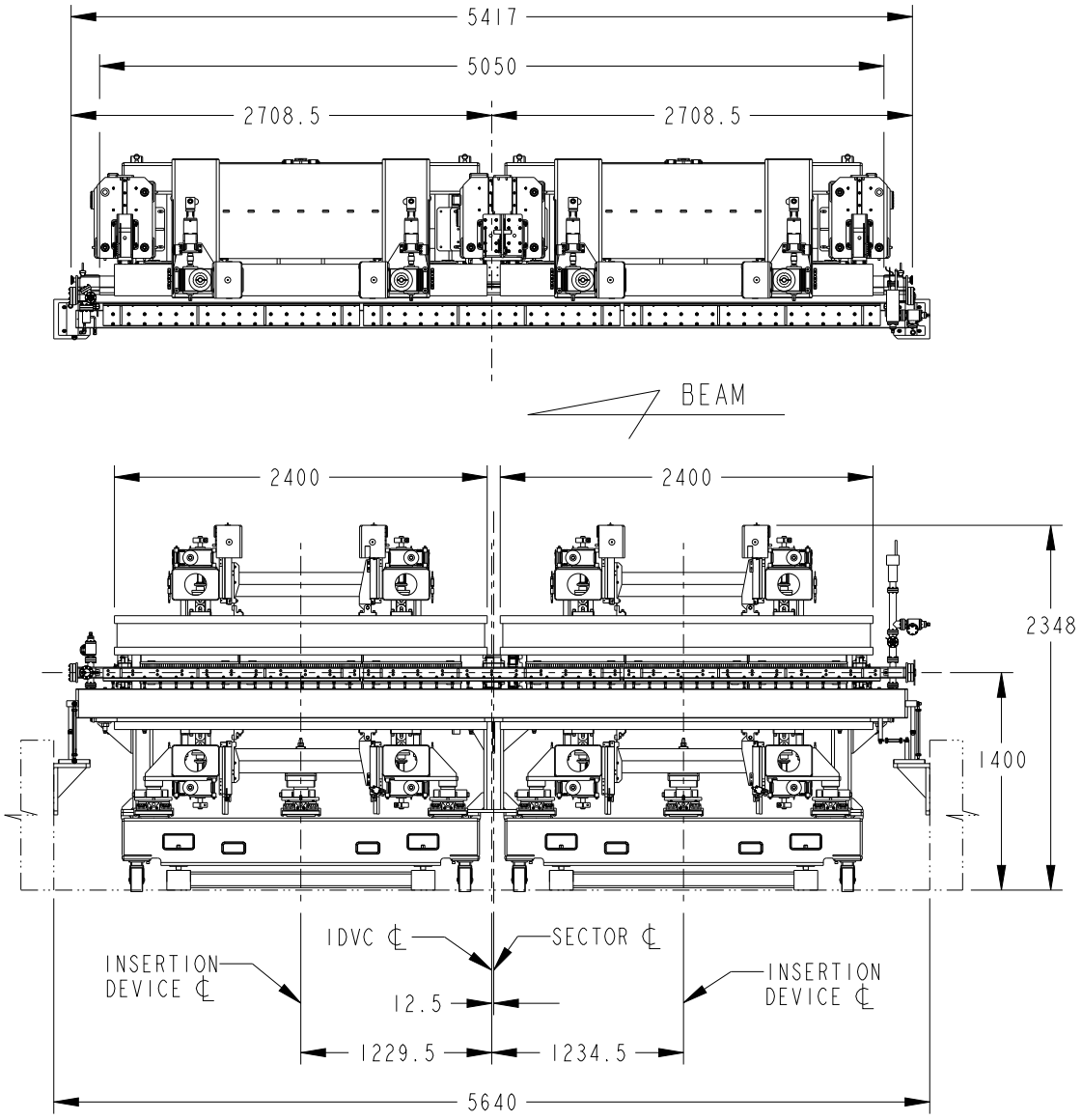

Figure 5.47. Plan and elevation views of the new straight section for canted geometry. The straight section consists of two undulators of 2.1m length each, two 0.5 mrad canting magnets in the upstream and downstream ends, and, a corrector and a central 1 mrad canting magnet in the middle of the straight section.

but this is otherwise a common configuration in the current APS. Several sectors employ a precise spacing between the undulators to optimize phasing at a specific X-ray energy, but no adjustable phasing provision has been made to date.

- Two HPM undulators in a canted configuration, such that each undulator is a source for a separate beamline branch. Either or both can be revolver undulators of ∼2.1 meter length. A canting dipole magnet will be used between the two undulators, together with horizontal/vertical corrector magnets as shown in (Figure 5.47). An RF-BPM between the two undulators may also be needed. While revolver undulators have not been used in dual, canted undulator sectors at the APS, this is otherwise a common straight section configuration, and most such sectors incorporate a BPM and a horizontal/vertical corrector electromagnet between the undulators and an electromagnet dipole. It is envisioned that APS-U will also use electromagnets for both dipole and corrector magnets; the same designs currently used will likely be employed, with new designs for their mounting structures and for their power supplies.
- A HPM undulator upstream of ∼2.3 m length and an SCU downstream of ∼1.1 m length, similar to two existing APS configurations (Sectors 1 and 6).
- Two SCUs inline in a single cryostat of ∼4.5 meters; each SCU would be about 1.75 meters in length. A phase shifter between them, horizontal/vertical corrector magnets and a BPM would also be needed, similar to the dual, inline planar permanent magnet undulator configuration. A 3D model of the long cryostat in the APS-U lattice is shown in Figure 5.48.
- Two SCUs canted in a single cryostat of ∼4.5 meters; each SCU would be about 1.5 meters in length. A canting dipole between them, horizontal/vertical correctors, and a BPM would also be needed. In addition two canting dipoles at either end will also be needed. This is similar to the dual, canted HPM undulator configuration; externally it would look like the configuration shown in Figure 5.48.
- A special circularly polarizing SCU (SCAPE) will be developed with the intent of using two such devices of length ∼1.75 meters in a common cryostat of ∼4.5 meters. The two SCAPE devices will be tuned to the same nominal energy with opposite circular polarization, and the fields will be varied slightly off-energy to facilitate a source with reversing polarization at a constant X-ray energy. The vacuum chamber is anticipated to be round with 6-mm inner diameter.
- A special Horizontal device (HGVPU) ∼4.6 meters long will be used to provide vertically polarized X-rays. This is a full-length device using the full straight section. A special vacuum chamber with small horizontal aperture and an ante-chamber for NEG pumping is envisioned.
- There is a unique electromagnetic ID (IEX) currently used at the APS, which is 4.8 meters long, and has both horizontal and vertical fields, allowing it to produce a variety of polarizations: linear vertical, linear horizontal, and right- or left-handed elliptical or circular. It is expected that this device will be reused, with either a unique IDVC or an evolution of the standard APS-U IDVC with a longer nose length.

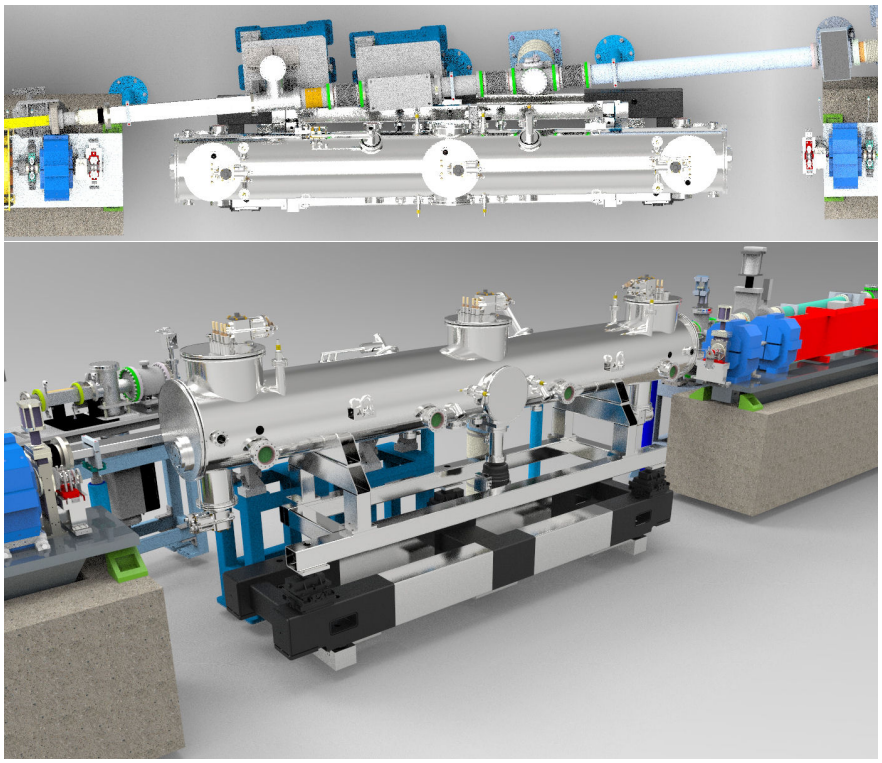

Figure 5.48. Plan and isometric views of the long SCU cryostat in the APS-U lattice. The plan view shows the proximity of the neighboring BM front end components. The isometric view shows the upstream and downstream plinths. The open space on either side of the cryostat will be for transitions from the storage ring vacuum system to the cryostat.

5-3.6 Hybrid Permanent Magnet Undulators

5-3.6.1 Planar Undulator Design

Planar undulators, using hybrid (pole/permanent magnet) magnet (HPM) arrays and variable magnetic gaps, are in wide use at the APS. Several periods of magnet structures designed and built by STI Optronics are used, with periods ranging from 1.8 cm to 3.3 cm. There are also numerous periods designed and built by the APS, ranging from 1.72 cm to 3.6 cm. The APS-built magnet arrays are modular, allowing them to be assembled in full-length or shortened version designs for inline use, or in dual, canted applications, respectively. The APS design will serve as the basis for final designs for the APS-U. The APS design is well-understood, both magnetically and mechanically, so it can be efficiently modified for other periods and further refined for more demanding undulator requirements. It features a value-engineered design, as shown in Figure 5.49. The design exploits high machining accuracy and repeatable assembly methods to provide ease of magnetic tuning to meet performance requirements.

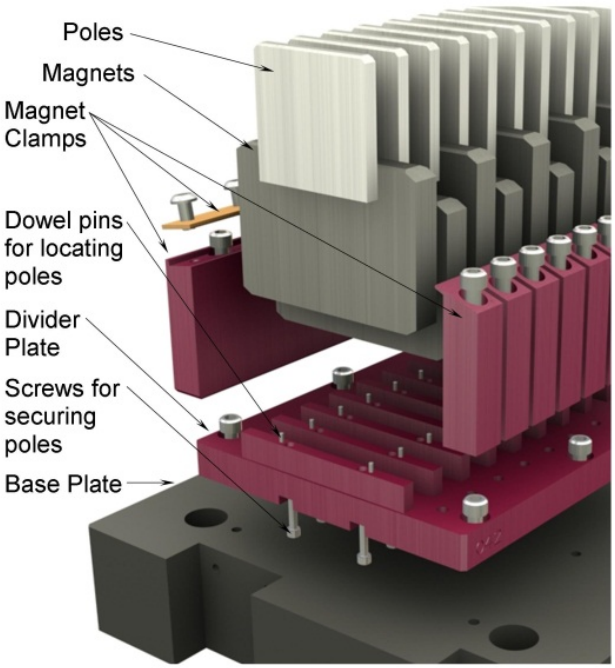

Figure 5.49. 3D model of a magnet assembly.

Some of the functional features and design improvements include:

- Pole registration "machined-in" to the magbase and poles.
- Positive pole z-axis registration rather than alignment of outside faces.
- Five "magbase" sections allow removal/installation of outer two sections so all devices can be switched between "normal" sectors and dual, canted undulator sectors.
- Minimized cost of manufacture by eliminating pole clamps and only using individual magnet clamps on one side.

5-3.6.2 Gap Separation Mechanism

Planar undulators (HPMU) for the APS-U will have two hybrid, planar magnet structures opposing each other vertically, mounted to a gap separation mechanism. These will maintain the functionality of the existing APS undulators (i.e. control by energy or gap, ability to taper, synchronous scan, etc.) and will be compatible with existing and planned APS-U undulator vacuum chambers. The gap separation mechanism for a planar, permanent magnet undulator provides precise, repeatable control of the magnetic gap and taper, while functioning reliably in a harsh radiation environment. The mechanism and its control system ensure safe operation, with multiple levels of safeguards and interlocks, and also allow distributed control from remote locations through EPICS, while enforcing access security.

It is expected that the majority of gap separation mechanisms for the APS-U will be reused from existing undulators currently in use in the APS storage ring. These mechanisms will be maintained and updated, as needed, by APS Operations to ensure they are ready for re-use at the beginning of the APS-U shutdown. Most of these will be the APS-designed "4-motor" gap separation mechanisms, shown in Figure 5.50, which feature a welded steel frame with four drive motors, one for each end of each magnet structure. The motors are synchronized through the control system, using feedback from four primary linear encoders or four backup rotary encoders. This device has a very conservative load capacity of ~5000 pounds (22,000 N), and is expected to be suitable for any magnet structure designed specifically for the APS-U, and for shorter period magnet structures reused from the existing APS stock.

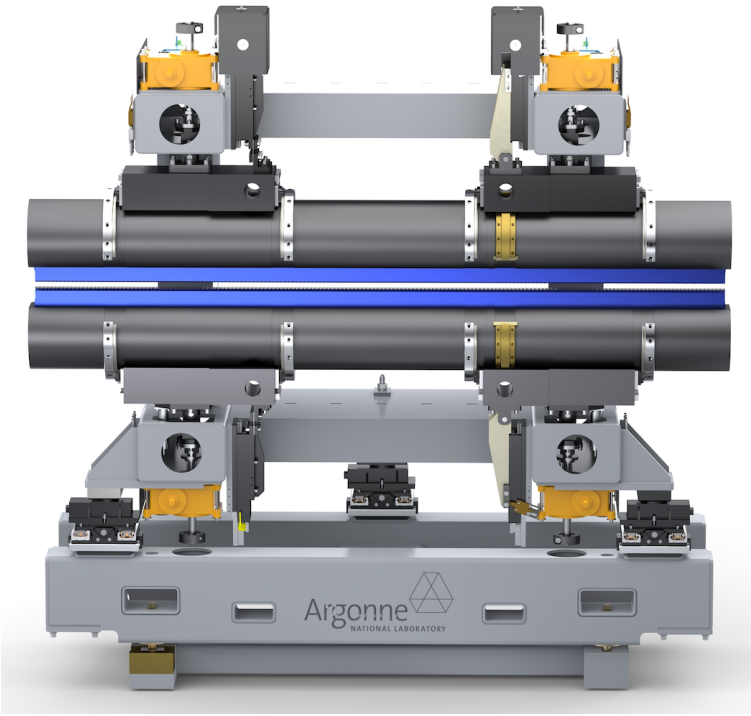

Figure 5.50. Four motor gap separation mechanism with revolver mechanisms, strongbacks, and magnetic arrays.

The undulator control system, located in the storage ring mezzanine above the undulator, coordinates motion between the four motors to achieve the desired gap based on readback of the encoders, while synchronizing the motion to be symmetrical about the IDVC (and electron beam). Multiple limit switches are used on the magnet structures and on the gap separation mechanism to protect the undulator and the IDVC from damage. Limit switches are also used as inputs to the beam position limits detector (BPLD) system, which in turn links to the machine protection system (MPS). These protect the storage ring and front end equipment from damage due to radiation produced from an off-trajectory electron beam.

Another gap separation mechanism in use at the APS, that will be reused for the APS-U, was designed and built by STI Optronics. This mechanism uses two drive motors, with mechanical linkages to synchronize upper and lower magnet structure drives on each end. Only two linear encoders are needed for primary feedback, and rotary encoders for backup feedback. The frame is assembled of bolted aluminum plates, as it was designed to maintain a larger "stay-clear" area for ferrous materials than the later APS 4-motor design. The 2-motor gap separation mechanism was also designed to operate at much larger magnetic attractive forces. Reuse of ∼7-10 of these mechanisms will provide a platform for longer period undulators reused from existing APS stock, which have wider poles than is expected to be needed for the APS-U and a correspondingly larger magnetic attractive force. The overall control system functionality is similar to the 4-motor version, with the key difference being there is no need to synchronize motion for vertical symmetry.

5-3.6.3 Revolver Undulator Designs

A revolver undulator offers a greater energy tuning range than any single-period undulator by combining two (or more) magnet structures in the space of one undulator. Each magnet structure can be optimized for a specific spectral range with higher average brightness than would be possible with a single device. A revolver undulator has been successfully developed at the APS, using the same gap separation mechanism as the single-magnetic structure planar undulators. The development program initially produced a prototype undulator with a single revolving jaw, which was magnetically measured and mechanically tested to validate the design. Then a full prototype was built, with 3.3-cm period and 2.7-cm period magnet structures on each of the two revolver strongbacks. This device was fully magnetically tuned, and further tested for repeatability and reliability, including an operational test simulating two years of actual use. Then the magnetic tuning was rechecked and the device was installed in Sector 35 of the APS storage ring in January, 2015, as a source for the new Dynamic Compression Sector (DCS) beamline. In May, 2015, the prototype was replaced with the DCS "production" revolver, featuring a 3.0-cm period/2.7-cm period combination. Figure 5.51 is an image of the first revolver undulator installed in sector 35 in the APS storage ring.

We have achieved a high degree of confidence in the APS revolver undulator from magnetic, mechanical, controls, reliability, and user-friendliness perspectives. As the design uses the well-proven APS gap separation mechanism (32 are currently installed), we can repurpose existing mechanisms as revolver undulators for the APS-U. The revolver undulator design accommodates undulator magnet structures up to 2.4 meters long. Any combination of the APS-designed undulator magnet structures, from 1.72- to 3.6-cm periods can be used, along with any periods envisioned for the APS-U.

A design study was further undertaken to explore capabilities for extending the "two-headed" re-

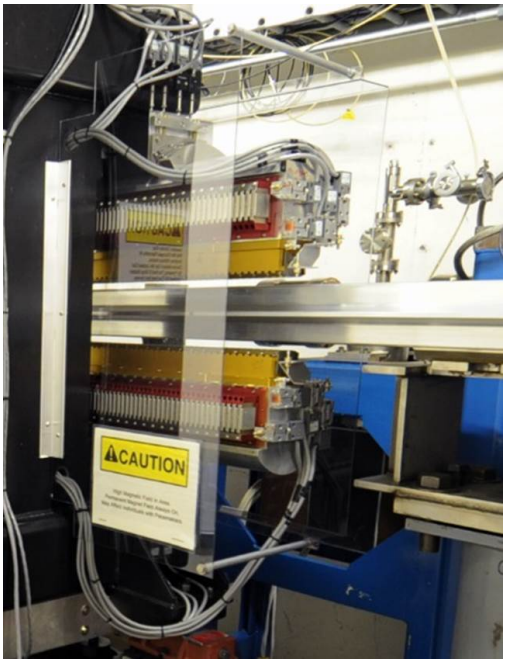

Figure 5.51. Revolver undulator installed in sector 35 in the current APS storage ring.

volver design to three magnet structures oriented at 45° to each other. Figure 5.52 is a rendering of a 3 headed revolver design concept on the existing 4 motor gap separation mechanism. This would require redesigns of the magnet structures and the ID vacuum chamber, but they appear compatible with the requirements of the APS-U lattice. Control and magnetic tuning issues also need to be addressed, but a "three-headed" revolver appears to be a very viable, cost-effective option for use with the APS-U lattice.

Revolver Undulator Design Highlights A major design criteria was the desire to reuse the existing gap separation mechanism, as it was reliable and cost-effective, and many were available for repurposing. With that constraint, the strongback is as large in diameter as practical. It is torsionally stiff, so a single revolver drive on each jaw is fine. The strongback is not as stiff in bending as the one used in the APS non-revolver undulators, but the strongback is supported in 4 places rather than 2, which minimizes differential gap deflection. The revolver strongback deflection analysis is shown in Figure 5.53.

The revolver drive uses a wormgear with a duplex design, which allows backlash adjustment without changing the center distance of the wormshaft/wormwheel pair. Backlash is adjusted by axial movement of the worm shaft with shims, similar to this illustration from Kohara Gear shown in Figure 5.54.

Our design uses a standard Kohara wormshaft with custom machining, and a custom wormwheel with a 100:1 ratio. The backlash is adjusted to about 70 microns at the radius of the magnet poles. There is no preload provision other than the moment load of the unused magnet structure.

The guide rails are THK HCR15, with standard bearing blocks and rails, but the rails are custom

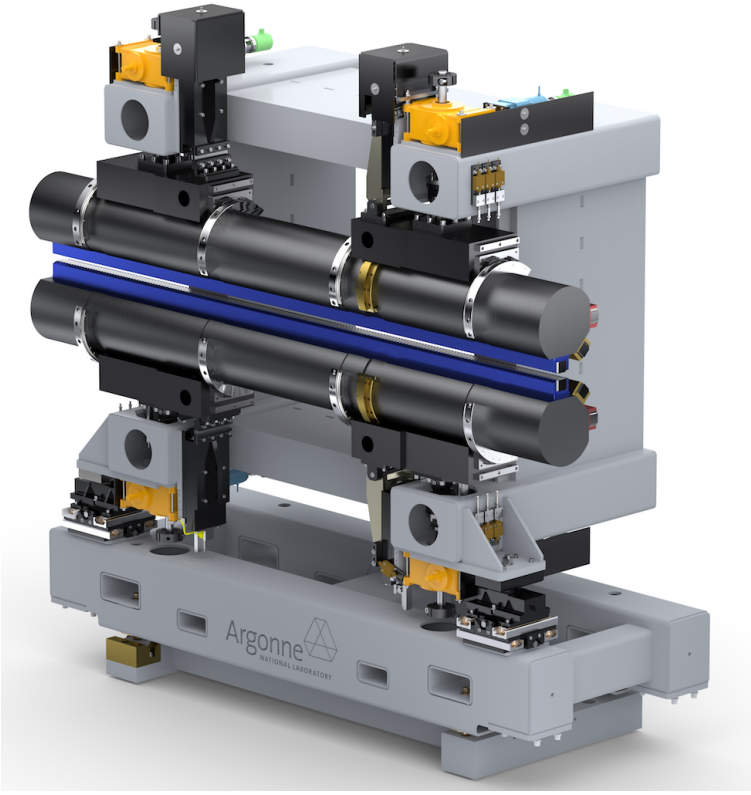

Figure 5.52. A 3D rendering of the 3 headed revolver design on a 4 motor gap separation mechanism.

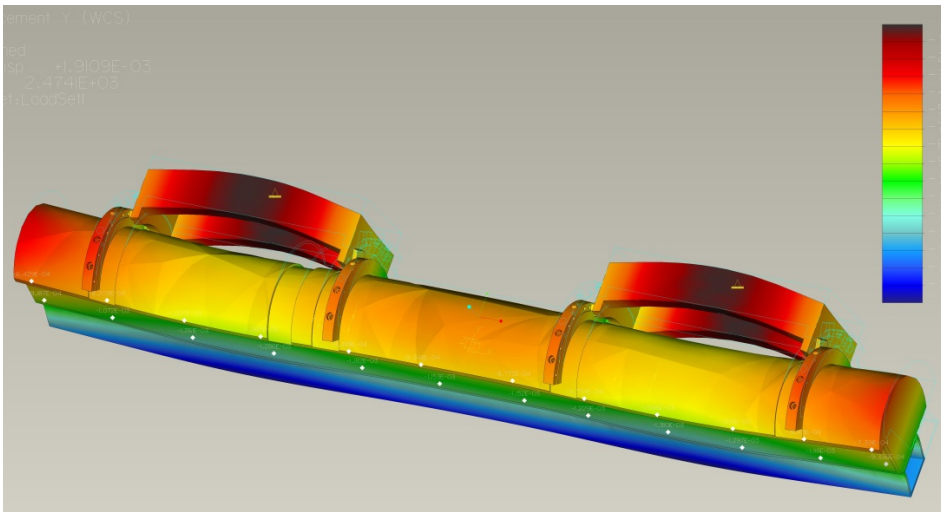

Figure 5.53. Revolver strongback deflection analysis.

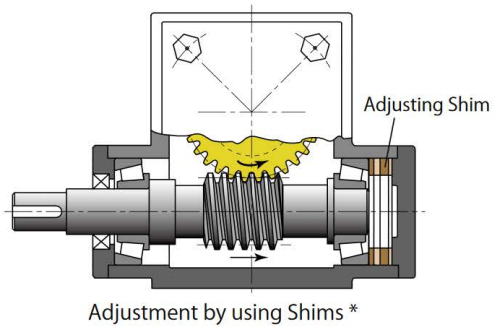

Figure 5.54. Revolver worm gear backlash adjustment method.

match-ground to the circumferential length we need. The rails and carriages are the only ferrous materials on the revolver mechanism. The rails mount to stainless steel semi-circular rail brackets, which are mounted to the strongback. Each bracket is butted against a shoulder on the strongback, and the THK bearing blocks have a light preload. To avoid overloading the bearings, we precisely shim between the mounting plates of the bearing blocks and their mating support plates.

The revolver drive motor and rotary encoder assembly are the same as the gap drive, but a 50:1 gearhead is used between the motor and the worm shaft. The worm gear set is self-locking by itself, and cannot backdrive the gearhead either, so no brake is used. Our gap drive employs a similar scheme with acme screws with wormgear reducers which cannot be backdriven, due to the combination of friction and the screw and Wormgear ratios.

Our control system uses resolution of .001°, but the encoder resolution is even finer. We use a series of limit switches together with encoder feedback to interlock the gap and revolver drives through software, gate array logic, and hard-wiring. The gap has to be open for the revolver to move; once it moves slightly, the gap drive is disabled until the 90° rotation is complete. Similarly, once the gap begins to close, the revolver drive is disabled. Figure 5.55 is a closeup view of the revolver drive mechanism and the array of limit switches used to sense and interlock revolver position.

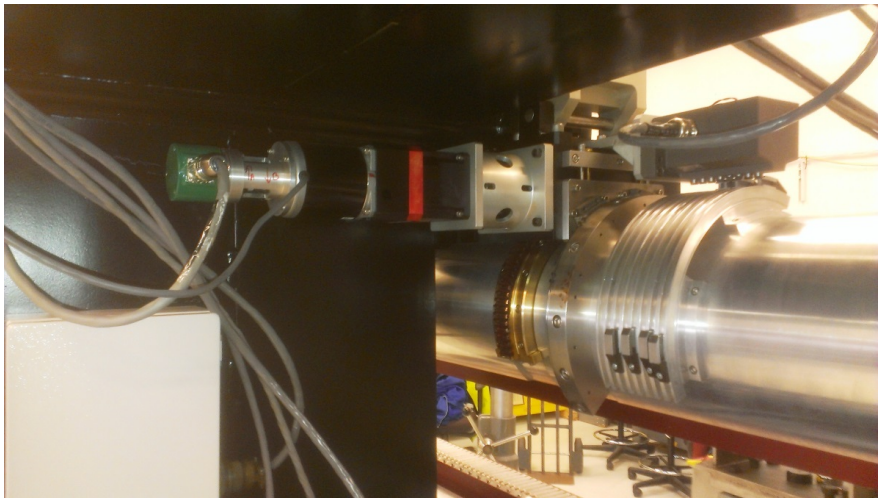

Figure 5.55. Revolver drive mechanism.

5-3.7 Canting Magnets and Phase Shifters

5-3.7.1 Canting Magnet

The APS dual, canted undulator sectors have been in operation for over a decade. In the original design, 3 electromagnetic dipole magnets were used to create a 3-bend chicane for the electron beam within the insertion device straight section: 0.5 mrad outboard -> 1 mrad inboard -> 0.5 mrad outboard. Later, the 0.5 mrad magnets were eliminated, with the electron beam entering the ID straight 0.5 mrad outboard and leaving the ID straight 0.5 mrad inboard, with the orbit corrected downstream of the ID straight. To conform to the APS-U MBA lattice/magnet requirements, the APS-U configuration will revert to the original 3 dipole configuration, and will use the existing magnet designs. Figure 5.56 shows the center canting magnet assembly and an image of that assembly installed in the current APS storage ring. The 3-bend chicane configuration can utilize beam position feedback from a BPM located near the center of the ID straight, but typical ID operation and storage ring orbit control do not require a BPM.

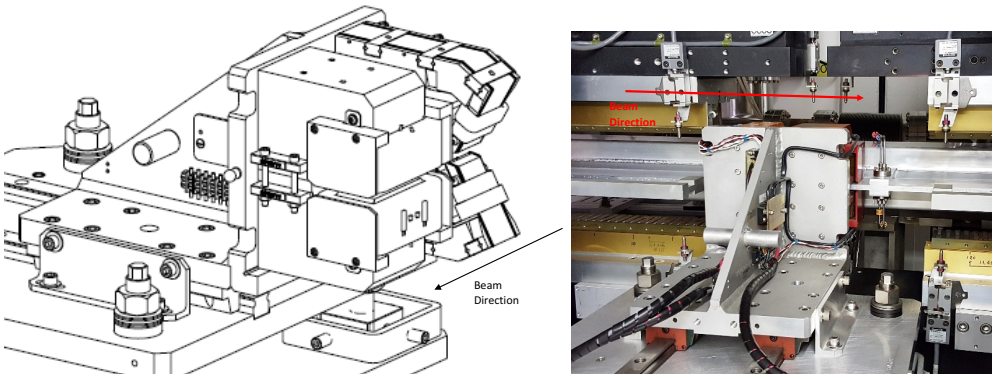

Figure 5.56. Center canting magnet assembly: corrector magnet (upstream) and dipole (downstream); image of assembly installed over IDVC between two HPMUs, with a BPM downstream of the dipole.

5-3.7.2 Phase Shifter

To provide a full-length (4.6 m), coherent X-ray source, APS-U have chosen to employ a permanent magnet, variable gap phase shifter between two undulators, each of 2.3 m length. This avoids the complexity and lack of interchangeability of a single long undulator approach. Another possibility considered was to move one undulator remotely in the z-direction, but this is not as efficient a use of source length as the phase shifter, among other drawbacks. The phase shifter is functionally a short undulator, and will employ a Halbach array of permanent magnets and a mechanism to allow precise gap adjustment while protecting the IDVC from contact or damage. A gap range from 9 mm to 80 mm will be provided. Changing the gap will vary the length of the electron path between the two undulators, and a stepper motor and absolute position encoder will be used to adjust the gap and provide control system feedback. The phase shifter will be mounted to a plate similar to the canting magnet assembly shown in Figure 5.56, and the same horizontal/vertical corrector magnet will be used. The plate provides 6 degrees of freedom adjustment, and allows the entire assembly to be retracted for installation, removal or service of the phase shifter or corrector magnet. The corrector magnet is required to meet the electron beam trajectory as discussed in Section 5-3.2.2.

5-3.8 Horizontal Gap Vertical Polarization Undulator

Conventional planar undulators currently in operation in synchrotron facilities are typically a pair of magnetic arrays which open and close in the vertical plane. These devices produce X-rays polarized in the horizontal plane. Special devices like the Advanced Planar Polarized Light Emitter (APPLE) provide variable polarization of the X-ray beam, but they also operate by magnetic arrays oriented above and below the plane of the particle beam. Recently a horizontal gap device known as HGVPU was developed at APS for the LCLS II facility. This device requires a small horizontal aperture for the particle beam vacuum chamber. The APS-U lattice with the on-axis injection allows the possibility of small horizontal apertures of 6 mm similar to the vertical aperture of 6 mm, thereby opening up the possibility for a horizontal gap device as a source for beamlines.

APS-U will be using a HGVPU of 4.6 m length as a the source for one of the beamlines. For the specific APS-U beamline geometry, vertical polarization coupled with the APS-U beam properties offer a superior X-ray source. The HGVPU developed for LCLS-II had numerous assemblies of conical springs which accurately compensated the undulator's magnetic attractive force, which varies exponentially with gap changes. This scheme allowed for use of a much smaller strongback (the beam which provides bending stiffness to the magnet structure). It also allowed for use of much smaller gap drive mechanisms than would be required without the spring compensation. The magnet/pole holders for the HGVPU allow smaller adjustments to the pole height than are possible with prior APS mechanical shimming. The overall, integrated design allows very precise gap adjustment, and maintains a much smaller gap variation over the length of the device than is achievable as economically from convention undulator designs. Figure 5.57 is a 3 m HGVPU prototype built at APS for the LCLS II project undergoing magnetic measurements.

Figure 5.57. The 3 m prototype of HGVPU built for LCLS II at APS.

For APS-U, the design will likely take the form of drive/force compensation systems located solely on the inboard side of the storage ring, with the HGVPU removable from underneath a special ID vacuum chamber supported only on the ends (as the standard APS-U IDVC will be, discussed later in Section 5-3.10). The HGVPU ID vacuum chamber will obviously have a small horizontal aperture and a larger vertical aperture (6.2 mm H x 8 mm V). Due to the need to intercept synchrotron

radiation from the upstream dipole over the length of the chamber, the chamber will have a thicker wall than the standard APS-U IDVC (1.5 mm vs 0.6 mm), and will have the antechamber for NEG pumping located above the beam aperture, rather than to the outboard side. Early design studies have been conducted to assure the feasibility of operating the HGVPU at a gap of 10 mm while maintaining the same design and operational safety margins as other APS-U ID and IDVC systems.

5-3.9 Superconducting Undulators

5-3.9.1 Scope

The technology of superconducting undulators was developed at the APS over the last decade. A superconducting undulator (SCU) employs a set of superconducting coils to generate a periodic magnetic field. Due to the high current-carrying capacity of superconductors, superconducting undulators outperform all other technologies in terms of peak magnetic field for a given period length and magnetic gap. For the APS-U , the SCUs are the preferred choice of undulators for beamlines requiring x-rays at 20 keV and beyond.

The SCU team has accumulated experience while building and operating three planar SCUs for the APS and a test undulator for the LCLS SCU R&D project. The parameters and status of the devices are listed in Table 5.22 [8, 9].

Table 5.22. List of planar superconducting undulators developed at the APS

Parameters	SCU0	SCU1 (SCU18-1)	SCU18-2	LCLS SCU
Period length (mm)	16	18	18	21
Magnetic gap (mm)	9.5	9.5	9.5	8
Magnetic length (m)	0.33	1.1	1.1	1.5
Design/Achieved field (T)	0.64/0.8	0.96/0.97	0.96/0.97	1.67/1.67
Status	Retired Jan2013-Aug2016	Operational since May2015	Operational since Sep2016	Project complete

The current scope of superconducting undulators for the APS-U include eight devices assembled in pairs in four long cryostats, as shown in Table 5.20 before and summarized in Table 5.23. The magnetic gap is assumed to be 8 mm. The APS-U project will capitalize on the existing infrastructure and experience of the team.

Table 5.23. Scope of APS-U superconducting undulators

Period length (mm)	Magnet length (m)	Configuration	Quantity of cryostats
16.5	1.8	Two in line	2
16.5	1.5	Two canted	1
18.5	1.2	Two canted	1

5-3.9.2 Supercounducting Magnet Design

A superconducting undulator magnet consists of two magnet cores separated by a magnetic gap where a beam chamber is accommodated, as shown in Figure 5.58.

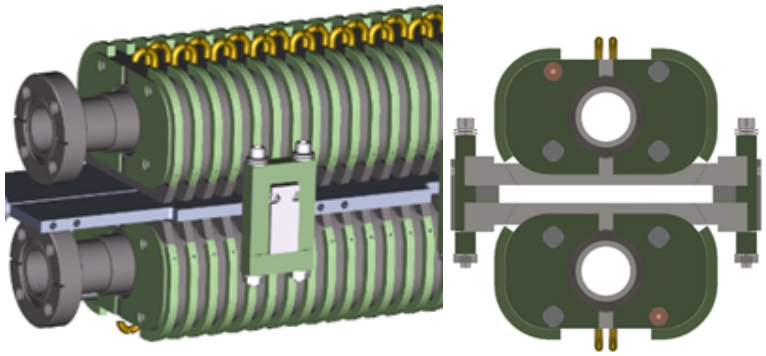

Figure 5.58. Assembly of two cores with precise spaces defining the magnetic gap.

A set of multiple racetrack coils are formed when a NbTi superconducting wire is wound into the core groves. The current is flowing in opposite directions in the adjacent coil packs, therefore generating an alternating field profile along the beam axis. In this scheme, the superconducting wire makes an 180-degree turn on the back side of the core around a pin (seen in Figure 5.58) after being wound into a groove. The number of wire turns in a winding pack depends on the undulator period length and the groove dimensions. For example, a 16-mm period SCU0 magnet contains 39 turns of 0.6-mm round wire in a groove. The core and the superconducting wire is cooled to the temperature of 4.2 K with liquid Helium passing through a channel in the core, also seen in Figure 5.58.

It should be noted that the quality of the magnetic field, i.e. repeatability of the peak magnetic field from one undulator period to another along the full device, strongly depends on the precision of grooves, quality of winding, and the uniformity of the magnetic gap. The high quality of APS SCU winding has already been demonstrated [10]. The SCU cores are typically machined to high precision with the coil winding groove dimensions within typically 15 μm RMS. It was noticed, that the cores are usually deformed after a technological operation of an epoxy impregnation. In the SCU18-1 magnet, for instance, the measurement of the pole face revealed that the cores had developed a bow that would cause the magnetic gap to be up to 200 μm larger once the cores were assembled. To address this issue, a dedicated R&D program was performed during the LCLS SCU project. As a result, a special technique for a gap correction was developed. It is based on a system of mechanical clamps that allows adjustment of the magnetic gap to a value defined by the extended gap spacers machined to a 10 μm precision. This system was fully implemented in the SCU18-2 magnet. As a result, the measured maximum variation in the gap over the length of that magnet was around 25 μm. Due to such a precise gap, the measured field errors in the SCU18-2 – the latest planar undulator built at the APS – are within 2° RMS. Figure 5.59 is cross-sectional view of the mechanical clamp used to correct the gap error. The APS-U undulators will be equipped with the similar gap correction system.

It should be noted that there are correction coils that are available to adjust the values of the first

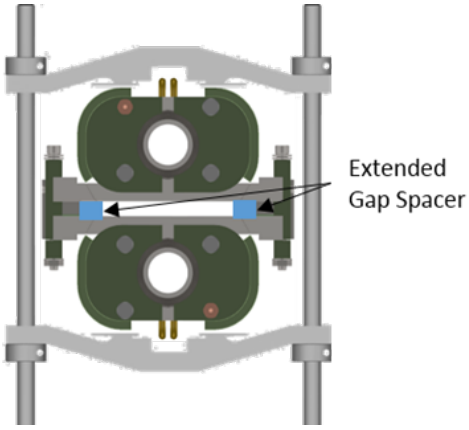

Figure 5.59. Assembled cores with external clamp and extended gap spacer.

and second field integrals in the vertical direction. These coils are external to the magnet assembly and are shown in Figure 5.60.

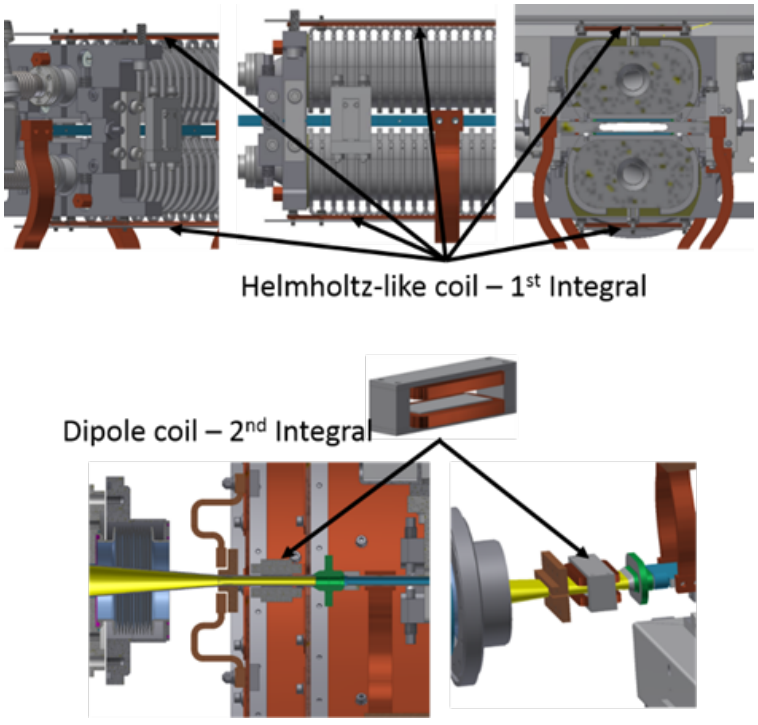

Figure 5.60. Vertical field integral correction coils.

5-3.9.3 Cryostat Design

The existing planar SCUs for the APS use a common cryostat design developed in collaboration with the Budker Institute of Nuclear Physics (BINP) [11]. The cryostat consists of a cylindrical end-loading vacuum vessel, multiple thermal radiation shields, and a liquid helium (LHe) reservoir connected to cooling channels within the core of each magnet. Refrigeration is provided at three different temperature levels using multiple cryocoolers. This cooling strategy keeps the heat load

on the LHe circuit to a manageable level and allows the cryostat to operate in a closed-loop, "zero boil-off" mode. Figure 5.61 shows design models and photos of the existing APS SCUs.

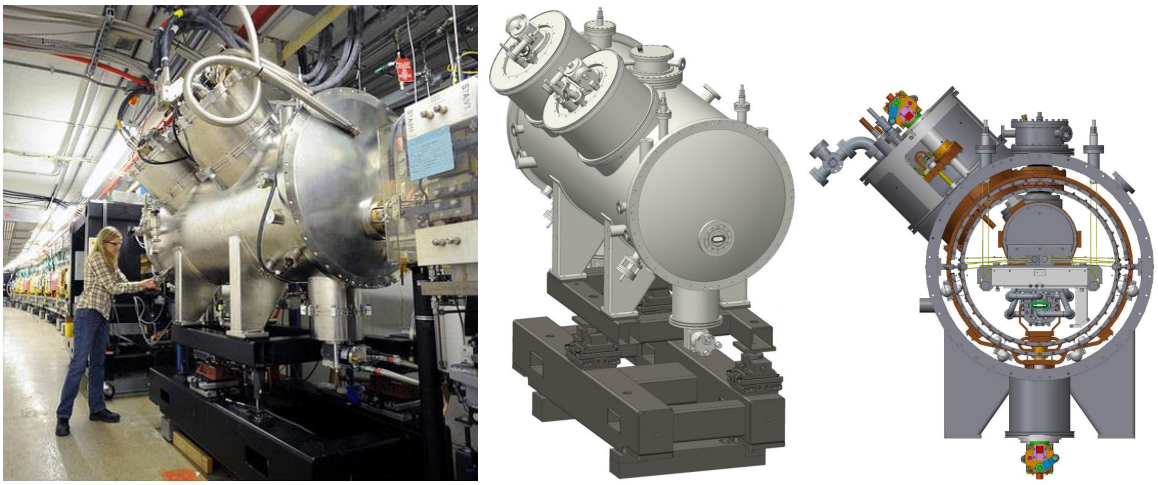

Figure 5.61. (left) installed SCU, (middle) CAD model, (right) CAD end section.

For the APS-U, a revised cryostat will be used. Lessons learned with the existing devices together with value engineering has yielded a cheaper and smaller design better suited to available ID locations in the storage ring. The new cryostat model is shown in Figure 5.62. Figure 5.63 shows the new design prototype compared with the original design.

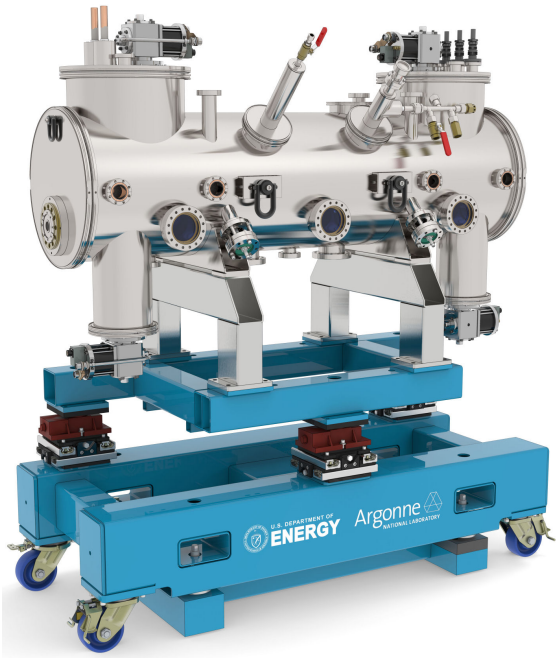

Figure 5.62. A 3D rendering of the new compact SCU cryostat.

The new compact cryostat is very modular and can be extended to larger lengths. The prototype was a 2m cryostat, however for the APS-U, the length of the cryostat will be scaled to the full straight section and is expected to be about 4.5m long. The single long cryostat will hold two

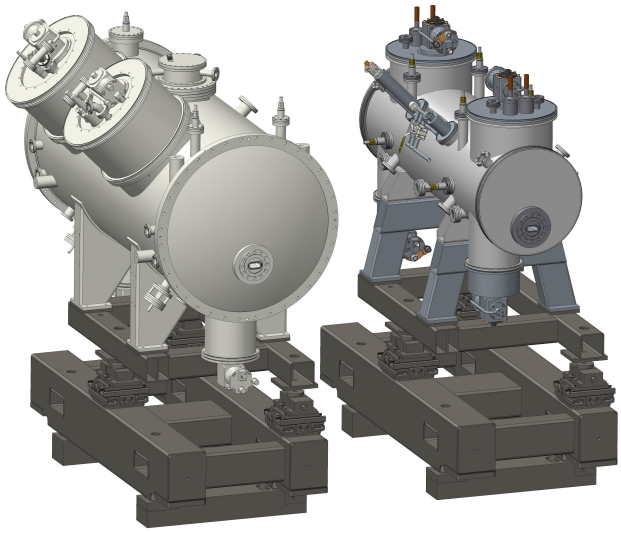

Figure 5.63. Comparison of the existing cryostat with the new cryostat.

sets of magnets either in tandem or in canted geometry. Figure 5.64 is a 3D rendering of the long cryostat in the APS-U straight section. The middle figure shows the top view and its coexistence with the bending magnet beamline on the outboard side.

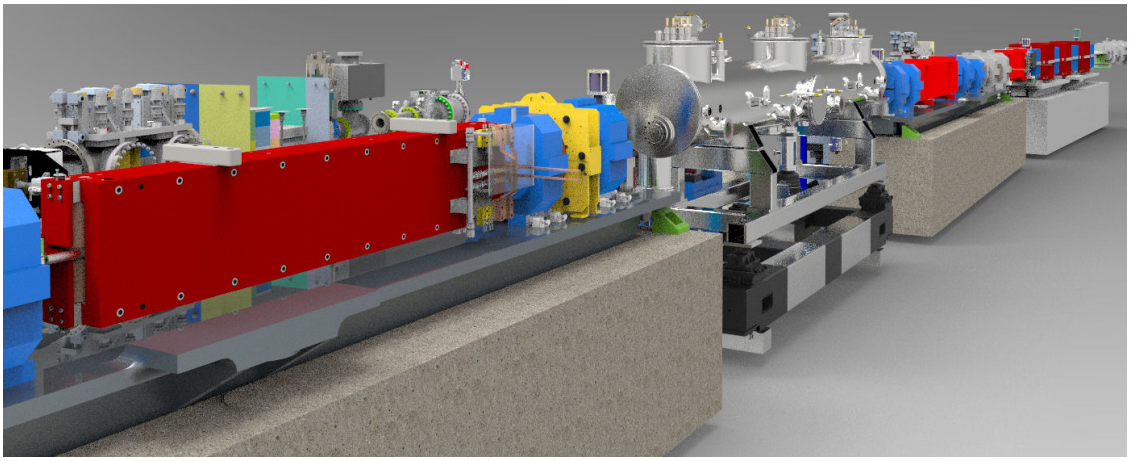

Figure 5.64. Rendering of long SCU cryostat in the APS-U straight section.

5-3.9.4 SCAPE

SCAPE stands for SuperConducting Arbitrary Polarized Emitter. It is a novel concept of a universal superconducting undulator capable of generating both planar and circular polarized radiation. The SCAPE magnetic structure consists of two pairs of a planar-like cores – one vertical and one horizontal – assembled around a beam vacuum chamber,as seen in Figure 5.65. The horizontal pair is shifted against the vertical one by a quarter of the period length. Such a magnet generates a planar magnetic field when one of the core pairs is energized – either the vertical or horizontal one, or it generates a helical field when all the core pairs are energized, as seen in Figure 5.66. Since the cores are wound with a superconducting wire, the magnetic field on axis exceeds the values reachable with a permanent magnet technology.

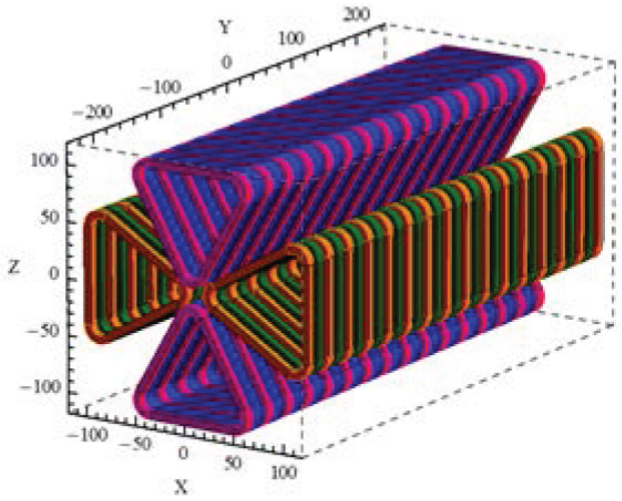

Figure 5.65. Magnetic model of SCAPE structure with two pairs of coil windings.

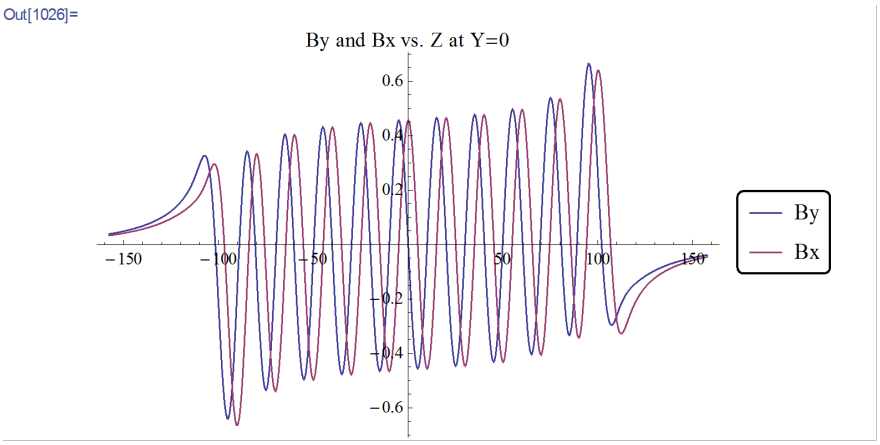

Figure 5.66. Simulated field profile in SCAPE when all four cores are energized.

The mechanical 3D model of a SCAPE magnet and a beam chamber is shown in Figure 5.67. The beam chamber is made of an Al extrusion containing a central tube with integrated longitudinal fins that are used for extraction of the electron beam generated heat. The magnet cores, which are also made of Al extrusion, contain magnetic pole tips. The cores and superconducting windings are cooled by liquid helium, which passes through the core channels.

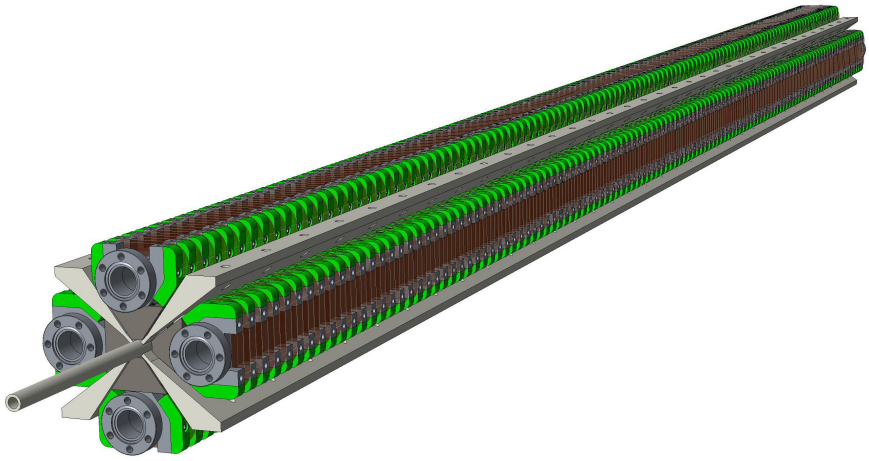

Figure 5.67. Solid model of SCAPE magnet with beam vacuum chamber.

The SCAPE undulator will use the same cryostat as the APS-U planar superconducting undulators. Two 1.75 m long SCAPE devices will be located in the same cryostat to provide switchable polarization for the beamline. R&D funded by the laboratory is in progress to develop a proof of principle device and also to study the switching of the field to be a viable device for the POLAR beamline.

5-3.10 Insertion Device Vacuum Chamber

5-3.10.1 Requirements

One of the main purpose of an accelerator vacuum system is to minimize interaction between the particle beam and gas molecules. Such interactions contribute to the instability and gradual loss of beam. The APS-U storage vacuum system must limit residual gas pressures so that the lifetime associated with gas scattering is no less than 30 hours while operating at 200 mA after 1000 A hours of machine operation. Moreover, to reliably serve the facility beamlines, the system must be robust enough for a life span of at least 25 years over which 5000 hours of beam per year are provided with at least 95% availability.

In addition to functional requirements, numerous design constraints are associated with interfaces to other technical systems. These interfaces include adequately limiting the electromagnetic interaction between the vacuum system and the beam, ensuring mechanical fit between vacuum components and magnets, ensuring that vacuum components do not compromise required magnet field strength and quality, keeping gas bremsstrahlung and other stray radiation within acceptable levels, providing signals as-needed for control and equipment protection systems, and making sure that the time needed for installation is accommodated by the project schedule. The APS-U insertion device vacuum system, although addressed separately, must meet the same standards as the rest of the APS-U storage ring vacuum system.

The current APS storage ring has 35 straight sections available for IDs. The usable length of the straight section for the insertion devices is 4.8 m. With the exception of a few specialty devices and super-conducting undulators (SCU), the nominal internal aperture of the planar insertion device vacuum chambers (IDVC) will be a 16-mm horizontal and 6.2-mm vertical modified ellipse. All of the planar IDVC assemblies will consist of a machined chamber extrusion supported by a rigid strongback support system. Each end of the strongback support system must attach to adjacent support plinth assemblies and allow for alignment in 6 degrees-of-freedom (DOF). More details are found in the APS-U Insertion Device Vacuum Chamber ICD.

The IDVC will be made of 6063-T5 aluminum extrusions. The extrusions will have a surface roughness of the aperture $\leq 1\mu$m, be exposed to a resistive wall heating of 7 W/m, and be able to have the aperture center aligned to within ± 50 μm.

All components will be designed so that during operational conditions, each component will have a maximum Von Mises stress less than 1.5 times the documented typical yield strength of the material, and a maximum Von Mises stress less than 2.4 times the documented typical ultimate strength of the material. The maximum material operating temperature will not exceed 30% of the melting temperature to ensure that material creep is negligible.

Water circuit topology, return and supply pressures, temperature, chemistry, fittings, and required monitoring and interlocking are described in the APS-U Insertion Device Vacuum Chamber ICD. Water joints will be designed so that water cannot enter vacuum spaces in the case of a failure of a joint. To minimize erosion, water passages will be designed so that the maximum water velocity does not exceed 3 m/s. A corrosion/erosion allowance of 0.010 mm per year will be used for all water channel boundaries. Operational water temperature shall not exceed 141°C at 40 psig.

5-3.10.2 Design

The APS-U storage ring vacuum chamber has a nominal 22 mm round aperture. At the ID straight sections, transitions will be made from the 22-mm round aperture to the 16 mm horizontal by 6.2 mm vertical, roughly elliptical aperture over a length of 120 mm within the extrusion by using a plunge EDM method of machining into the raw extrusion. The raw extrusion will be designed with enough material to machine the transitions directly into the ends of the extrusions. After final machining is complete, the IDVC will have nominal wall thickness of 0.6 mm at the largest beam aperture, over 5050 mm of its 5417 mm overall assembly length to allow for electron beam interaction with the insertion devices' magnetic field. This vacuum chamber allows a minimum magnetic gap of 8.4 mm for the IDs. Figure 5.68 shows a cross-section of the new extrusion for the APS-U lattice.

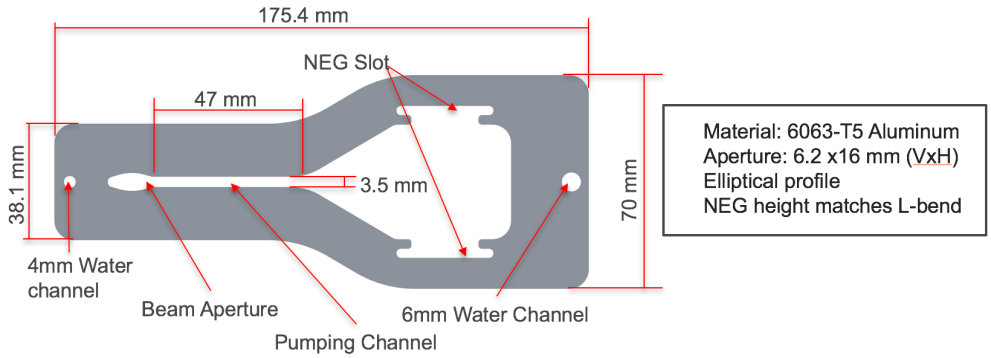

Figure 5.68. Cross-section of ID vacuum chamber extrusion.

Analysis has been performed to verify that the chamber will meet the specified requirements for Von Mises stress after machining of the thin wall, and to examine the deflection of the pumping channel as seen in Figure 5.69.

Figure 5.70 is a 3D view of the downstream end of the ID straight section, where the transition box has been machined into the Al extrusion. The chamber has an ante-chamber to accommodate the installation of NEG strips for distributed pumping down the entire length of the chamber. The spacing of the NEG strips is consistent with the L-bend vacuum chamber so that the same feed-through flange can be utilized for both chamber designs. The vacuum chamber assembly will be fabricated from materials that will allow all internal surfaces to reach a temperature of 130℃ for the purposes of a vacuum bake-out. This chamber design is also compatible with the "three-headed" revolver undulators.

The end box assembly is shown in Figure 5.71. The upstream and the downstream end boxes are identical, with the major exception of the the photon absorber in the downstream end box. Both end boxes have a small ion pump of 25 l/s capacity. In addition two NEG strips running the whole length of the ID straight section provides pumping along the straight section.

Flanges on the particle beamline will be 316L stainless steel of the QCF type similar to the rest of the storage ring vacuum chambers. As the vacuum chamber body is made of extruded T6063 aluminum, an explosion-bonded Al 2219 – SST 316L transition between the flange and chamber will

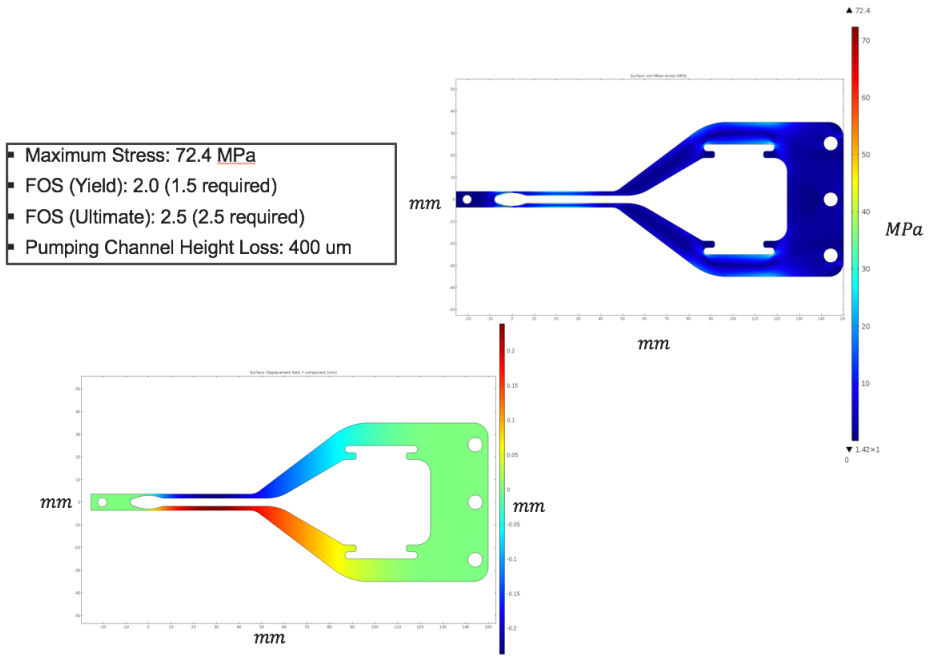

Figure 5.69. Vacuum chamber stress and deflection results.

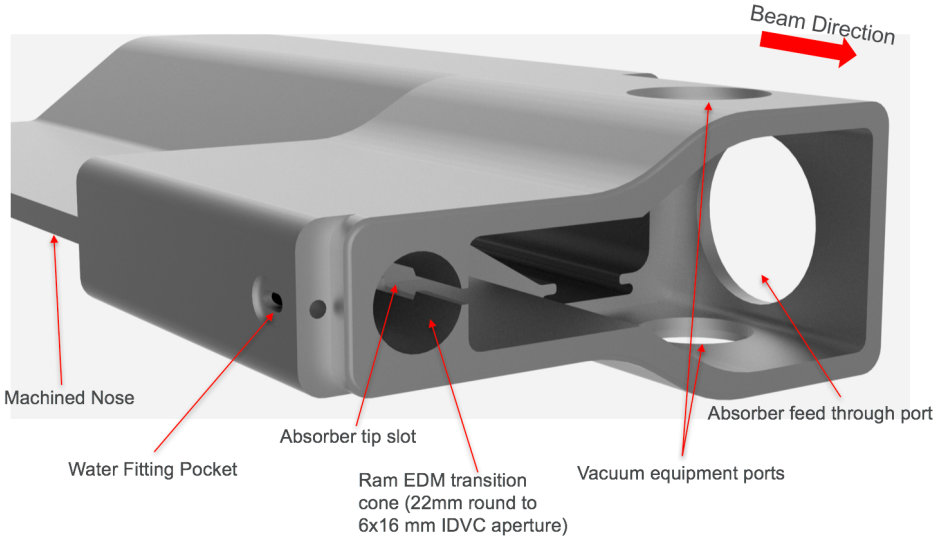

Figure 5.70. View of the downstream end box, which is machined into the end of the extrusion.

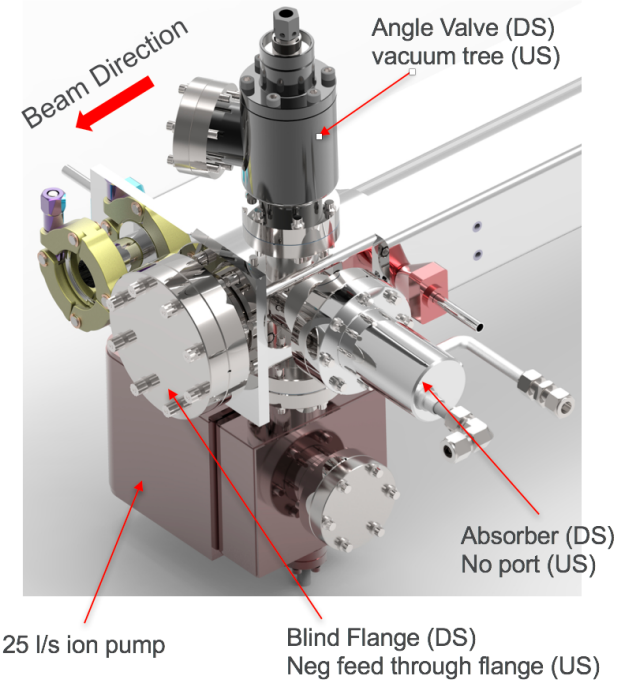

Figure 5.71. The downstream (DS) end box assembly with a photon absorber. The upstream end box (US) is identical with the exceptions noted in the figure (mainly, no photon absorber).

be utilized. Gaskets for these flanges will be annealed copper. All flanges on the particle beamline will be specially machined to minimize the "gap" between flanges exposed to the particle beam. This gap will be no more than 0.2 mm long and 3 mm deep. In addition, it will be ensured that the offset between flanges in the radial direction cannot exceed 0.2 mm. Radio frequency (RF) shielding springs or other such devices will not be used.

Flanges not on the particle beamline will be 316L stainless steel and be of bolted CF type. Because the vacuum chamber body is aluminum, an explosion-bonded Al 2219 – SST 316L transition between the flange and chamber will be used. Gaskets for these flanges will be non-annealed copper.

Photon absorbers are tasked with shadowing sensitive components from direct incident synchrotron radiation under all expected missteering scenarios. A photon absorber will be placed at the downstream end of the ID straight section to intercept the synchrotron beam from the M1 dipole upstream of the straight section. The narrow slot in the IDVC between the beam chamber and the ante-chamber plays a dual role - it provides a vacuum pumping access for the beam chamber from the NEG pump, and it allows all the synchrotron radiation from the upstream dipole magnets M1.1 and M1.2 to pass through under normal beam conditions. Figure 5.72 shows the calculated ray tracing of the synchrotron radiation from the upstream dipole magnet M1 impinging on the photon absorber at the downstream end of the straight section. A photon absorber is located at the downstream end box to handle about 728 W of beam box. A small amount of about 100 W passes through the opening in the beam chamber along with the particle beam. The photon absorber protects the downstream components and also protects the BPM and the gate valve immediately downstream of the ID straight section. The photon absorber is expected to be fabricated with Glid-Cop to

ensure that the the stress and the temperature are within the acceptable levels. The beam strike surface of the photon absorber is tapered to avoid normal incidence with the synchrotron radiation. Figure 5.73 shows the thermal analysis of the photon absorber. Currently no synchrotron radiation deposition is expected to strike the IDVC itself. Off orbit ray tracing criteria is being developed.

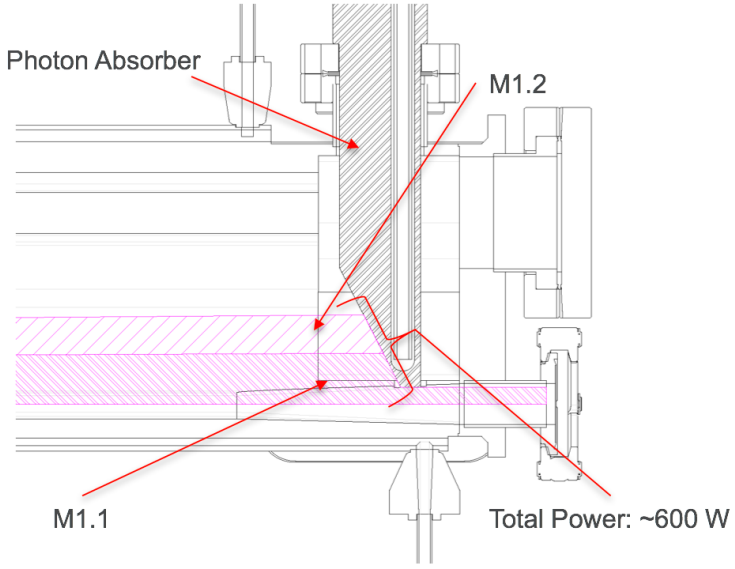

Figure 5.72. Radiation from upstream dipole M1.1 and M1.2 intercepted by the photon absorber at the downstream end of the IDVC.

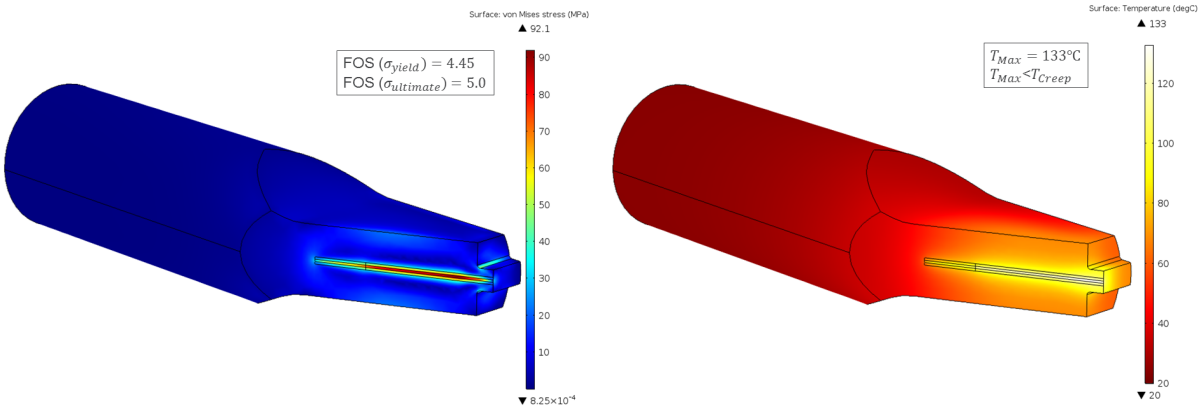

Figure 5.73. Temperature and stress analysis of the downstream absorber (Top) Stress (Bottom) Temperature of the surface.

The IDVC support system will provide distributed support across the length of the IDVC and provide beam aperture alignment to ±50 μm. The IDVC support beam will be machined from a 6061-T6 aluminum extrusion. The support beam must deflect an order of magnitude less than the IDVC when simply supported by itself. This ensures that any deflection in the IDVC can be removed. The IDVC support beam will be mechanically coupled to two support brackets, both welded from 6061-T6 aluminum. These support brackets will mount directly to the upstream and downstream plinths. The brackets must be capable of supporting the entire IDVC assembly and IDVC support load. Figure 5.74 is an overview of the IDVC with the support structure. The bottom

panel is a 3D rendering of the IDVC support system without the IDVC. Connecting the brackets to the support beam are six strut assemblies. Each assembly will consist of a hex-rod strut-beam, 1x fine thread bearing rod end, and 1x coarse thread bearing rod end. All parts of the strut assembly will be made from 316L SST. The IDVC will be mechanically coupled to the support system, as shown in the bottom panel of Figure 5.74, through a series of threaded rod connections on the top of the support beam. The threaded rod will be silver plated and fine thread to ease the alignment process. The number and locations of the threaded rod will be minimized to ease assembly time while also meeting alignment requirements as mentioned in the ID FReD. Analysis of the beam weldment was completed to examine the stress under load.

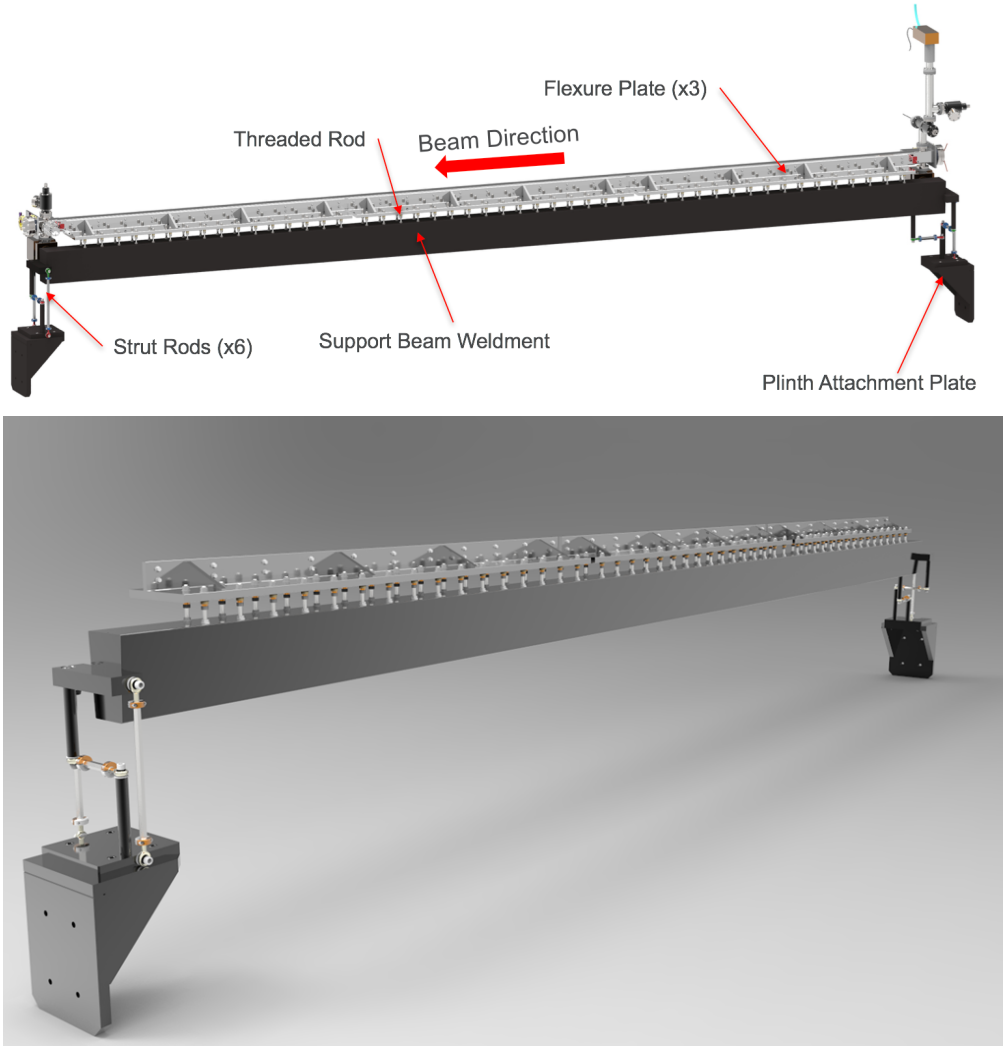

Figure 5.74. (Top) Overview of the IDVC with its integrated support system (Bottom) 3D rendering of IDVC support system.

5-4 Bending Magnet Sources

5-4.1 Introduction and Scope

The current APS has 20 Bending Magnet (BM) beamlines in operation. he beamlines are provided with a 6 mrad horizontal fan of radiation from one of the two dipole magnets per sector. The current storage ring has two dipoles per sector and only one of the dipole sources is used for BM beamlines. The other dipole just downstream of the ID straight section is not used. The separation between the ID and the BM source is currently set to 5.0625°. All beamlines have been built with this geometry.

The APS-U is a MBA lattice and has 7 bending magnets per sector. The lattice has been optimized to keep the ID beamline tangent line the same to avoid having to realign all the ID beamlines. However by keeping the separation between the ID and BM line the same, the new source point for the BM beamlines lies 43.6 mm inboard of the current location. The center of the source point for the BM beamline is positioned between the transverse gradient dipole (M4) on the upstream and the quadrupole (Q8) downstream. Figure 5.75 is an elevation view of the FODO section of the lattice showing the location of the BM source point. In addition, the source point has also shifted upstream by 2.929 m relative to the current APS BM beamline source.

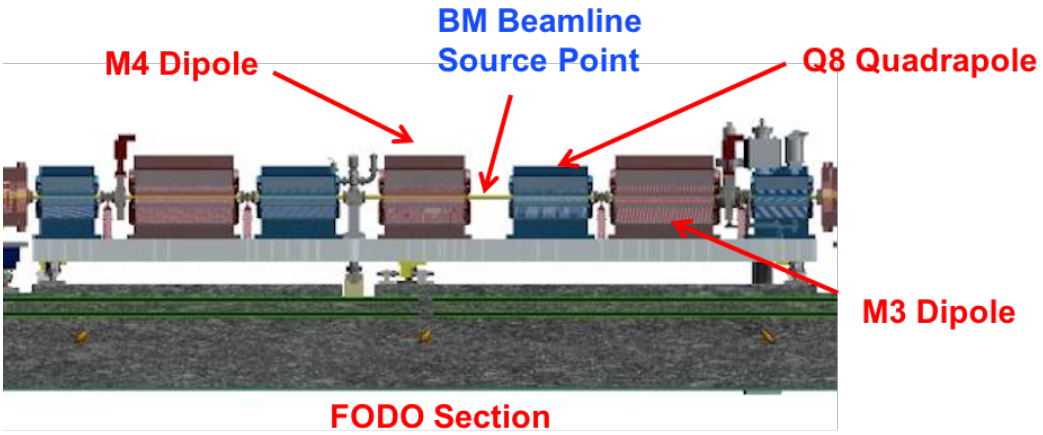

Figure 5.75. An elevation view of the BM source location in the FODO section.

5-4.2 Requirements

The APS-U lattice was designed with the possibility of inserting a small three pole wiggler (3PW) at the BM source point. The 3PW can be installed in the short space between the A:M4 and B:Q8 magnets and has about 15 cm of available space. The main requirement for the 3PW is to provide higher flux than that of the current APS BMs at higher energies.

In the APS-U lattice, as designed, the BM beamlines will receive a combination of radiation from the M4 and M3 transverse gradient dipoles. In addition, the reverse bend lattice makes it more complex as the quadrupole Q8 between the M4 and M3 magnet provides a 5 mrad of reverse bend. The net result for the beamline will be a combination of all these dipole sources and the 3PW.

The current plan is to reuse the existing BM front ends. The radiation fan delivered to the beamlines is determined by the masks in the front end and is limited to 6 mrad. However, most beamlines do not use more than 1 mrad of fan, with the exception of 3 beamlines that split the 6 mrad fan into two branches. With the shift of the source point upstream by 2.929 m, the spatial fan of radiation delivered to the beamlines will be the same, but will be provided by a combination of sources of about 5.2 mrad equivalent.

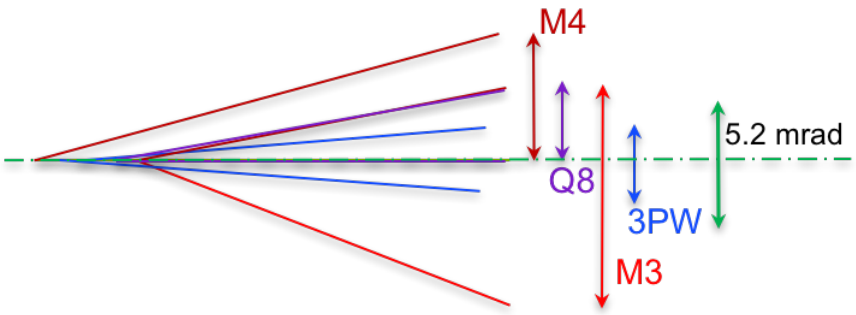

Figure 5.76. A schematic view of the radiation fans on the BM source centerline.

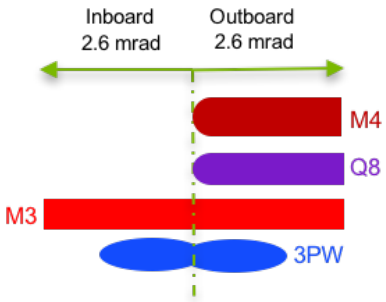

Figure 5.77. A schematic view of the radiation from the multiple sources as viewed from a beamline.

Figure 5.76 is the rendition of the radiation fan received by the beamlines on the horizontal plane. Figure 5.77 is a schematic view of what the beamlines will see on the 5.2 mrad fan they receive. The contributions from the various sources are shown. Multiple versions of 3PW have been magnetically designed and all of them provide a double lobe at most energies. At very high energies, this becomes

a Gaussian due to the strong center pole of the 3PW. At this time, based on the spectral properties discussed in the next section and the beamline by beamline specific case, the 3PW as a BM beamline source will not be pursued.

5-4.3 Spectral Flux of BM source

The current APS bending magnet has 0.599 T field and is operating at 7 GeV with 100 mA of stored beam. For the APS-U, the storage ring will operate at 6 GeV with 200 mA of current. The field of the upstream transverse gradient dipole is about 0.61 T and the downstream transverse gradient dipole M3 is 0.66 T. In addition, the quadrupole Q8 in the reverse bend has 0.18 T of dipole fields. These magnet field strengths are approximate and may change during the final design due to optimization of the storage ring magnet design. As shown in Figure 5.77, the radiation pattern is different along the 5.2 mrad fan received by the beamline. The inboard fan of about 2.6 mrad is a clean radiation from the downstream M3 magnet. The outboard radiation is a combination of the upstream M4, the downstream Q8, and the M3 magnets. Due to spacial distribution and the discrete nature of the radiation from multiple sources, it may be possible during focusing to isolate the specific source. For most beamlines, the use of the clean M3 radiation on the inboard side will be advantageous. The introduction of a 3PW will result in the 3PW radiation having a background radiation from the M3 and on the outboard side there will be the edge radiations from the M4 and Q8 magnets.

A comparison of the various sources are shown in Table 5.24. The APS BM is shown in the table for 7 GeV and 100 mA while the other sources are for 6 GeV at 200 mA. The horizontal fan in the table is what is received by the beamline based on the front end configuration. The power per mrad is for the horizontal fan of 1 mrad at 25 m from the source for the current configuration. For the APS-U, the increased source distance has been compensated. Figure 5.78 is the comparison of the spectral flux at current 25 m point of the beamline for an aperture of 25 mm horizontal by 2 mm vertical. The M3 magnet radiation has increased flux up to 38 keV over the current BM source.

Table 5.24. Comparision of the different BM beamline sources

Source	Field [T]	Critical Energy [keV]	Horizontal Fan [mrad]	Power/mrad [W]
APS BM	0.599	19.519	6	87
M3	0.66	15.815	5.2	121
M4	0.61	14.652	2.6	112
Q8	0.18	4.357	2.6	33
M3+M4+Q8	-	-	2.6	266
3PW	0.99	23.731	1.4	261

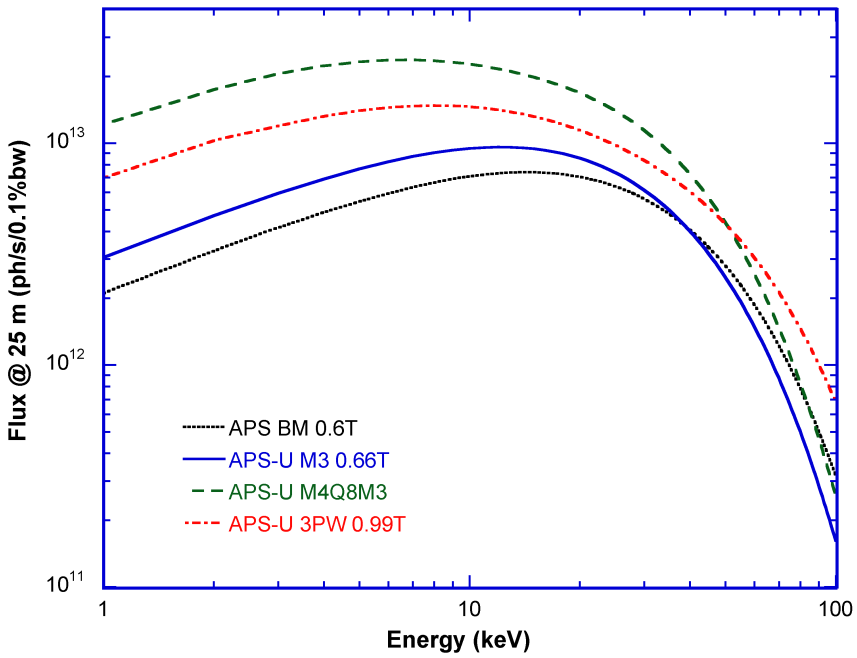

Figure 5.78. Calculated spectral flux at current 25 m point through an aperture of 25 mm horizontal and 2 mm vertical. The 3PW (red curve), the inboard M3 dipole radiation (blue curve), and the combined outboard radiation from M3, M4, and Q8 (green curve) for a beam energy of 6.0 GeV and a current of 200 mA are shown. The performance of the current APS BM for a beam energy of 7.0 GeV and a current of 100 mA (black curve) is shown for comparison.

References

[1] Yifei Jaski. Thermal analysis of the components of the insertion device front ends fev1.2 and fev1.5. In *ANL/APS/TB-50*, Argonne, IL, 2005.

[2] Y. Jaski, E. Trakhtenberg, J. Collins, C. Benson, B. Brajuskovic, and P. D. Hartog. Thermomechanical analysis of high-heat-load components for the canted-undulator front end. In *MEDSI 2002 Conference Proceeding*, pages 390–397, 2002.

[3] Yifei Jaski. New front-end design for multiple in-line undulators at the advanced photon source. In *AIP Conference Proceedings 705*, pages 356–359, 2004.

[4] J. T. Collins, J. Nudell, G. Navrotski, Z. Liu, and P. D. Hartog. Results from studies of thermomechanically-induced fatigue in glidcop®. In *MEDSI 2014 Conference Proceeding*, Melbourne, Australia, 2014.

[5] Glenn Decker and Om Singh. Method for reducing x-ray background signals from insertion device x-ray beam position monitors. *Physical Review ST Accelerators and Beams*, 2:112801, Nov 1999.

[6] B.X. Yang, G. Decker, S. H. Lee, and P. Den Hartog. High-power hard x-ray beam position monitor development at the APS. In *Proceedings of BIW10*, pages 235–237, Santa Fe, NM, 2010.

[7] B.X. Yang, G. Decker, S. H. Lee, P. Den Hartog, T. L. Kruy, J. Collins, M. Ramanathan, and N. G. Kujala. High-power beam test of the APS grazing-incidence insertion device x-ray beam position monitor. In *Proceedings of BIW2012*, page 235, Newport News, VA, 2012.

[8] Yury Ivanyushenkov and et. al. Development and operating experience of a short-period superconducting undulator at the advanced photon source. *Physical Review ST Accelerators and Beams*, 18:040703, 2015.

[9] Yury Ivanyushenkov and et. al. Status of development of superconducting undulators for storage rings and free electron lasers. In *Proceedings of NA PAC2016*, Chicago, IL, 2016.

[10] Efim Gluskin. Development and performance of superconducting undulators at the advanced photon source. *Synchrotron Radiation News*, 28, 2015.

[11] N. A. Mezentsev and et. al. Superconducting magnets for sr generation in budker inp. In *Proceedings of of Russian Particle Accelerator Conference*, Dubna, Russia, 2006.